2017-12-07

Bioluminescent Sensing Systems for Cytokines and Cancer Biomarker Detection

Xiaowen Yu
University of Miami, xwyu.wendy@gmail.com

UNIVERSITY OF MIAMI

BIOLUMINESCENT SENSING SYSTEMS FOR CYTOKINES AND CANCER CELL BIOMARKER DETECTION

By

Xiaowen Yu

A DISSERTATION

Submitted to the Faculty
of the University of Miami
in partial fulfillment of the requirements for
the degree of Doctor of Philosophy

Coral Gables, Florida

May 2017

UNIVERSITY OF MIAMI

A dissertation submitted in partial fulfillment of
the requirements for the degree of
Doctor of Philosophy

BIOLUMINESCENT SENSING SYSTEMS FOR CYTOKINES AND CANCER BIOMARKER DETECTION

Xiaowen Yu

Approved:

_____
Sylvia Daunert, Ph.D.
Professor of Biochemistry and
Molecular Biology

_____
Leonidas G. Bachas, Ph.D.
Professor of Chemistry

_____
Roger M. LeBlanc, Ph.D.
Professor of Chemistry

_____
Guillermo Prado, Ph.D.
Dean of the Graduate School

_____
Sapna Deo, Ph.D.
Associate Professor of Biochemistry and
Molecular Biology

YU, XIAOWEN (Ph.D., Chemistry)

Bioluminescent Sensing Systems for Cytokines and Cancer Biomarker Detection. (May 2017)

Abstract of a dissertation at the University of Miami.

Dissertation supervised by Professor Sylvia Daunert.
No. of pages in text. (122)

The implementation of highly sensitive analytical platforms that can perform rapid and reliable detection of disease biomarkers is critical for early diagnosis and monitoring of disease. Bioluminescence is the generation of light through a natural oxidation chemical reaction, thus avoiding the need for an external light source which eliminates background fluorescence. This results in higher signal-to-noise ratio when compared to fluorescence, making it suitable for use as a label in ultra-sensitive detection applications. In that regard, the work in this dissertation focuses on the development of bioluminescent sensing platforms for biomarkers of disease in different biological systems.

The trend for improved, more precise diagnosis and management of disease relies on the measurement of panels of biomarkers, which highlights the need for technologies that can detect more than one biomarker without interferences from other analytes present in the same sample, i.e., multiplexed detection. To date, one drawback that limits the application of bioluminescence in multiplexed detection is the lack of versatility in the emission profiles and decay kinetics of the available bioluminescent labels. Recent efforts in solving this issue only expanded the application of bioluminescence to the simultaneous detection of two analytes. Herein, as part of the work of the second chapter of this dissertation, we have demonstrated that by combining both temporal and spatial resolution

strategies, the multiplexing capabilities of the photoprotein aequorin (AEQ) can be expanded. Chapter two of this dissertation describes the design and development of a multiplexed assay to measure three analytes simultaneously in a single solution by employing the variants of the photoprotein aequorin (AEQ). Aequorin, natively found in jellyfish *Aequorea victoria*, can emit a flash-type light at 469 nm with a half-life around 0.5-1 s after the binding of calcium ions (Ca^{2+}). The emission profiles, decay kinetics, and thermostability of AEQ have been tuned significantly from the native AEQ through site-specific mutations and use of synthetic coelenterazine analogues, expanding the applications of AEQ in versatile and miniaturized analytical systems. Specifically, the AEQ mutants AEQY82F and AEQF113W have been genetically conjugated to three main pro-inflammatory cytokines, namely, interleukin 6, interleukin 8, and tumor necrosis factor alpha (IL-6, IL-8, TNF-α) resulting in cytokines labeled with AEQ mutants. The three fusion proteins in conjunction with different synthetic coelenterazine analogues were applied as bioluminescent labels for the detection of all three cytokines simultaneously through the combination of spatial and temporal windows. The validity of the assay was demonstrated in serum by employing human pooled serum spiked samples and comparing our results with commercially available individual tests for each of the three cytokines.

Another topic in this dissertation is the establishment of a highly sensitive cancer cell detection technique using bioluminescence. In Chapter three, we demonstrate a bioluminescence-based approach to detect and image cancer cell lines *in vitro* and *in vivo*. The bioluminescent protein *Gaussia* luciferase (Gluc), native from the marine copepod *Gaussia princeps*, was employed as a sensitive detection label, taking advantage of the attractive properties of its bioluminescence emission. In addition, the surface biomarker

epidermal growth factor receptor (EGFR) that is overexpressed in various cancer cells was chosen as the binding target to increase the specificity of the detection reagent in the cancer cells. Herein, Gluc was genetically conjugated to the recognition molecule human epidermal growth factor (EGF), the ligand of EGFR, to construct a bioluminescence-based probe that can be directed to the EGFR receptors in the cancer cells, and thus, if such cells are present, then binding between Gluc-EGF and the EGFR occurs and we can visualize the cells by the bioluminescence emission of Gluc. In this work, the EGF-Gluc fusion protein was applied to detect three common cancers including head and neck squamous cell carcinoma (HNSCC), breast cancer, and pancreatic cancer, showing high sensitivity, specificity, and resolution.

In Chapter four, a different method that uses a bioluminescent probe to detect head and neck cancer, specifically, HNSCC CAL-27 cells was described, using the photoprotein aequorin as the reporter. The biomarker CD44 that is overexpressed on the surface of the HNSCC cells was chosen as the binding target for our bioluminescent probe. Aequorin mutant S5CF113W (AEQS5CF113W) was chemically conjugated to the anti-human CD44 antibody to construct a detection probe with specific targeting capability. The anti-CD44 antibody-AEQS5CF113W conjugate was employed in the development of the bioluminescent assay of the HNSCC cells, demonstrating the high sensitivity of aequorin as a new detection label/reporter for head and neck cancer.

Acknowledgement

First, I would like to express my sincere gratitude to my research mentor, Dr. Sylvia Daunert, who has given me great support, guidance, help, encouragement and patience during my graduate study. Her continuous support and encouragement have helped me overcome all the difficulties and obstacles I have faced during my research study.

I want to take this great opportunity to express my love and thanks to my parents, Binzhou Yu and Liping Zhang, who always support me to chase my dream. Their unconditional love is the most precious and beautiful thing in my life.

I want to express my sincere thanks to my committee members Dr. Leonidas G. Bachas, Dr. Roger M. LeBlanc and Dr. Sapna Deo, for their help, support, patience and suggestions during my graduate study. I would like to thank Dr. Emre Dikici who has taught me how to perform experiments and make high-quality figures, and read and edit my manuscripts for content as well as English. I also want to thank my laboratory member Yu-Ping Yang for his help and encouragement, and for the construction of the bioluminescent probe used in Chapter 3 of this dissertation. My thanks are also for Dr. Smita Joel and Ms. Pratibha Joshi for their help and the animal work described in Chapter 3 of this dissertation. I want to thank Dr. Jean-Marc Zingg for his help and suggestions on my research. I also would like to thank Dr. Elizabeth J. Franzmann for kindly providing the head and neck squamous cell carcinoma CAL-27 cells to support my research. I want to thank Dr. Joaquin Jimenez for kindly providing the mouse models transplanted with tumors. I want to thank all my laboratory members and friends here who are not only friends but also family to me in the USA.

TABLE OF CONTENTS

Pages

LIST OF FIGURES vi

LIST OF TABLES viii

Chapter

1 Introduction

1.1 Bioluminescence 1
1.2 The mechanism and chemistry of aequorin 6
1.3 Tuning the light emission 7
1.4 Applications 9
1.4.1 Calcium detection 9
1.4.2 Immunoassays 12
1.4.3 Hybridization and homogeneous assays 15
1.4.4 Whole-cell biosensors 17
1.4.5 BRET assays 19
1.4.6 Multiplexed assays 20
1.4.7 Molecular switches 22
1.4.8 *In vivo* detection and imaging 24
1.5 Summary and significance 26

2 Multiplexing cytokine analysis: toward reducing sample volume needs in clinical diagnostics

2.1 Overview 28
2.2 Introductory remarks 29
2.3 Experimental section 34
2.3.1 Reagents 34
2.3.2 Apparatus 36
2.3.3 Construction and expression of cytokine-aequorin fusion proteins 36
2.3.4 Half-Lives of the emission of cytokine-aequorin fusion proteins 41
2.3.5 Emission spectra of cytokine-aequorin fusion proteins 41
2.3.6 Concentration optimization of the EGF-Gluc fusion protein 42
2.3.7 Binder dilution curves for cytokine-aequorin fusion proteins 42
2.3.8 Dose-response curves for individual cytokines 43
2.3.9 Simultaneous dose-response curves for multiplexing cytokines in buffer 44
2.3.10 Simultaneous dose-response curves for multiplexing cytokines in serum 45
2.4 Results and discussion 46

2.5 Summary and significance 61

3 Detecting and imaging tumor cells in *vivo* using a bioluminescent probe

3.1 Overview 64
3.2 Introductory remarks 65
3.3 Experimental section 70
3.3.1 Reagents 70
3.3.2 Apparatus 71
3.3.3 Engineering, expression, and purification of the fusion protein EGF-Gluc 72
3.3.4 Decay kinetics of EGF-Gluc 75
3.3.5 Emission spectrum of EGF-Gluc 75
3.3.6 Concentration optimization of the EGF-Gluc fusion protein 75
3.3.7 Cell culture 76
3.3.8 Distinguishing cancer cells and normal cells using EGF-Gluc 76
3.3.9 Detecting EGFR overexpressing HNSCC CAL-27 cells using EGF-Gluc 77
3.3.10 *In vivo* bioluminescence imaging 77
3.4 Results and discussion 78
3.5 Summary and significance 88

4 Detection of the biomarker CD44 expressed on the head and neck cancer cells using an aequorin variant

4.1 Overview 89
4.2 Introductory remarks 90
4.3 Experimental section 93
4.3.1 Reagents 93
4.3.2 Apparatus 95
4.3.3 Engineering, expression, and purification of AEQS5CF113W 96
4.3.4 Chemical conjugation of the anti-human CD44 antibody and AEQS5CF113W 98
4.3.5 Decay kinetics of free and conjugated AEQS5CF113W 99
4.3.6 Emission spectra of free and conjugated AEQS5CF113W 100
4.3.7 Bioluminescent detection of CD44 overexpressed HNSCC cells 100
4.4 Results and discussion 101
4.5 Summary and significance 107

5 Conclusions and future perspectives 109

References 112

LIST OF FIGURES

Pages

Figure 1. Bioluminescent proteins 2

Figure 2. The bioluminescent reaction of aequorin 4

Figure 3. The bioluminescent reaction of the firefly luciferase catalyzed by ATP 5

Figure 4. Ribbon representation of aequorin and native coelenterazine 7

Figure 5. Native coelenterazine and its synthetic analogues 9

Figure 6. Sandwich-type immunoassay for AFP 14

Figure 7. The scheme of the DNA hybridization assay 16

Figure 8. Schematic representation of one type of molecular switch 24

Figure 9. The 3-D scheme of the multiplexed competitive assay for cytokines 34

Figure 10. The 2-D scheme of the simultaneous competitive assay for cytokines..... 48

Figure 11. Three-dimensional crystal structure of aequorin..... 49

Figure 12. The scheme of the overlap extension PCR..... 50

Figure 13. The SDS-PAGE gels of the cytokine-aequorin fusion proteins 51

Figure 14. The bioluminescence emission properties of the three fusion proteins 54

Figure 15. Individual binder dilution curves 56

Figure 16. Dose-response curves for the individual cytokines in a buffered solution 57

Figure 17. Simultaneous dose-response curves for multiplexing cytokines in buffer 59

Figure 18. Simultaneous dose-response curves for multiplexing cytokines in serum..... 60

Figure 19. The scheme of imaging tumors *in vivo* using the EGF-Gluc fusion protein.. 70

Figure 20. Crystal structures of EGF and the extracellular domain of EGFR 79

Figure 21. The scheme of the overlap extension PCR..... 80

Figure 22. SDS-PAGE of the fusion protein EGF-Gluc 80

Figure 23. Bioluminescence intensity from EGFR-overexpressed cancer cells and the corresponding negative controls 83

Figure 24. Bioluminescence emission from the EGFR-overexpressed CAL-27 cells labeled with EGF-Gluc 84

Figure 25. Image of the mouse showing a transplanted pancreatic tumor by bioluminescence 86

Figure 26. Image of the mouse with transplanted triple-negative breast tumor and metastasized (smaller) tumor labeled by the binding of EGF-Gluc 86

Figure 27. Light intensity from the triple negative breast cancer detection in mouse with the FOs during a 80-min period 87

Figure 28. Scheme of binding AEQS5F113W mutant labeled anti-CD44 antibody to the CD44 expressed HNSCC CAL-27 cells 93

Figure 29. Crystal structure of the AEQC5F113W mutant with the locations of the two mutations (Cys5 and Trp113) 102

Figure 30. SDS-PAGE of the prepared aequorin mutant AEQS5CF113W 103

Figure 31. Optimization for the conjugation temperature for the first hour 105

Figure 32. Bioluminescence intensity from the CD44 overexpressed CAL-27 cells 107

LIST OF TABLES

Pages

Table I The primer sequences for each overlap extension PCR..... 39

Table II The bioluminescence emission properties of the fusion proteins 52

Table III Comparison of serum levels of TNF-α, IL-6 and IL-8 measured by the nude mice bioluminescent assay and ELISA kits 61

Table IV The primer sequences for the overlap PCR for the construction of the EGF-Gluc fusion protein..... 73

Table V Bioluminescence maximum wavelengths and the half-lives of the fusion protein EGF-Gluc and Gluc 81

Table VI The primer sequence for the engineering of AEQS5CF113W 97

Table VII Bioluminescence emission maxima and half-lives of AEQS5CF113W..... 104

Chapter 1: Introduction

1.1 Bioluminescence

Advances in science and technology come from humans' curiosity about the law of nature. For thousands of years, bioluminescence, a naturally occurring phenomenon, has attracted plenty of attention from humans because of its beauty and magic. Before modern analytical and biological technologies were developed, bioluminescence had been a mystery to humans for a long time. People's imagination across cultures ran wild and created countless myths to explain the enigma. Meanwhile, the scientific community never gave up discovering the natural essence of this phenomenon. Only in recent years, as the progress of protein engineering techniques and molecular biology advanced, the nature of bioluminescence was brought to light, which opened a new page in the applications of this phenomenon. The interest in bioluminescence for applications in the analytical field emerged in 1962 (1), when Osamu Shimomura and his group discovered the photoprotein aequorin and the green fluorescent protein (GFP) in the jellyfish *Aequorea victoria*, and uncovered the nature surrounding the bioluminescence mystery of marine organisms, in particular, the jellyfish. Varieties of other bioluminescent proteins such as obelin (2), firefly luciferase (Fluc) (3), *Gaussia* luciferase (Gluc) (4), and *Renilla* luciferase (Rluc) (5) were discovered in their corresponding organisms (**Figure 1**) (6). Bioluminescent proteins generate light through a natural oxidation reaction, eliminating the need for an external light source for excitation, therefore, avoiding background fluorescence, and thus allowing for a higher signal-to-noise ratio when compared to fluorescence, making it suitable for ultra-sensitive detection. Taking advantage of this unique property, bioluminescent proteins have been employed in many biological detection systems such as *in vivo* imaging,

immunoassays, calcium detection, hybridization assays, and bioluminescence resonance energy transfer (BRET) assays (7, 8). In 2008, Osamu Shimomura was awarded the Nobel Prize, together with Martin Chalfie and Roger Tsien, for the discovery of GFP, honoring their invaluable contribution to discovery science as well as to the advancement of the biomedical and analytical fields through the impact that GFP had in the development of a myriad of new technologies (9).

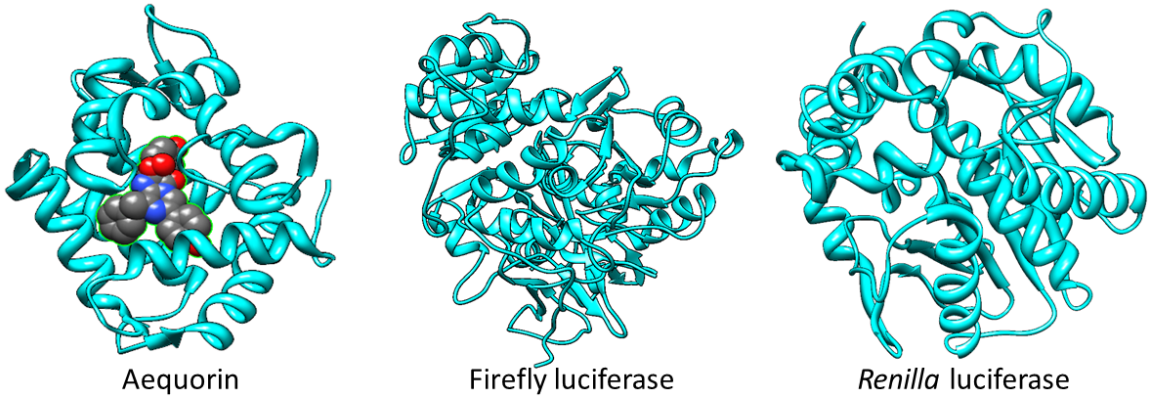

Figure 1. Bioluminescent proteins. (Aequorin PDB Code: 1EJ3, FLuc PDB Code: 1LCI, Rluc PDB Code: 2PSD).

Bioluminescent proteins are mainly classified in two broad categories, photoproteins and luciferases. The main distinction between the two are, the number of photons emitted by photoproteins is proportional to the concentration of the photoprotein itself, when there is an excess amount of the substrate. On the other hand, the light intensity emitted from luciferase catalyzed reactions is proportional to the concentration of the substrate, luciferin, when there is an excess amount of the luciferase. This difference comes from their respective mechanism of light emission. For instance, the photoprotein aequorin forms a tight complex with its substrate, coelenterazine. When calcium ions (Ca^{2+}) are present in

the protein's environment, aequorin binds Ca^{2+} in the three high-affinity Ca^{2+}-binding sites and, subsequently, the resulting conformational change oxidizes coelenterazine to an excited state coelenteramide, which upon relaxation to the ground state releases one photon during its decay to the ground state (**Figure 2**) (10). It should be noted that the number of photons emitted by aequorin is proportional to its concentration when there is an excess amount of coelenterazine. Luciferases, such as firefly luciferase, Fluc, produce the light through a different mechanism. Fluc catalyzes the oxidation of the luciferin in the presence of ATP and molecular oxygen to form oxyluciferin in the excited state. One photon is emitted through the relaxation of the excited oxyluciferin to its ground state (**Figure 3**) (11). After this reaction, however, Fluc releases the consumed oxyluciferin very rapidly and is ready to catalyze more luciferin immediately. Therefore, provided that there is an excess of luciferase present, the light intensity of the emitted bioluminescence is proportional to the concentration of luciferin.

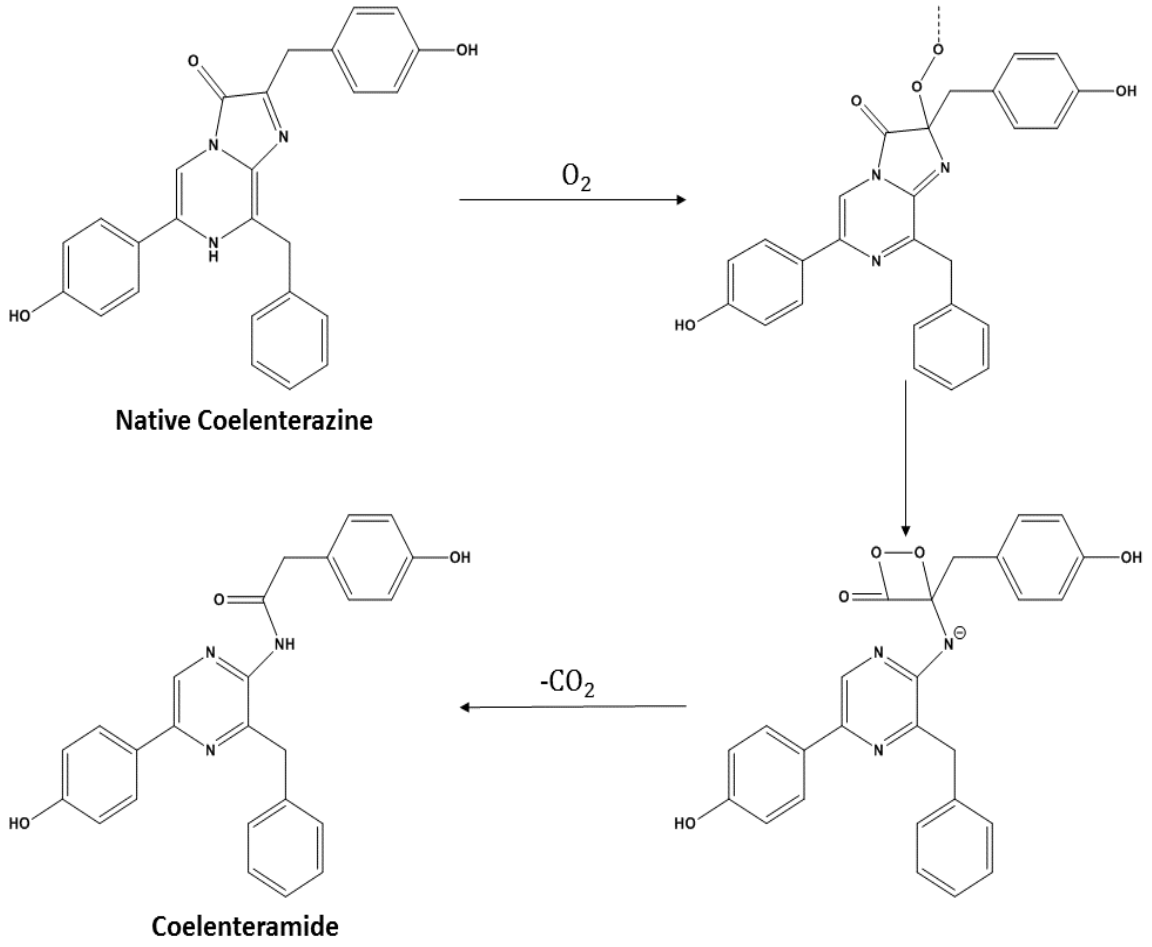

Figure 1. The bioluminescent reaction of aequorin. In the presence of Ca^{2+}, aequorin oxidizes coelenterazine to coelenteramide through its conformational change.

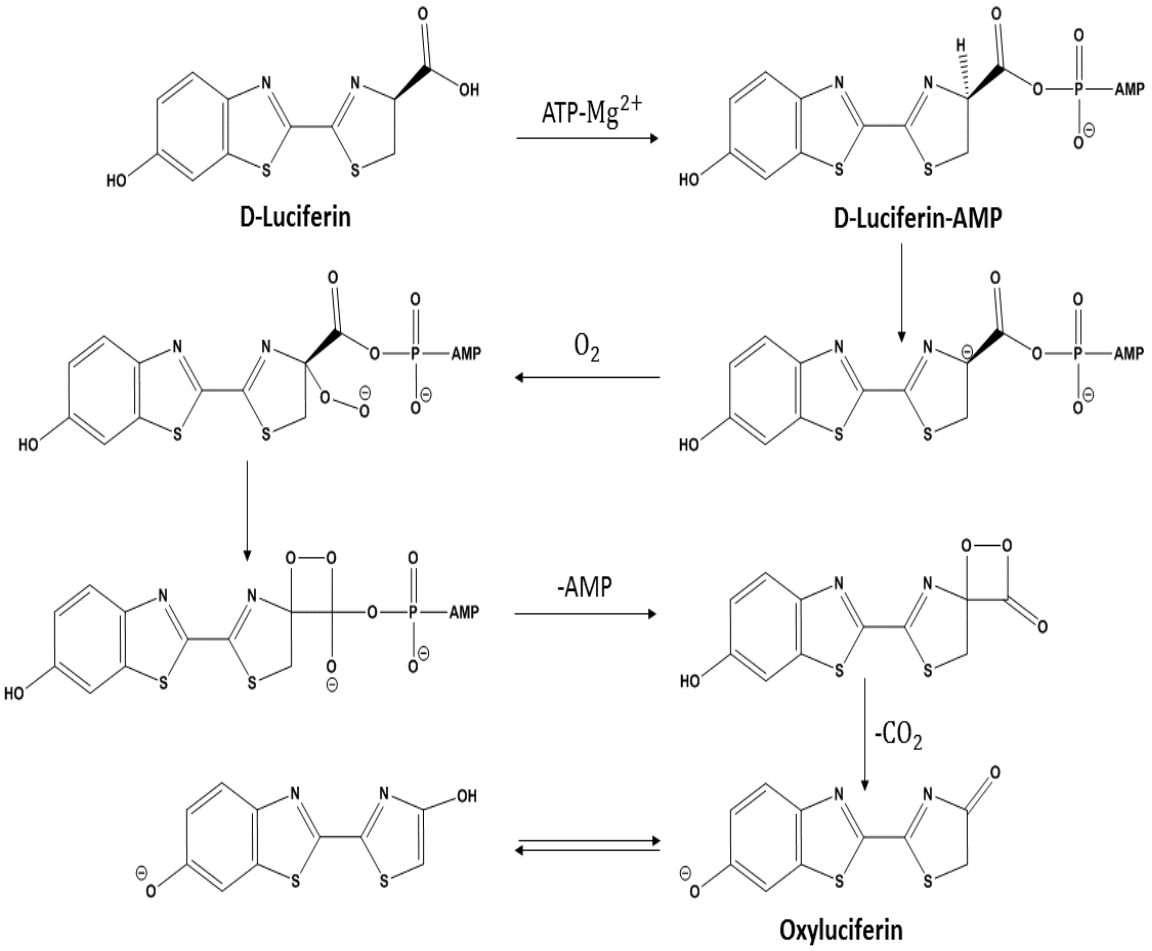

Figure 2. The bioluminescent reaction of the firefly luciferase catalyzed by ATP.

Despite all the advantages, however, unlike fluorescence-based detection, which can be performed at multiple emission wavelengths using different fluorophores or fluorescent proteins, bioluminescent proteins have similar emission characteristics. Their use in multiplexed analysis is scarce since it is hard to find luminescent proteins with sufficiently different bioluminescence emission characteristics. This drawback is due to the lack of diversity in the emission profiles as well as the broadness of their emission spectra. Fortunately, the crystal structure and the emission properties of photoprotein aequorin have been studied thoroughly, leading to the successful tuning of its emission half-life and

spectra by engineering the protein employing rational design (12). Benefiting from its tunable emission profiles, aequorin has been widely applied in calcium signaling, drug discovery, immunoassays, and *in vivo* imaging (8). Along those lines, this chapter will focus on describing the chemistry, engineering, and applications of the photoprotein aequorin.

1.2. The mechanism and chemistry of aequorin

There are several milestones in the research of photoprotein aequorin. Native aequorin was originally discovered in the jellyfish *Aequorea victoria* by Shimomura *et al.* in 1962 (1). In 1985, the DNA for aequorin was cloned into bacterial hosts and expressed for the first time by Inouye *et al.* (13). However, it was not until the start of the new millennium, in 2000 that Head *et al.* determined the crystal structure of this protein (12).

The active form of this 22 kDa protein consists of apoaequorin, chromophore coelenterazine, and molecular oxygen (**Figure 4**). The apoaequorin molecule contains 189 amino acids, which form four EF-hand domains (helix-loop-helix) and a hydrophobic pocket, sharing a similar primary structure with other Ca^{2+}-regulated photoproteins, such as obelin and clytin (14). The imidazopyridine chromophore coelenterazine is incorporated into the hydrophobic pocket non-covalently in the 2-hydroperoxidized form. Calcium ions bind to three high-affinity Ca^{2+}-binding sites on EF-hand loops (I III and IV), causing a conformational change of the protein, which leads to the oxidation of bound coelenterazine to excited state coelenteramide (10). A flash-type light at 469 nm is emitted upon the relaxation of the excited state coelenteramide to the ground state, transferring the chemical bond energy to light energy. The protein complex at the same time decomposes to apoaequorin, coelenteramide, and carbon dioxide. The role of EF-hand II is not entirely

clear because it cannot bind with Ca^{2+}. However, it is thought to help the protein to form a stable scaffold (10).

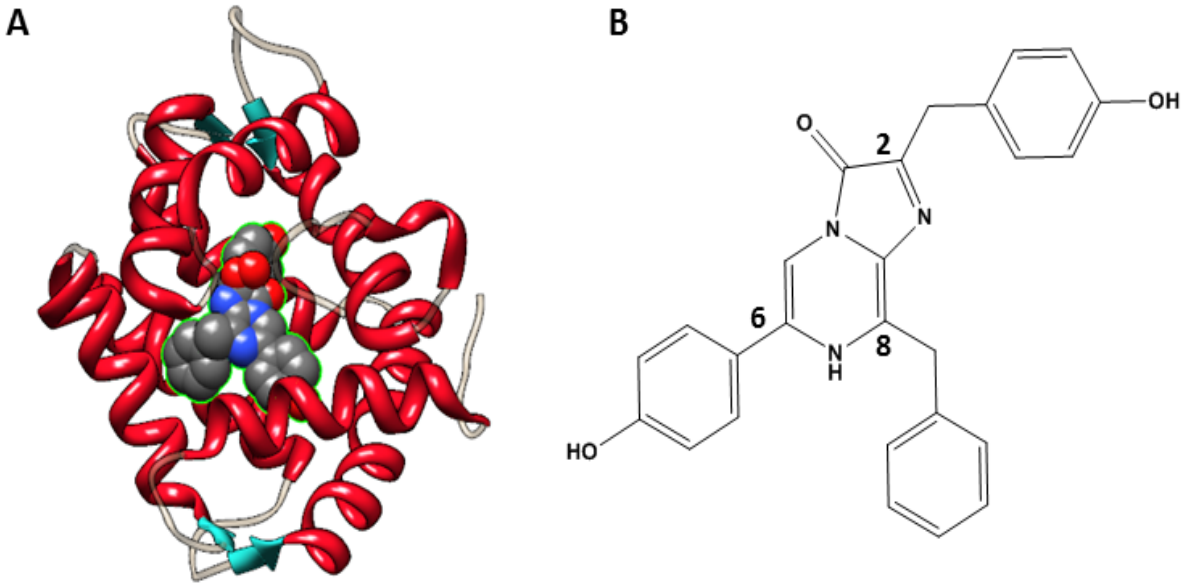

Figure 4. (A) Ribbon representation of aequorin with coelenterazine (PDB Code: 1EJ3); (B) Native coelenterazine

1.3. Tuning the light of aequorin

As mentioned above, the main drawback of bioluminescence is the lack of diversity in the emission spectra and decay kinetics, which limits the applications of bioluminescence in multiplexed detection and imaging. Since the crystal structure and the reaction mechanism of aequorin have been studied thoroughly, a lot of progress has been made to overcome this deficiency. The wavelength of the bioluminescence emission of aequorin depends on the interactions between apoaequorin and coelenterazine. Thus, the emission spectrum can be tuned by altering these interactions, including hydrogen-bonds, $\pi - \pi$ interactions, and hydrophobic interactions. Employing rational design, random and direct evolution

strategies, these alterations can be first designed and then introduced into the protein structure. Specifically, diverse aequorin photoproteins can be obtained by changing the functional groups on apoaequorin through random (15) and site-directed mutagenesis (16, 17), as well as incorporation of non-natural amino acids (18), or creation of semi-synthetic aequorin variants through the incorporation of synthetic coelenterazine analogues (**Figure 5**) (19-21). Our group was one of the pioneers in this field and created a library of aequorin mutants and semi-synthetic aequorins and their combinations with altered emission characteristics (21). For example, a combination of aequorin mutant AEQY82F and coelenterazine *i* red-shifted the emission maxima from 469 nm to 519 nm, resulting from the reduction of the H-bond interactions and the bulky group on the C2 position of coelenterazine. In contrast, aequorin mutant AEQF113W paired with coelenterazine *hcp* blue-shifted the emission maximum to 446nm, benefiting from the increasing of the $\pi - \pi$ interactions and the smaller five-members ring at the C8 position of coelenterazine. On the other hand, the half-life of the emission was prolonged to 50.09 s from less than 1 s by the combination of mutant AEQW86F and coelenterazine *i*, due to the heavy atom effect of iodine (22). The existence of the heavy atom iodine in coelenterazine *i* increases the probability that the excited electron transits to the triplet state, which is a forbidden state that, in turn, prolongs the relaxation time. The emission profiles can also be altered by incorporating, site-specially, non-natural amino acids into the apoaequorin sequence. These aequorin variants or semi-synthetic AEQs have enough separation within the spatial and temporal spaces that can enable them to simultaneous multi-analyte detection in a single well, expanding the applications of AEQ to sensitive and versatile analytical systems.

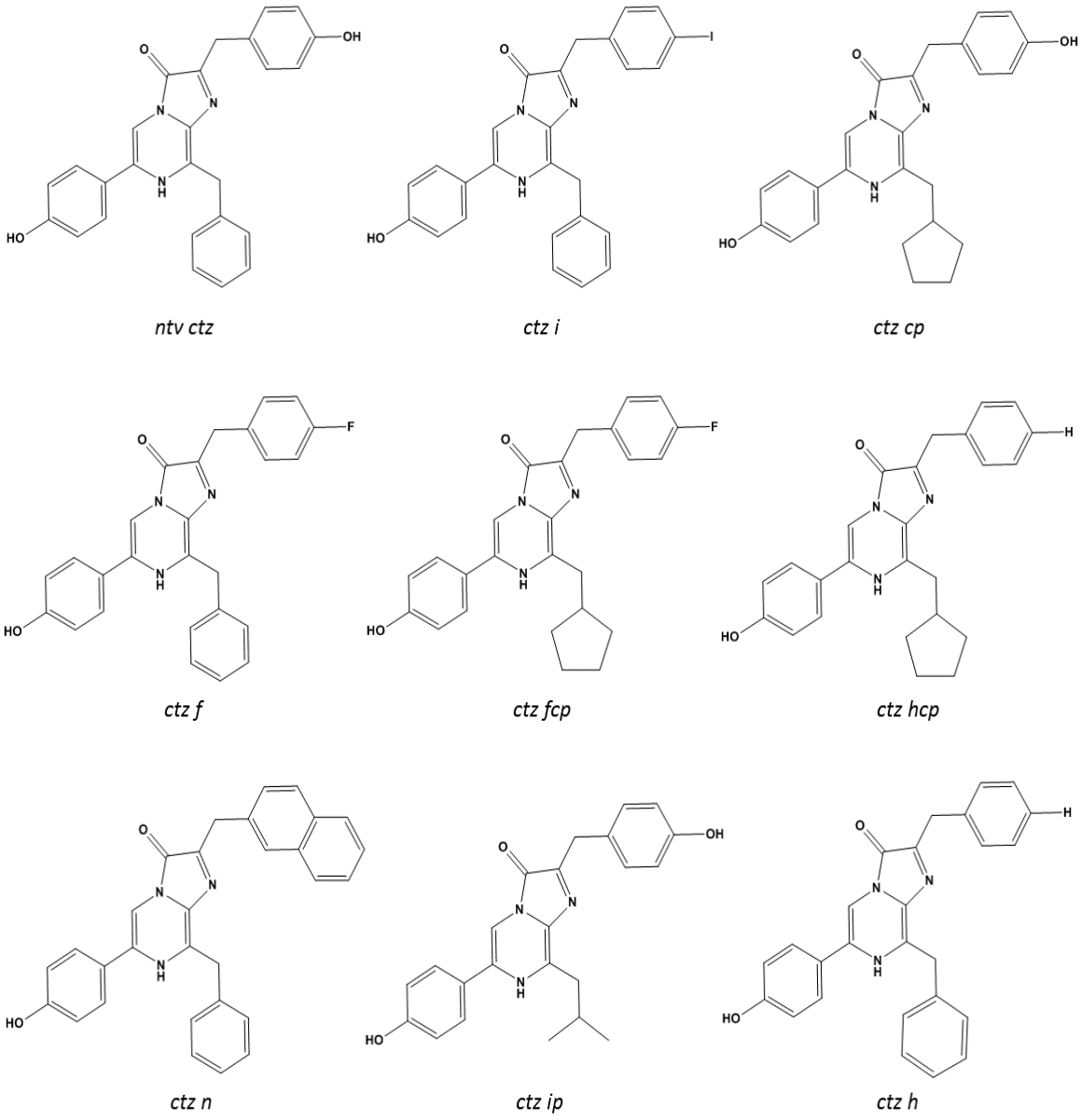

Figure 5. Native coelenterazine and its synthetic analogues.

1.4. Applications

1.4.1 Calcium detection

One of the most important applications of aequorin is the *in vivo* monitoring and imaging of intracellular calcium ions (23). Calcium ions are involved in a variety of physiological processes such as signaling, muscle contraction, bone formation and nerve impulse (24,

25). Therefore, monitoring the dynamic of intracellular calcium concentration is critical to investigate the mechanism of these processes and corresponding function of the calcium ions. Aequorin is the ideal tool for calcium detection for several reasons. First, the light intensity of aequorin is ultra-sensitive to calcium concentration, emitting over a large dynamic range spanning from attomolar to millimolar (26, 27). In addition, aequorin is non-toxic to living organisms and has been expressed in various living systems, from prokaryotic one-cell organisms to eukaryotic whole transgenic animals. Additionally, the gene of aequorin might be fused with targeting sequences to form recombinant aequorin chimeras, that can be targeted to emit light at particular cellular locations (28).

Owing to all these advantages, aequorin-based calcium probes have been widely used in plants, mammalian cells, cell compartments, and yeasts. For instance, aequorin has been applied to study calcium dynamics in mitochondria of HeLa cells (27). Three changes have been performed on aequorin in order to make it suitable to measure mitochondrial calcium. First, a binding sequence (the N-terminal peptide from the human cytochrome *c* oxidase subunit VIII) was fused to the N-terminus of aequorin, resulting in a mitochondria-binding aequorin chimera (mtAEQ). Second, mutated aequorin (AEQD119A and AEQN28L) with lower affinity to calcium was used instead of mtAEQ to measure the relatively high concentration of calcium ions in mitochondria. Third, coelenterazine *n*, which has a lower affinity with apoaequorin than native coelenterazine, was used instead of native coelenterazine. The mutated form of aequorin coupled with coelenterazine *n* has been employed to measure the concentration of calcium up to millimolar levels. Up-to-date, aequorin mutants and chimeras have been used to measure calcium in most intracellular compartments, including cytosol, nucleus, endoplasmic reticulum (ER), Golgi apparatus,

plasma membrane, and peroxisomes (28). Specifically targeting aequorin chimera was also used to study the roles of the plant Golgi apparatus in cellular calcium homeostasis (29). Zonin *et al.* also monitored calcium ion levels in plant cells successfully with a transactivator of transcription (TAT) aequorin fusion protein (30). Similarly, cytosol expressing aequorin has been used to track the calcium elevation triggered by the biotic and abiotic stimuli such as pathogens, drought, and salt in a transgenic *Arabidopsis* mutant, proving that the elevation was related to the accumulation of defense-related compounds (31).

Another application of aequorin in calcium detection is imaging the dynamics of calcium with the fusion of green fluorescent protein and aequorin (GAP). GFP and aequorin are both originally isolated from the same species of jellyfish, and in jellyfish, aequorin is the excitation source of GFP (32). This application simulates the natural function of aequorin as the excitation source of fluorescent proteins. Rodriguez-Garcia *et al.* fused GFP variant to the N-terminus of apoaequorin to form a bioluminescence resonance energy transfer (BRET) system (33). GAPs combined with specific targeting sequences were expressed in mammalian cells and transgenic mice, tracking the calcium dynamics through imaging. This chimeric protein system combines the advantages of both bioluminescence and fluorescence, such as high signal-to-noise from bioluminescence and tunable emission wavelengths and half-lives of fluorescence. This GFP-aequorin probe was expressed and used in *in vivo* calcium detection in intact plants as well (34).

The sensitivity of aequorin to calcium ions makes it valuable in drug discovery as well. G protein-coupled receptors (GPCR) are the prime targets for drug discovery as they can bind to various ligands and compounds, affecting cell signaling, and thus, trigging the

transportation of calcium ions (35, 36). Therefore, the response of cells to different drug candidates can be studied through tracking the fluctuations of calcium ions in the close vicinity to targeted GPCRs, which can be then reported by aequorin. For instance, Menon *et al.* have applied aequorin in a high-throughput screening assay for drug development (37). In their research, the Chinese hamster ovary (CHO) cells that co-expressed apoaequorin, the G-protein Gqi5, and the G-protein-coupled dopamine receptor were used to screen 8,106 compounds to check their interactions with GPCRs. Compared to fluorescent assays, aequorin-based bioluminescent assays were more cost-efficient and showed lower background signals, and therefore, lower false-positive rates (38).

1.4.2 Immunoassays

An immunoassay is a bioanalytical method that measures the concentration of a target analyte employing the specific affinity binding of antibodies to their specific antigens. In some situations, in particular for the detection of disease biomarkers in small volume physiological samples, the levels of the analytes can be very low, requiring the use of high-sensitive detection labels. Aequorin and its variants are capable of ultra-sensitive detection because of their high signal-to-noise ratios leading to low background in physiological fluids, and consequently, low detection limits. Because of these unique characteristics, aequorin and its variants have been extensively used as ultra-sensitive detection labels in immunoassays to detect analytes in competitive and sandwich immuno- and binding assays.

When employed in competitive immunoassays, aequorin needs to be linked to the analyte of interest. After labeling, the aequorin labeled analyte needs to compete with free analyte in a sample for binding to immobilized antibodies. Thus, in competitive assays, the bioluminescence signal decreases as the concentration of the analyte increases. On the

other hand, in sandwich-type immunoassays, the aequorin molecules are linked to the antibodies that bind to the immobilized analyte. Therefore, the bioluminescence intensity increases when the level of the analyte increases. Because sandwich-type assays need two different types of antibodies that recognized the different epitopes of the same analyte, competitive assays are preferred when only one such antibody is available.

Aequorin can be conjugated to analytes, and other single domain binding moieties genetically. For instance, to set-up a competitive assay for angiotensin II, Qu *et al.* fused the gene of aequorin to the C-terminus of the gene of angiotensin II, constructing a heterogeneous fusion protein (39). This fusion protein was then used to compete with free angiotensin II to generate a dose-dependent response curve with detection limits as low as 1 pg/mL. Aequorin fusion proteins have been employed in sandwich-type immunoassays as well. An example of this application is the measurement of the cancer biomarker α-Fetoprotein (AFP) (40). In this work, aequorin is fused to the C-terminus of streptavidin. The AFP-aequorin fusion proteins are then linked to biotinylated anti-AFP antibodies through a biotin-streptavidin interaction. The aequorin-antibody complex is applied to a sandwich-type assay, yielding a detection range for AFP from 0.02 to 200 ng/mL (**Figure 6**).

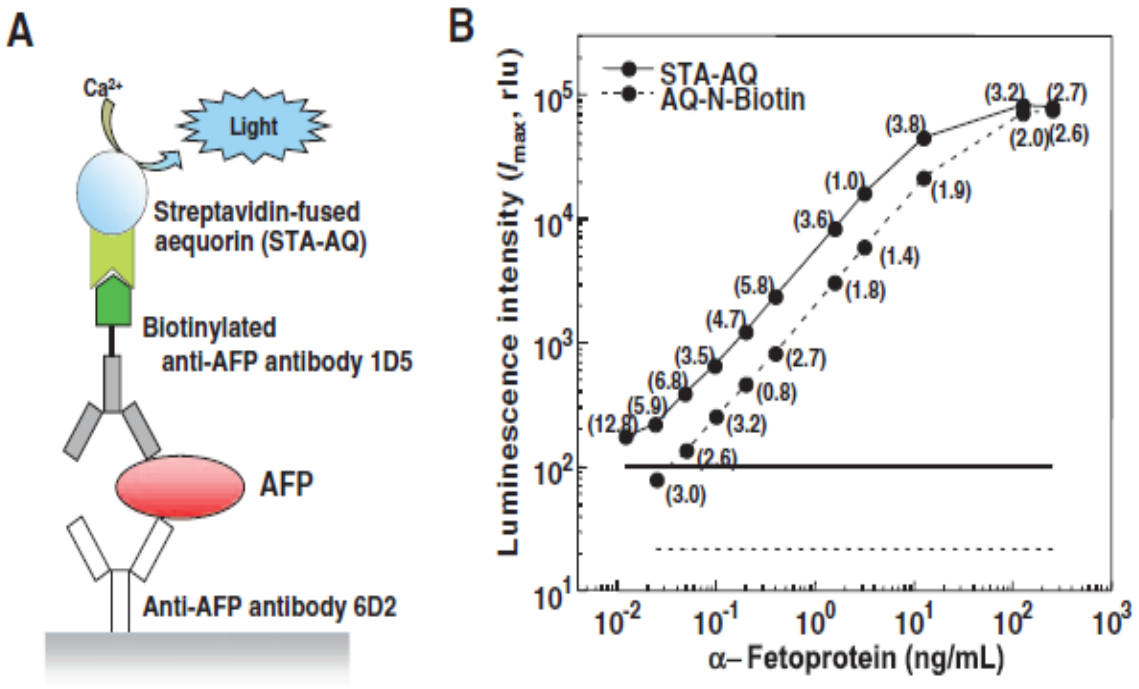

Figure 6. Sandwich-type immunoassay for AFP yielding a detection range from 0.02 to 200 ng/mL. A: The scheme of the immunoassay for AFP. B: The AFP concentration in relation to the bioluminescence intensity with STA-AQ (solid line) and streptavidin biotinylated aequorin (AQ-N-Biotin) (dashed line). The points in parentheses represent the intra-assay coefficient of variation (%CV). The horizontal solid and dashed lines equal to the blank + 3 standard deviation (SD) for assays using STA-AQ and AQN-Biotin. Reprinted with permission from (Inouye S, Sato J. Comparison of luminescent immunoassays using biotinylated proteins of aequorin, alkaline phosphatase and horseradish peroxidase as reporters. Biosci Biotechnol Biochem. 2008;72(12):3310-3. Epub 2008/12/09. PubMed PMID: 19060386.). Copyright (2008) Taylor & Francis.

On occasions, genetic modification of proteins encounters difficulties at the protein expression and folding levels. In such cases, alternative strategies such as chemical conjugation or modification can circumvent these issues. In that regard, aequorin has also been modified by chemical conjugation, once it is expressed, isolated and purified. Modification and conjugation can occur through the reactive residues on the surface of the protein, such as the amine groups of lysines or the carboxylic groups of acidic amino acids, such as glutamic acid and aspartic acid. Other residues used for crosslinking modification

are cysteines and tyrosine residues. For instance, Inouye *et al.* conjugated an aequorin mutant with a reactive cysteine residue to the maleimide-activated antibody against α-fetoprotein (AFP) that is a tumor biomarker through a heterobifunctional crosslinker sulfosuccinimidyl 4-(N-maleimidomethyl)cyclohexane-1-carboxylate (Sulfo-SMCC) (41). Sulfo-SMCC solution was mixed with anti-AFP antibody 1D5 solution, reacting with the primary amine groups in the antibody, producing maleimide-activated anti-AFP antibody 1D5. The activated antibody reacted with the thiol group of the cysteine residue in the aequorin mutant, forming the aequorin labeled antibody (aequorin-Ab1D5). Aequorin-Ab1D5 was employed to set up a sandwich-type immunoassay of AFP, obtaining a measurable range of AFP from 0.02 to 200 ng/mL.

1.4.3 Hybridization and homogeneous assays

Aequorin and its variants have been employed to develop highly sensitive hybridization and homogeneous assays. In a hybridization assay, aequorin is linked to the target oligonucleotide that binds to a complementary immobilized oligo sequence, in order to detect and quantify the amount of the target oligonucleotide. The sensitivity of these types of assays can be increased several orders of magnitude by incorporating an amplification step using the polymerase chain reaction (PCR) in which a small amount of target oligonucleotide present in the sample is amplified millions of folds, thereby expanding the scope of the hybridization assay. Christopoulos *et al.* have combined the reverse transcriptase-polymerase chain reaction (RT-PCR) and aequorin-based hybridization assays to measure prostate-specific antigen (PSA) mRNA, detecting PSA with a linear detection range from 5 attomoles to 10 femtomoles (42). Doleman *et al.* established a DNA hybridization assay for the detection of *Plasmodium falciparum* without the use of PCR

(**Figure 7**) (43). In this study, the aequorin labeled target malaria DNA competed with free target DNA to establish a competitive assay, obtaining a detection limit of 3 pg/µL, the lowest achieved for malaria detection.

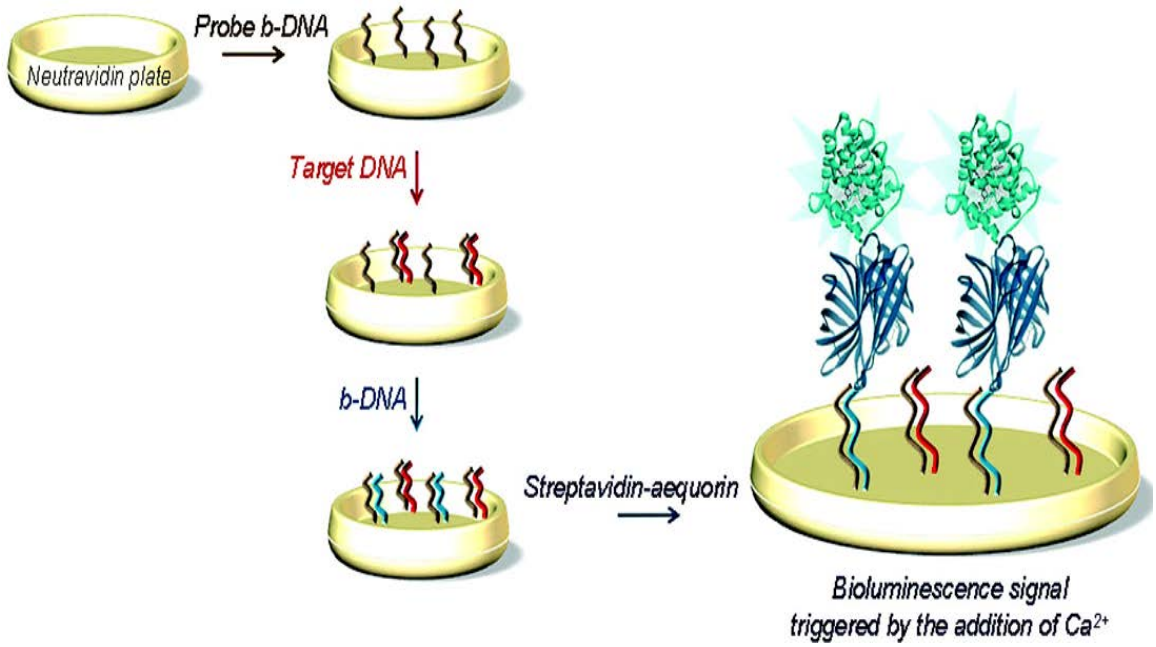

Figure 7. The scheme of the DNA hybridization assay to detect *P. falciparum* with the aequorin labeled streptavidin (b represents biotin). Reprinted with permission from (Doleman L, Davies L, Rowe L, Moschou EA, Deo S, Daunert S. Bioluminescence DNA hybridization assay for Plasmodium falciparum based on the photoprotein aequorin. Anal Chem. 2007;79(11):4149-53. Epub 2007/05/05. doi: 10.1021/ac0702847. PubMed PMID: 17477506.). Copyright (2007) American Chemical Society.

The sensitivity, high signal to background ratio, and nontoxicity of bioluminescence expanded the application of photoproteins to homogeneous assays as well. Homogeneous assays offer much simpler detection methods than heterogenous assays. In a homogeneous assay, the binding of the analyte to the receptor leads to a measurable signal change directly, eliminating the need for phase separation, incubation, and washing steps, thus, decreasing the assay time significantly. Rowe *et al.* developed a fast and sensitive aequorin-based

homogeneous assay for detecting cortisol in saliva samples (44). In this assay, aequorin was conjugated to a cortisol derivative chemically, and the conjugate competed with free cortisol molecules to bind with cortisol antibodies. The assay results showed a decreased bioluminescence output with increasing free cortisol concentration. With this assay, Rowe and colleagues could detect free cortisol as low as 1 x 10^{-10} M in saliva.

1.4.4 Whole-cell biosensors

Immunoassays and hybridization assays detect the concentrations and monitor the presence of certain analytes, but they are not capable of reporting on the bioavailability and synergistic effects of toxins on living systems directly. In contrast, whole-cell sensors provide a rapid and sensitive way to monitor the bioavailability and toxic effects of organic and heavy metal pollutants, pathogens, and other bioreagents (45). One disadvantage of whole-cell sensors is the difficulty in maintaining the stability of the assay during transportation and storage. Several methods have been developed to overcome this limitation including sporulation (46) and immobilization of cells in biocompatible platforms such as paper strips, sol-gel, and biochips (47). These methods increase the shelf-life of whole-cell sensors and simplify the transportation and storage procedures, expanding the applications of whole-cell sensors.

Aequorin has been utilized in whole-cell sensors to monitor the effects of toxins and levels of calcium ions through the change of bioluminescence intensity by taking advantage of its biocompatibility in various living systems. Aequorin-based whole-cell sensors depend on two principles; the interaction between target analytes and the whole-cell sensors affect the intracellular calcium ion levels; and the presence of particular analytes

that bind to transcriptional regulator promoters and genes that are linked to the photoprotein and affect its transcription.

For instance, Araki *et al.* developed a cell-based assay to detect thyroid-stimulating antibodies (TSAb) that are responsible for hyperthyroidism in Graves' disease (GD) (48). The crosslinking of the TSAb with the corresponding receptors increase the intracellular cyclic adenosine monophosphate (cAMP) levels, which activate the cAMP-gated calcium channel, leading to influx of calcium ions. The elevated levels of calcium ions can be measured by the intracellularly expressed aequorin. This cell-based assay obtained positive results in 98.9% of the GD patient samples in 4 h, demonstrating that it is more sensitive and faster than conventional methods. Also, a whole-cell assay based on recombinant aequorin transfected *Aspergillus awamori* was developed to study short-term toxicity induced by the toxins, including Cr^{6+} , Zn^{2+}, and 3,5-DCP (49). The particular toxin creates a stimulus at different concentrations, causing a unique effect on the cytosolic calcium concentration, which was monitored by intracellular recombinant aequorin. Additionally, a whole-cell sensor for pathogens was established based on transient changes in calcium ion levels caused by the interactions of pathogens and membrane-bound antibodies (50). On the other hand, there is a whole-cell sensor for toluene and related compounds based on the regulation of the transcription of cytosolic aequorin (51). Toluene-like compounds can bind to xylR protein, activating the transcription of the lower pathway promoter that is in charge of the expression of aequorin, thus, promoting the expression of cytosolic aequorin. Therefore, the presence of toluene-like pollutants can be monitored by the whole-cell sensor through the bioluminescence emission.

1.4.5 BRET assays

Bioluminescence resonance energy transfer (BRET) is a special type of resonance energy transfer methods, in which the energy donor is a bioluminescent protein and the energy receptor is a fluorescent protein or fluorophore. When the donor and the receptor are in close proximity to each other (usually closer than 10 nm) and the emission profile of the bioluminescent protein overlaps the excitation profile of the fluorescent acceptor, the energy emitted by the bioluminescent reaction can be transferred to the fluorescent protein efficiently, thereby exciting the fluorescent acceptor. The other two resonance energy transfer-based methods are Forster resonance energy transfer (FRET) and homogeneous time resolved fluorescence (HTRF). BRET has the benefit that it can be employed in cells that suffer from high autofluorescence and sensitivity to excitation sources because it does not need an external light source for excitation. In addition, various BRET systems have been expressed *in situ* in various living organisms, eliminating the laborious expression and purification procedure. Given that the donor and acceptor in a BRET system need to be physically close to each other, BRET has been employed in various systems to study close interactions between analytes, including protein-protein interactions (PPI), receptor activation, and protein conformational changes (52-54). Furthermore, BRET shifts the emission spectrum and prolongs the emission half-life of the original donor molecule. Aequorin and GFP form a natural BRET system in the jellyfish *Aequorea victoria* (55). As noted above, in 2008, Shimomura, Chalfie, and Tsien were awarded the Nobel Prize in Chemistry for the discovery of GFP and the corresponding BRET system, which highlights the importance of this discovery (9). Aequorin-based BRET systems have been used in bioanalytical and bioimaging sensors. For instance, a GFP-aequorin chimeric protein (G5A)

was expressed in intact plants to monitor weak calcium activities, in particular in the highly autofluorescent plant tissues (34). In this work, the gene of G5A was cloned into the pGWB502Ω plasmid, and transfected into *Agrobacterium tumefaciens* to image calcium activity in response to various stimuli. The G5A BRET system emitted five times more light than aequorin itself, suggesting that this system can be used as an ultra-sensitive sensor for plants in cases when there is weak calcium secretion and activity. Aequorin has also been conjugated with other fluorescent proteins beyond GFP to construct various BRET systems. Bakayan *et al.* fused a variety of orange and red fluorescent proteins to aequorin to construct red fluorescent protein-aequorin fusion proteins for calcium monitoring in living organisms given that red light is better in penetrating the tissues due to its less propensity for scattering (56). Among all the fusion proteins, the tandem-dimer Tomato-aequorin (tdTA) showed highest BRET efficiency and faster fluorescent maturation. In this research, tdTA was bright and sensitive enough to monitor the calcium level changes not only in single cells, but also in whole mice.

1.4.6 Multiplexed assays

Accurate clinical diagnosis usually requires detection of multiple biomarkers, considering the complexity of most diseases. In addition, to reduce the pain and financial burden for patients, especially for pediatric and elderly patients, novel techniques that are highly sensitive and capable of multiplexed detection are urgently needed. Further, efforts towards the miniaturization of detection systems also highlight the requirement for more sensitive and versatile labels. State-of-the-art multiplexed detection methods include microarray assays and bead array assays that are based on either fluorescence or absorbance detection. Compared to them, bioluminescence has the potential to generate better detection

technologies by taking advantage of its sensitivity and their ultra-low background in physiological samples. One drawback of bioluminescence that limits its application in multiplexed detection is the lack of versatility of their bioluminescence emission profiles. Efforts by a number of researchers have been devoted to solve this problem. Recent progress in this area includes using two different naturally available photoproteins to achieve resolved signals, genetically engineered bioluminescent proteins exhibiting tuned emission profiles (15, 17, 57), incorporation of non-natural amino acids (18), and semi-synthetic aequorin with differentiated spatial and temporal resolution strategies (19-21). Based on all these efforts, simultaneous detection of two analytes were available due to the availability of spectrally distinct or time-resolved mutants.

As described in Chapter 2, semi-synthetic aequorin mutants can have altered emission spectra and decay kinetics, therefore, expanding the application of aequorin in multiplexed assays. For instance, semi-synthetic aequorin mutants have been used to detect two important cardiovascular molecules 6-keto-prostaglandin-FI-α and angiotensin II in a single well simultaneously (57). In this research, 6-keto-prostaglandin-FI-α was linked to aequorin chemically through the use of a N-hydroxy succinimide (NHS) linker, while angiotensin II was fused to aequorin genetically. 6-keto-prostaglandin-FI-α-aequorin was combined with the native coelenterazine (*ntv ctz*) to form a semi-synthetic aequorin construct with a half-life of 0.5 s. In contrast, angiotensin II-aequorin was combined with the coelenterazine *i* (*ctz i*), yielding a construct with a half-life of 11 s. Thus, the bioluminescence signals emitted by these two conjugates were differentiated through time resolution with two time intervals 0-6 s and 6.01-25 s.

1.4.7 Molecular switches

Another kind of protein engineering technique used in bioanalytical detection assays is protein splicing, which separates the reporter protein into two separate components, leading to a loss of the bioluminescence activity. The bioluminescence activity can be regained through the reassembly of the split fragments. The splicing and reassembly of the protein construct an on-off switch of the light emission, which can be controlled by the conformational changes induced by the analyte binding. The switch can be built in two ways: (1) insertion of a recognition sequence of the target analyte into the bioluminescent protein and (2) fusion of a binding sequence to the separate components of the protein. Thus, the binding of the analyte to its recognition sequence changes the distance and the orientation of the split fragments, altering the emission intensity. Therefore, incorporating the on-off property of the switch with the specific analyte binding, one can develop a sensitive detection assay of the analyte. The molecular switches developed have been used to investigate protein-protein interactions (PPI), cell signaling, and *in vivo* imaging as well.

As previously mentioned, aequorin has 189 amino acid residues and four EF-hand sequences in its structure (See Figure 4). Researchers have found that there is a flexible loop between the first and the second EF-hand that can be modified without disrupting the tertiary structure of the protein (58). Thus, the recognition sequence of the target analyte can be inserted into this flexible loop (amino acid residues 46-51) to develop a molecule on-off switch in response to the binding of the analyte. For instance, this principle of construction has been applied for the detection of the cyclic AMP. Scott *et al.* have inserted the cyclic AMP receptor protein (CRP) between the forty-seventh and the forty-eighth amino acids (59). Without the presence of the cyclic AMP, aequorin-CRP fusion protein

folds normally and shows strong bioluminescence emission. As the concentration of the cyclic AMP increases, it can bind to the CRP, separating the two fragments of aequorin, interrupting the tertiary structure of the fusion protein, thus, decreasing the bioluminescence emission. In this application, the switch is turned off by the presence of the analyte. On the other hand, in another application an aequorin-based molecular switch was used in the detection of glucose (58). The glucose binding protein (GBP) was inserted between the forty-seventh and the forty-eighth amino acids of aequorin as well. In this case, the insertion of GBP disrupts the folding of the fusion protein, separating the two fragments of aequorin too far apart from each other, preventing the bioluminescence emission. When glucose binds to the GBP, the fusion protein undergoes a conformational change, bringing two components of the aequorin close enough to each other to trigger the bioluminescence process and emission of light. This molecular switch detects glucose by turning the switch on through binding of the fusion protein with the glucose molecule. A schematic representation of this type of molecular switch is displayed in **Figure 8** (8).

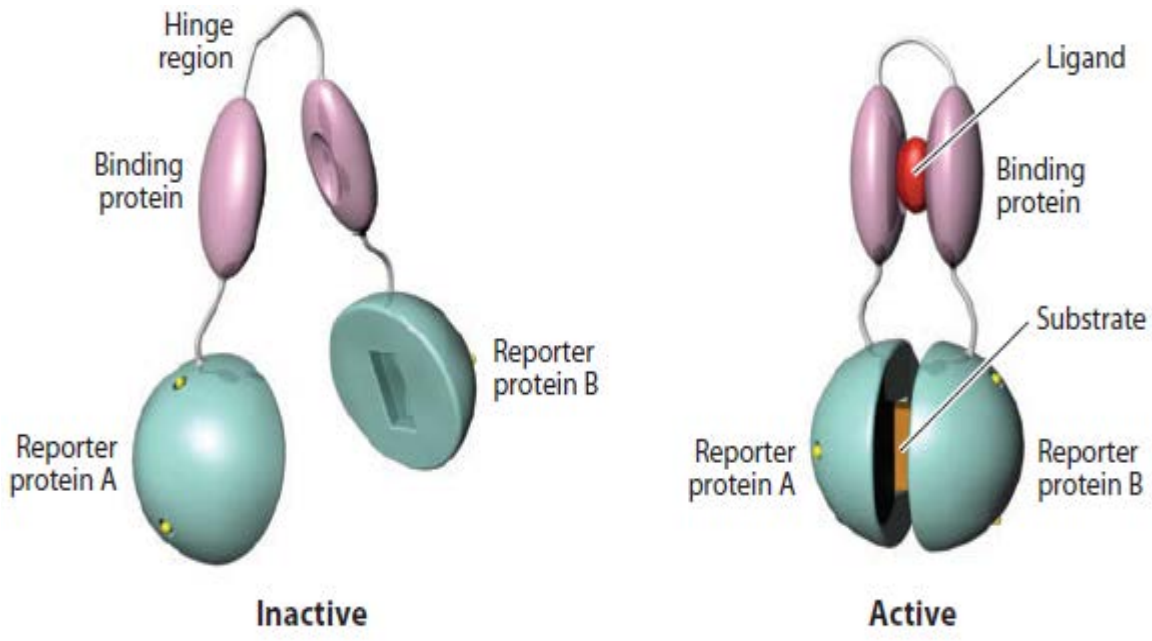

Figure 8. Schematic representation of one type of molecular switch. The presence of the analyte turned on the switch. When the analyte binds to the binding protein, the conformational change of the binding protein can bring the two fragments of the bioluminescent protein together to resume the light emission. Reprinted with permission from (Scott D, Dikici E, Ensor M, Daunert S. Bioluminescence and its impact on bioanalysis. Annu Rev Anal Chem (Palo Alto Calif). 2011;4:297-319. doi: 10.1146/annurev-anchem-061010-113855. PubMed PMID: 21456969.). Copyright (2011) Annual Reviews.

1.4.8 *In vivo* detection and imaging

In vivo detection and imaging provide a convenient method to study and monitor molecular events, pathways, and metabolic processes in living systems. This application demands more from the detection labels because it is employed in a complex environment, especially when used in deep tissue imaging. The key factors of the detection probes required to achieve high-resolution imaging include penetration depth in tissues, quantum yield, background, biosafety, and the capability of loading (60). Compared to other commonly used probes such as fluorescent dyes and radiolabels, bioluminescent labels such as aequorin have the similar advantages that was explained previously. These advantages

include no autofluorescence, ultra-low background, high biocompatibility, and the availability of local expression (eliminating the need for the laborious extraneous injection process). However, the emission maxima of aequorin is in the blue region of the visible portion of the electromagnetic spectrum (469 nm), and, therefore, it is a relatively high energy emission with short wavelengths, which is very susceptible to scattering. This causes the blue-light emission to have a high adsorption rate in tissues and low photon yield (one photon each reaction). Therefore, the low photon yield when compounded with the low penetration rate of bioluminescence emission, it limits its application for *in vivo* imaging. Research has proven that light with longer wavelengths, such as red light, can penetrate biological tissues more efficiently because of lower scattering and higher absorption rate (61). Thus, red-shifting the bioluminescence emission of aequorin is a key point to improve its application in *in vivo* imaging.

The BRET system, as shown above, can red-shift the bioluminescence emission, as well as increase the photon yield, and Bakayan *et al.* fused red fluorescent protein tdTA to aequorin to form a BRET system emitting red light. They also optimized the configuration of the linker in tdTA to achieve a BRET system with maximum energy transfer rate, named Redquorin, shifting the emission wavelength above 575 nm (62). Moreover, these investigators successfully imaged calcium ion oscillations and transients in single HEK-293 cells and zebrafish embryos using the Redquorin. Aequorin variants with red-shifted emission spectra have the potential to be used as imaging reporters by themselves, without need for BRET. To that end, Grinstead *et al.* incorporated the non-natural amino acid L-4-methoxyphenylalanine into positions 82 and 86 of the aequorin protein (18). This variant, when paired with coelenterazine *i,* the emission maxima had a 56 nm red-shift to 526 nm,

making it suitable for *in vivo* applications. This variant was injected into the eyes of mice, followed by the topical addition of coelenterazine *i*, and then the emission was detected by an *in vivo* imaging system (IVIS).

1.5. Summary and significance

Bioluminescent proteins comprising of photoproteins and luciferases can generate light emission through a chemical reaction, eliminating the need for an external light source, therefore, reducing background fluorescence, and making them suitable as ultra-sensitive detection indicators. Among of them, the photoprotein aequorin, a naturally occurring photoprotein from the jellyfish *Aequorea victoria* has been engineered to produce various mutants, variants, chimeras, and fusion proteins that expand its applications in the biomedical and bioanalytical fields. Taking advantage of advanced protein engineering technologies and the sensitivity of luminescent detectors, aequorin and its variants have been widely employed in many biological detection systems such as immunoassays, calcium detection, hybridization assays, BRET assays, molecular switch assays, and *in vivo* imaging. The inherent low background, nontoxicity, and the availability of local expression associated with these photoproteins have allowed for their use in tracking activities inside the cells such as PPI, as well as in drug discovery.

Despite to all the benefits that employing aequorin has, its bioluminescence emission still has some drawbacks that need improvement, such as low quantum yield, high tissue absorption, and limited spectral diversities, which limit the applications of aequorin in multiplexed detection in small volumes of samples and in *in vivo* detection. Therefore, in the future, further modifications need to be performed on aequorin and its variants in order to increase their photon yields and alter their emission properties, which are essential for

establishing easy-to-use, sensitive, and accurate miniaturized diagnostic methods that can operate on platforms such as lab-on-a-chip or lab-on-a-CD, as well as in high-throughput systems. Finally, creation of new aequorin variants with tuned emission properties should allow for expanding the applications of this photoprotein in ultra-sensitive bioanalysis and diagnostics.

Chapter 2: Multiplexing cytokine analysis: toward reducing sample volume needs in clinical diagnostics

2.1 Overview

The trend for improved more precise diagnostics and management of disease relies on the measurement of panels of biomarkers in physiological samples of patients. The need for large volumes of blood to perform the assays for the biomarkers has resulted in a renewed interest in miniaturization of diagnostic and detection systems, which in turn has highlighted the need for the design of versatile yet sensitive reporters/labels for use in these systems. Ideally, the goal is to detect as many clinically relevant biomarkers as possible in a single drop of blood, achieving quick, sensitive, reproducible, and affordable detection in small volume physiological samples, reducing the physical suffering of patients when blood is drawn too frequently. Bioluminescent proteins generate emission through a natural oxidation chemical reaction, eliminating the need for an external light source, therefore, eliminating background fluorescence, and has, therefore, higher signal-to-noise ratio when compared to fluorescence, making it suitable for ultra-sensitive detection. However, to date, one defect limits the application of bioluminescence in multiplexed detection is the lack of versatilities of their emission profiles and decay kinetics. Herein, we have demonstrated that by combining both temporal and spatial resolution strategies, the multiplexing capabilities of the photoprotein aequorin (AEQ) can be expanded. Recent efforts in solving this issue only expanded the application of bioluminescence to the simultaneous detection of two analytes. Thus, in this study, we designed a multiplexed assay to measure three analytes simultaneously in a single solution by employing the variants of the photoprotein aequorin (AEQ). Aequorin, natively found in jellyfish *Aequorea victoria*, can emit a flash-

type light at 469 nm with a half-life around 0.5-1 s after the binding of calcium ions. In our lab, the emission profiles, decay kinetics and thermostability of AEQ have been tuned significantly from the native AEQ through site-specific mutations and use of synthetic coelenterazine analogues, expanding the applications of AEQ in versatile and miniaturized analytical systems. In this study, the AEQ mutant AEQY82F and AEQF113W have been genetically conjugated to three main pro-inflammatory cytokines, namely interleukins 6, 8 and tumor necrosis factor alpha (IL-6, IL-8, TNF-α), resulting in cytokines labeled with AEQ mutants. The three fusion proteins in conjunction with different synthetic coelenterazine analogues were employed as bioluminescent labels for the detection of all three cytokines simultaneously through the combinations of different spatial and temporal windows. The validity of the assay was demonstrated in serum by employing human pooled serum spiked samples and comparing our results with commercially available individual tests for each of the three cytokines.

2.2 Introductory remarks

The fully understanding of disease biomarkers is the crucial point for the precise and fast diagnosis of many diseases (63). The boom of translational science has undoubtedly helped in the identification of new biomarkers that are proving to be key in the more precise diagnosis and monitoring of disease. While biomarker identification has soared, and contributed to the field of precise medicine, analytical detection technologies for the newly discovered biomarkers still rely on traditional techniques. The most common technique for detection of biological markers is the enzyme-linked immunosorbent assay (ELISA), which is designed for the analysis of only one analyte per sample, and, typically, uses quite large volume of samples for accurate diagnosis. Detection of multiple biomarkers or panels

of biomarkers is a trend that has proved to be effective in precise medicine for diagnosis and management of disease. Often, the biomarkers are used to assess the effectiveness of treatment, and, therefore, their analysis needs to be performed often, requiring for drawing samples from patients on daily, weekly or monthly regimes. While the value of obtaining the information needed for precise management of disease outweighs any other drawbacks, there are some important parameters affecting patient's overall health and comfort, as well as financial burdens that need to be considered. If the panel of biomarkers needs to be detected in blood, then, this undoubtedly increases the physical burden in patients, especially for pediatric, elderly and chronically ill patients. Thus, there is a need for a better solution for monitoring these patients. A potential solution to this problem will involve the implementation of highly sensitive assays that can perform rapid and reliable detection in small volumes of physiological samples. The development of such assays come with a series of non-trivial requirements, that include detection of low levels of a target biomarker/analyte selectively in the presence of other components in a complex physiological sample, versatility to be incorporated into miniaturized analytical platforms, reproducibility, accuracy and precision of the analysis.

State-of-the-art multiplexed detection methods include microarray assays (64, 65) and bead array assays (66, 67). For protein microarray assays, the immobilized capture reagents specific for distinct analytes are arrayed at fixed positons on a solid surface. Quantitative signals are read through each microspot to realize simultaneous detection of multiple analytes. Unlike microarray assays, the bead array assays are based on pre-coated and internally dyed spherical beads instead of planar surface. Each bead population coated with

distinct binding reagents are identified by its specific fluorescent spectrum. The intensity of a second signal from the reporting label is measured as the quantitative identifier.

All of these commercially available assays are either based on fluorescence or absorbance. While very valuable newly discovered biomarkers are present in physiological fluids at very low concentrations, and neither absorbance nor fluorescence-based assays can reach such low detection limits. Luminescent proteins, including luciferases, when employed as label in assays encompass many distinct advantages over absorbance or fluorescent reporters. For instance, bioluminescence is a biochemically-driven reaction that eliminates the need for an external light source therefore eliminating background fluorescence, making it suitable for ultra-sensitive detection. In addition, bioluminescent proteins are highly biocompatible, having been expressed in a variety of biological systems (68). Benefiting from these properties, bioluminescent proteins have established themselves as vital components of the biosensing toolbox for an assortment of applications including *in vivo* imaging, immunoassays, whole cell sensors, drug discovery, and the study of protein-protein interactions (PPI) (8, 69-75). Despite all the advantages, bioluminescent proteins lack the capability of the multiplexed detection however, compared to fluorescent labels, which can perform multiple emission wavelengths. This is due to the lack of diversity in the emission profiles, as well as the broadness of their emission spectra. Recent efforts in solving this issue include shifting the bioluminescence-emission properties of these proteins by genetic mutation (76), incorporating non-natural amino acids into their structure (18), or using two proteins with different emission profiles to discriminate signals from different analytes (77). However, all the progress was still limited to detection of only two analytes. In this study, we designed a multiplexed assay to

measure three biomarkers of inflammation simultaneously in a single sample solution employing for the first time a combination of space and time resolution strategies in bioluminescence detection with the goal of, expanding the application of bioluminescent proteins in multiplexed analysis. Specifically, in this research, the photoprotein aequorin (AEQ) and its variants have been engineered and incorporated with different coelenterazine analogues to obtain shifted spectra and decay kinetics, and then have been employed in detection of three clinically common biomarkers simultaneously in a single well, through the combinations of the spatial and temporal differences.

The photoprotein aequorin (AEQ), is natively found in the jellyfish *Aequorea Victoria* (78). The active form of this 22 kDa protein is generated upon binding with the chromophore coelenterazine and molecular oxygen (79). When calcium is present in the protein's environment, aequorin binds calcium ions in the three high affinity binding sites and, subsequently, coelenterazine binds to the active site of aequorin and is oxidized to an excited state coelenteramide, which goes down to the ground state, which concomitant release of one photon during its decay to the ground state (10, 12). The protein complex at the same time decomposes to apoaequorin, coelenteramide, and carbon dioxide. In our lab, the emission profiles, decay kinetics, and thermostability of AEQ have been tuned significantly from the native AEQ through site-specific mutations and use of synthetic coelenterazine analogues (7, 21, 80). These different aequorin variants or semi-synthetic AEQs have spatial and temporal space features that can make them amenable to simultaneous multi-analyte detection in a single well, expanding the applications of AEQ in not only sensitive, but also versatile and miniaturized analytical systems. Herein, we propose to develop a multiplexed assay for three main pro-inflammatory cytokines, namely

tumor necrosis factor alpha, interleukin 6 and interleukin 8, (TNF- α, IL-6, IL-8) to prove the detection capabilities of the semi-synthetic AEQs (**Figure 9**). These cytokines play an important role in a variety of biological processes, including inflammation, disease pathogenies, cancer progression and response to inflammation, can serve as biomarkers for the diagnosis and monitoring/management of a variety of diseases with inflammatory components, including, among others, rheumatoid arthritis, Crohn's disease, ulcerative colitis, cardiovascular diseases, diabetes, cancer, lupus, and hyperalgesia (81-83). These cytokines are routinely analyzed when diagnosing and monitoring the health of patients suffering from these chronic or long-term diseases. Given that and the fact that, as stated earlier, small volume detection is highly desirable in the health management of patients with long-term illnesses, the development of a rapid, sensitive, and multiplexed assay for the detection of biomarkers such as cytokines, is an example of how clinical diagnostics and management of disease in precision medicine can be improved.

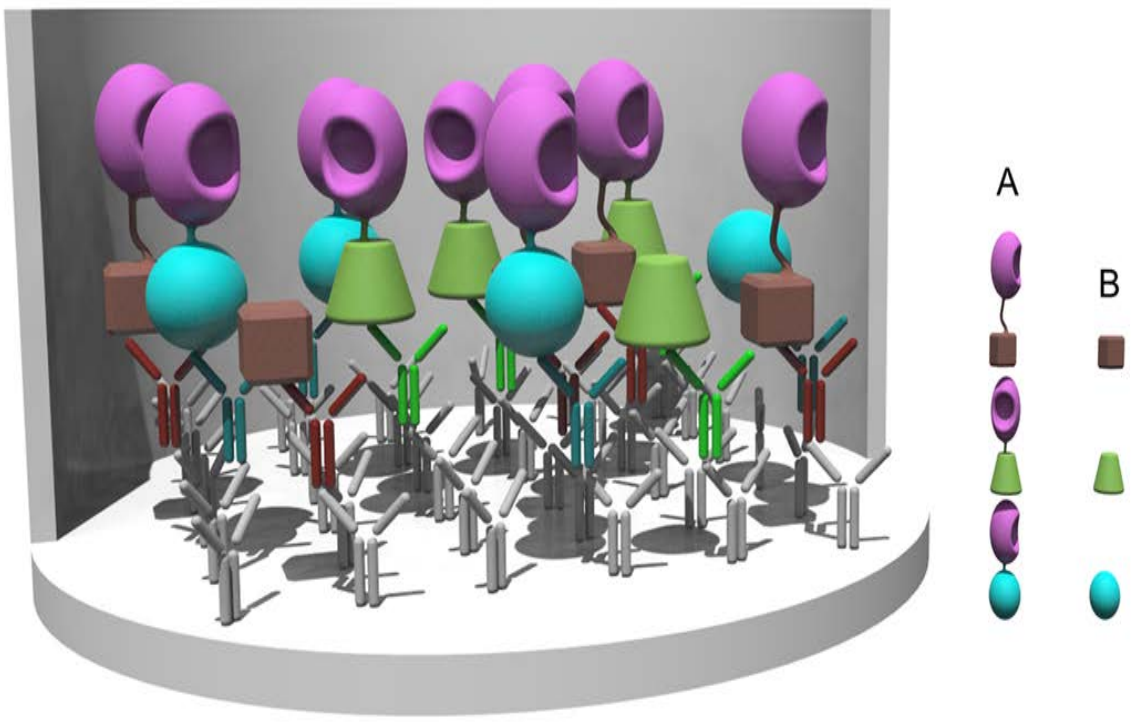

Figure 9. The 3-D scheme of the multiplexed competitive assay for TNF-α, IL-6 and IL-8. The grey Y-shaped structures located at the bottom of the plate represent the goat anti-mouse IgG antibodies coated on the 96-well plates. The red, green, and cyan Y-shaped structures captured on the plates represent the mouse anti-human TNF-α, IL-6, and IL-8 antibodies respectively. The structures captured by the antibodies represent the free cytokines and aequorin-cytokine fusion proteins. The structures in the column A represent the cytokine-aequorin fusion proteins. The structures in the column B represent the free cytokines. TNF-α is the brown cube, and IL-6 is the green cone represents, while IL-8 is the blue sphere. In the assay, the fusion proteins and the free cytokines compete to bind to the captured antibodies bound on the plate.

2.3 Experimental section

2.3.1 Reagents

Disodium ethylenediaminetetraacetate (EDTA) was purchased from Fisher Scientific (Fair Lawn, NJ). Luria-Bertani (LB) Agar was purchased from EMD Millipore (Darmstadt, Germany). LB Broth, pET-30 Xa/LIC Vector kit, KOD Hot Start DNA Polymerase, and Factor Xa Kits were purchased from Novagen (Darmstadt, Germany). LB Lennox was

purchased from Alfa Aesar (WardHill, MA). Sodium dodecyl sulfate (SDS) was purchased from J. T. Baker (Center Valley, PA). Plasmid mini-prep kits, gel extraction kits and Ni-NTA agarose were purchased from Qiagen (Valencia, CA). *Eco*RI, *Hind*III, *Nde*I, and *Bam*HI, restriction enzymes were purchased from New England BioLabs (Ipswich, MA). Sodium phosphate, imidazole, calcium chloride, reduced and, oxidized glutathione and all the oligonucleotides were purchased from Sigma Aldrich (St. Louis, MO). Tween-20 was purchased from VWR (Radnor, PA). Isopropyl-beta-D-thiogalactoside (IPTG) was purchased from Gold Biotechnology (St. Louis, MO). Tris(hydroxymethyl)amino methane (Tris) free base, sodium chloride, glycerol and Urea were purchased from BDH Chemicals (distributed by VWR, West Chester, PA). Precision plus protein dual color standards were obtained from BIO-RAD (Hercules, CA). Bench top 1Kb DNA ladder was purchased from Promega (Madison, WI). Coelenterazine sampler kit was ordered from Biotium (Hayward, CA). The cDNA clones of human TNF-α was purchased from GeneCopoeia (Rockville, MD). The cDNA clones of human IL-6, and IL-8 were purchased from ATCC (Manassas, VA). Kanamycin sulfate and potassium chloride were obtained from AMRESCO (Solon. OH). Chloramphenicol and guanidinium chloride were purchased from Calbiochem (La Jolla, CA). The standard human TNF-α protein and human TNF-α monoclonal antibody were purchased from Abcam (Cambridge, MA). The standard human IL-6, and IL-8 proteins, human IL-6 monoclonal antibody, and human CXCL8/ IL-8 monoclonal antibody were purchased from R&D systems (Minneapolis, MN). The BL21(DE3)pLysS chemical competent cells were obtained from Invitrogen (Carlsbad, CA). The pooled human serum was obtained from Innovative re-search (Novi, MI). The Rosetta (DE3) competent cells suitable for electroporation were prepared in our lab. The protein-free (PBS) blocking

buffer, BCA protein assay reagent (bicinchoninic acid) and Reacti-Bind goat anti-mouse IgG coated white 96-well plates and Pierce Protein Refolding Kit were from Pierce Biotechnology (St. Louis, MO). All chemicals were reagent grade or better and all aqueous solutions were prepared using 18 MΩ deionized distilled water produced by a Milli-Q water purification system (Millipore, Bedford, MA).

2.3.2 Apparatus

Polymerase chain reactions (PCR) were completed with the Eppendorf gradient thermo-cycler (Hamburg, Germany). DNA electrophoresis gels were showed with a UV Transilluminator (UVP, Upland, CA). The optical densities (OD) were read through a Spectronic 21D UV-Vis Spectrophotometer (Milton Roy, Ivy Land, PA). Rosetta (DE3) cells were electroporated by Eppendorf Eporator (Ham-burg, Germany). *E. coli* that expressed the proteins were incubated in the Fisher Scientific orbital shakers (Fair Lawn, NJ). The cells were centrifuged down by a Beckman coulter Avanti J-E centrifuge (Palo Alto, CA). The cells harvested were lysed using a Fisher Scientific 550 dismembrator (Pittsburgh, PA). Purified proteins were concentrated by Centrifugal Filter Units 10K from Millipore (Darmstadt, Germany). The concentrated proteins were dialyzed into the right buffers by Slide-A-Lyzer Dialysis Cassettes from Thermo Scientific (Rochford, IL). Bioluminescence intensity were measured by the Polarstar Optima luminometer from BMG Labtech (Cary, NC), while the emission spectrums were scanned with a liquid cooled CCD named SpectroScan.

2.3.3 Construction, expression, and purification of cytokine-aequorin fusion proteins

For this study, three different fusion proteins were constructed and expressed for cytokine proteins TNF-α, IL-6, and IL-8 respectively. The gene of AEQY82F was genetically linked

to the 3’ end of the genes of cytokine IL-6 and TNF-α respectively to form IL6-Y82F and TNFα-Y82F fusion proteins, while AEQF113W was genetically linked to the 3’ end of IL-8 to form IL8-F113W fusion protein through an overlap extension PCR. Each fusion protein contained a spacer sequence composed of serine and glycine (SGGGGS) between the genes of the cytokine and the aequorin mutant.

For instance, the sequence of the cytokine TNF-α was amplified with the TNF-α forward primer that introduced a LIC/Xa cloning site and a *Nde*I restriction site on the 5′ end, and the TNF-α reverse primer that introduced the space linker. The sequence of AEQY82F coding sequence was amplified using the aequorin forward primer, which introduced the linker sequence, and the *Bam*HI aequorin reverse primer that introduced a *Bam*HI restriction site and a LIC/Xa cloning site on the 3′ end of the aequorin gene sequence. The amplified products were purified and then combined. The mixture was amplified using the overlap extension PCR with the TNF-α forward and the *Bam*HI aequorin reverse primer to obtain the gene of the fusion protein TNFα-Y82F. The steps of the PCR reaction were started at 95 ºC for 2 min for polymerase activation, and then repeated for 25 cycles for the next steps, 95 ºC for 20 s, and 65 ºC for 10 s, followed by 70 ºC for 15 s/k pairs. Similarly, the sequence of the cytokine IL-6 was amplified with the IL-6 forward primer that introduced a LIC/Xa cloning site and an *Eco*RI restriction site on the 5′ end, and the IL-6 reverse primer that introduced the space linker. The sequence of the AEQY82F mutant coding gene was amplified using the aequorin forward primer, which introduced the linker sequence, and the *Hind*III aequorin reverse primer that introduced a *Hind*III restriction site and a LIC/Xa cloning site on the 3′ end of the aequorin gene sequence. The amplified products were purified and combined, and then amplified using

the overlap extension PCR with the IL-6 forward and the *Hind*III aequorin reverse primer to obtain the gene of the fusion protein IL6-Y82F. Finally, the sequence of the cytokine IL-8 was amplified with the IL-8 forward primer that introduced a LIC/Xa cloning site and an *Eco*RI restriction site on the 5′ end, and the IL-8 reverse primer that introduced the space linker. The sequence of the AEQY82F mutant coding gene was amplified using the aequorin forward primer, which introduced the linker sequence, and the *Bam*HI aequorin reverse primer that introduced a *Bam*HI restriction site and a LIC/Xa cloning site on the 3′ end of the aequorin gene sequence. The amplified products were purified and combined and then amplified using the overlap extension PCR with the IL-8 forward and the *Bam*HI aequorin reverse primer to yield the gene of the fusion protein IL8-F113W. The primer sequences are displayed in **Table I**.

Table I. The primer sequences for each overlap extension PCR for the construction of the cytokine-aequorin fusion proteins

Primer	Sequence (5′-3′)
Aequorin Forward	TCTGGCGGTGGCGGTTCTGTGAAACTGACCAGCGACTTCGACAACCCAAGA
Aequorin Reverse *Bam*HI	AGAGGAGAGTTAGAGCCGGATCCTTAGGGGACAGCTCCACCGTAGAGCTTTT CGGAAGC
Aequorin Reverse *Hin*dIII	AGAGGAGAGTTAGAGCCAAGCTTTGATTGTTAGGGGACAGCTCCACCGTAGA GCTTTTC
TNF-α Forward	GGTATTGAGGGTCGCCATATGATGGTTCGTTCTAGCTCCCGTACCCCGTCTGA CAAA
TNF-α Reverse	AGAACCGCCACCGCCAGACAGCGCGATGATACCGAAGTAAACCTGACCAGA
IL-6 Forward	GGTATTGAGGGTCGCGAATTCCAATCAATGAACTCCTTCTCCACAAGCGCCTT CGGTCCAGTTGCC
IL-6 Reverse	TTTCACAGAACCGCCACCGCCAGACATTTGCCGAAGAGCCCTCAG
IL-8 Forward	GGTATTGAGGGTCGCGAATTCCAATCAATGAGTGCTAAAGAACTTAGATGTCA GTGCATAAAGACA
IL-8 Reverse	TTTCACAGAACCGCCACCGCCAGATGAGTTCTCAGCCCTCTTCAA

The three fusion protein coding sequences were inserted into lac operator containing pET-30 plasmid by using Novagen pET-30 Xa/LIC Cloning Kits. The DNA genetic sequences were measured by the Sylvester Comprehensive Cancer Center Oncogenomics Core Facility at the University of Miami to confirm the gene sequences of the fusion proteins. The plasmids containing the gene for TNFα-Y82F and IL8-F113W were transferred into BL21(DE3)pLysS *E. coli* cells and grown through shaking at 250 rpm at 37 ºC in 500 mL LB broth containing 30 μg/mL Kanamycin to an OD_{600} ~ 0.6 in the incubator. The fusion proteins were expressed in the cells after the addition of 1 mM IPTG. The cells expressing TNFα-Y82F were collected after 8 h's incubation at room temperature,

while the cells expressing IL8-Y82F were collected after 3 h's incubation at 37 ºC. The cell pellets were then resuspended in the Ni-NTA native lysis buffer and lysed by using a dismembrator and then purified using immobilized metal affinity chromatography (Ni/NTA). The proteins were loaded into a gravity column containing Ni/NTA Agarose beads in 50 mM NaH_2PO_4 pH 8.0, 300 mM NaCl, and 10 mM imidazole buffer. A sequential washing with buffers of 30 mM NaH_2PO_4 pH 8.0, 300 mM NaCl, and 20, 50 and 70 mM imidazole, were then applied to the column. The fusion proteins were washed off by an elution buffer with 30 mM NaH_2PO_4 pH 8.0, 300 mM NaCl, and 100 mM imidazole. Ten fractions of 1.5 mL volume were collected and fractions containing high concentrations of the fusion proteins, determined by SDS-PAGE, were pooled. Similarly, the plasmid containing the IL6-Y82F gene was transformed into Rosetta (DE3) *E. coli* cells and grown with shaking at 250 rpm at 37 ºC in 500 mL of LB broth containing 30 µg/mL kanamycin to an OD_{600} ~ 0.6. The proteins were expressed in the cells for after the addition of 1 mM IPTG. These cells were then collected after the incubation at room temperature for 8 h, lysed by sonication and then purified through Ni-NTA affinity chromatography under denaturing conditions. The proteins were loaded onto a Ni-NTA beads column in a 100 mM NaH_2PO_4 pH 8.0, 10 mM Tris·Cl, and 6 M GuHCl buffer. A sequential washing with buffers of 100 mM NaH_2PO_4, 10 mM Tris·Cl, 8 M Urea with pH 6.3 and 5.9 adjusted by HCl, were performed followed by the elution of the fusion using an elution buffer with 100 mM NaH_2PO_4 pH 4.5, 10 mM Tris·Cl, and 8 M Urea. Pure fractions were pooled and dialyzed in the refolding buffer (55 mM Tris pH 8.2, 21mM NaCl, 0.88mM KCl, 1 mM EDTA, 2 mM GSH and 1mM GSSG) for 24 h at 4 ºC followed by 2 h at room temperature. The fusion proteins were then dialyzed into 30 mM Tris/HCl pH 7.4, containing 2 mM

EDTA, 150 mM NaCl (buffer A) for 24 h to change the buffer for further use, and stored at 4 ºC. Protein concentration was determined by the Pierce BCA protein assays.

2.3.4 Half-Lives of the bioluminescence emission of cytokine-aequorin fusion proteins

The bioluminescence decay kinetics of the combinations of each cytokine-aequorin fusion protein and each coelenterazine analogue (coelenterazine *ntv, i, f, cp, hcp, fcp, n, fcp, h*) were examined respectively. Each of the fusion protein was incubated with each synthetic coelenterazine analogue (three molar excess than the amount of the fusion protein) in buffer A for 18 h at 4 ºC. The bioluminescence intensity was measured with the Polarstar luminometer as follows. A volume of 10 µL of the coelenterazine activated fusion protein solution was added into one well of a microtiter plate, and then 50 µL of 30 mM Tris/HCl buffer containing 100 mM $CaCl_2$, pH 7.5 (buffer B) was injected into the well to trigger the bioluminescent reaction. The light intensity was then monitored for 50 s for semi-synthetic aequorin consisting with coelenterazine *i* and *n*, with readings taken every 200 ms. For the semi-synthetic aequorin consisting with other coelenterazine analogs, the light intensity was monitored for 10 s, with readings taken every 40 ms. The half-lives of these proteins were calculated by Grahpad Prism 5.0. The light intensity and the corresponding time frames were imported into Prism 5.0 and analyzed using the non-linear, one phase exponential decay fitting.

2.3.5 Emission spectra of cytokine-aequorin fusion proteins

The bioluminescence emission maximum is the other factor for the signal differentiation. In this research, the emission spectra were scanned by a liquid cooled SpectroScan CCD camera in a luminometer. Same steps as the measurement of decay kinetics were taken to prepare the samples. The volume of 10 µL of each sample was loaded into each well of the

96-well plate, and the spectra were scanned through the range of 400-700 nm while the injection of 50 µL of buffer B was then injected in the well and the emission photons were collected for 5.250 s. The light intensity and the corresponding wavelengths were recorded and imported into the Microsoft Excel to determine the emission maximum (the wavelength corresponding to the highest intensity).

2.3.6 Concentration optimization of cytokine-aequorin fusion proteins

An aliquot of 10 µL of serial dilutions of TNFα-Y82F with coelenterazine *f* were added to the wells of a microtiter plate, and 50 µL of buffer B was added to trigger the bioluminescent reaction. The bioluminescence intensity was recorded by the Polarstar Optima luminometer with 420 nm and 520 nm filters for both 0-6 s and 6-25 s windows. Same steps were taken for the concentration optimization of IL6-Y82F with coelenterazine *i* as well as IL8-F113W with coelenterazine *cp*.

2.3.7 Binder dilution curves for cytokine-aequorin fusion proteins

The binding of the fusion protein and its corresponding antibody, as well as the optimized antibody concentration for further research, were determined by the binder dilution research. The pierce goat anti-mouse IgG antibody coated white plates were used to capture the cytokine-specific monoclonal antibodies, and perform the binder dilution study. Monoclonal anti-human TNF-α antibody was serially diluted in Pierce protein-free (PBS) blocking buffer (buffer C), with an initial concentration of 1.0×10^{-4} µg/mL. Each well of the goat anti-mouse IgG plate was washed three times with 200 µL of buffer C to remove the super blocking buffer. Then a volume of 100 µL of each antibody dilution was loaded into each well and incubated at room temperature with shaking at ~500 rpm for 1 h for capturing the antibodies. The wells of the plate were then washed three times with 30 mM

Tris·HCl, pH 7.4 containing 2 mM EDTA, 150 mM NaCl and 0.05% Tween-20 (buffer D) to remove the excess antibodies to decrease the randomly binding. After washing, a volume of 100 µL of TNFα-Y82F fusion protein with coelenterazine *f* at the optimized concentration measured in the last step (1.04 x 10^{-8} M) was added to the wells, and incubated for 1 h at room temperature at ~500 rpm. After incubation, the wells were completely emptied and washed well again three times with 200 µL buffer D to remove the excess amount of the TNFα-Y82F fusion protein. The bioluminescence intensity was recorded by the Polarstar Optima luminometer after the injection of 50 µL of buffer B. The same procedures were employed for IL6-Y82F and IL8-F113W. The concentration of 7.00 x 10^{-8} M of IL6-Y82F fusion protein was used, as well as the concentration of 5.81 x 10^{-8} M of IL8-F113W fusion protein was used. The bioluminescence intensity was imported into Prism 5.0 and analyzed to obtain the antibody binder dilution curve.

2.3.8 Dose-response curves for individual cytokines

The competition between each cytokine-aequorin fusion protein and its corresponding free cytokine was studies through a competitive immunoassay. The detection limits of the competitive immunoassays were determined by the dose-response curves. For this study, the wells of the goat anti-mouse IgG plate were washed three times with 200 µL of buffer C to remove the pre-blocking buffer. A volume of 100 µL of anti-human TNF-α and IL-6 antibodies at a concentration of 1.0 µg/mL and anti-human IL-8 antibody at a concentration of 0.5 µg/mL that were optimized from the last step were then applied separately to each well, incubating for 1 h at ~500 rpm and room temperature. After incubation, the wells were washed three times with 200 µL of 10 mM PBS pH 7.4 containing 0.05% Tween-20 (buffer E) to remove the unbound antibody molecules. During the incubation, each human

cytokine standard was serially diluted in 10 mM PBS buffer pH 7.4 (buffer F). Then a volume of 100 μL of each dilution was loaded into each well and incubated for 1.5 h at ~500 rpm and room temperature. Each well was then washed three times with 200 μL of buffer D to remove the excess free cytokines. After washing, a volume of 100 μL of the corresponding fusion protein with desired concentration was added to each well, and incubated for 1 h at ~500 rpm and room temperature. After the incubation, the last washing step was repeated three times with buffer D. After washing, the bioluminescence intensity was recorded by the Polarstar Optima luminometer. Upon 50 μL of buffer B was injected into each well, the bioluminescence intensity was recorded through dual luminescence emission detection wavelengths combined with two kinetic windows. Channel A: 420 nm filter; channel B: 520 nm filter. Kinetic window 1: 0-6 s; kinetic window 2: 6-25 s. Then, the bioluminescence intensity for each fusion protein from the specific window was imported into Prism 5.0 for the dose-response curves and the detection limits.

2.3.9 Simultaneous dose-response curves for multiplexing cytokines in buffer

The dose-response curve of each cytokine was set up in the presence with the other two cytokines as well as the antibodies and fusion proteins specific to other cytokines. In addition, the detection limit of each cytokine of was determined by the corresponding dose-response curve. For this study, the wells of the goat anti-mouse IgG plate were washed three times with 200 μL of buffer C to remove the pre-blocking buffer. A volume of 100 μL of the mixture of each of the anti-human cytokine antibodies with the concentrations optimized in the binder dilution studies were loaded into each well, and incubated for 1 h at ~500 rpm and room temperature. After the incubation, the wells were washed three times with 200 μL of buffer E to remove the unbound and randomly bound antibodies. After

washing, a serial dilution of each cytokine to be analyzed was prepared in buffer F, while keeping the concentrations of the other two cytokines at 1000 pg/mL. Then a volume of 100 µL of each serial dilution was loaded into each well, and incubated for 1.5 h at ~500 rpm and room temperature. The wells were washed three times with 200 µL of buffer D to remove the excess free cytokines. After washing, a volume of 100 µL of the mixture of all three fusion proteins with their optimized concentrations was added to each well, and incubated for 1 h at ~500 rpm and room temperature. Then the wells were washed three times with 200 µL of buffer D to remove the excess amount of free fusion proteins. The bioluminescence intensity was recorded by the Polarstar luminometer. Upon 50 µL of buffer B was injected into each well, the bioluminescence intensity was recorded through dual luminescence emission detection wavelengths combined with two kinetic windows. Channel A: 420 nm filter; channel B: 520 nm filter. Kinetic window 1: 0-6 s; kinetic window 2: 6-25 s. Then, the bioluminescence intensity for each fusion protein from the specific window was imported into Prism 5.0 for the analysis of the dose-response curves and the detection limits.

2.3.10 Simultaneous dose-response curves for multiplexing cytokines in serum

For the simultaneous dose-response curves in human serum, the same procedure as the ones measured in buffer was followed except that instead of buffer C we have used a pooled serum sample that was diluted 10 times with buffer C. This diluted serum was than spiked with cytokines the same way above to prepare the cytokine samples used in the assay. The establishment of the assays and the calibrations curves were performed the same as the multiplexed assays in buffer. At last, the levels of TNF-α, IL-6 and IL-8 in the serum-

spiked sample were measured through the newly developed bioluminescent assays, as well as by the ELISA kits to validate the assays developed in this research.

2.4 Results and discussion

Recently, there has been a lot of discussion in the scientific as well as in the non-scientific press regarding the need of small volume detection of analytes in clinical samples. This has been highlighted especially by the controversy generated by the company Theranos and their widely publicized small volume test, which failed short on the delivery of their promised technology (84-87). While, unfortunately, Theranos misfortune in not being able to demonstrate without question that their tests conform to the analytical parameters needed for a reliable clinical assay, has also highlighted further the absolute need for better technology that can achieve sensitive, reproducible and low detection assays in small volume physiological samples. This is even more pressing given the fast pace discovery of new biomarkers and the trend of modern medicine to use the levels of these biomarkers in the diagnosis and management of disease. In addition, the issue of detection of panels of biomarkers and the burden imposed on patients when drawing large volumes of blood in high frequency is also an important consideration that highlights the need for technologies that can perform biological assays in small volumes. Granted this is not a trivial task, and we must recognize that the current move towards miniaturization of a number of analytical methods that can reliably detect low analyte concentrations in physiological samples requires, among other parameters, extremely sensitive labels. The ability to multiplexed assays is under such conditions would also greatly improve the value of the newly discovered biomarkers in diagnostic and monitoring of disease. Bioluminescent proteins offer several distinguished advantages such as high signal-to-background ratios than

fluorescent labels because of no need for the excitation energy sources. In addition, advanced protein engineering and signal detection technologies make bioluminescent proteins suitable for multiplexed detection applications. For example, semi-synthetic aequorin has been applied to detect two analytes simultaneously based on time resolution (57). In this study, we would like to prove that the multiplexed detection capabilities can be further expanded to three analytes or more by combining both time and wavelength resolution strategies. Herein, three pro-inflammatory cytokines (TNF-α, IL-6 and IL-8) were chosen as biomarker candidates for the proof of principle for multiplexed detection system based on the fact that their simultaneous detection would be beneficial in the diagnosis of a number of diseases (81, 88-91) (**Figure 10**). Indeed, these cytokines are routinely employed in the management of diseases including, among others, rheumatoid arthritis, Crohn's disease, ulcerative colitis, cardiovascular diseases, diabetes, cancer, lupus, and hyperalgesia (81-83).

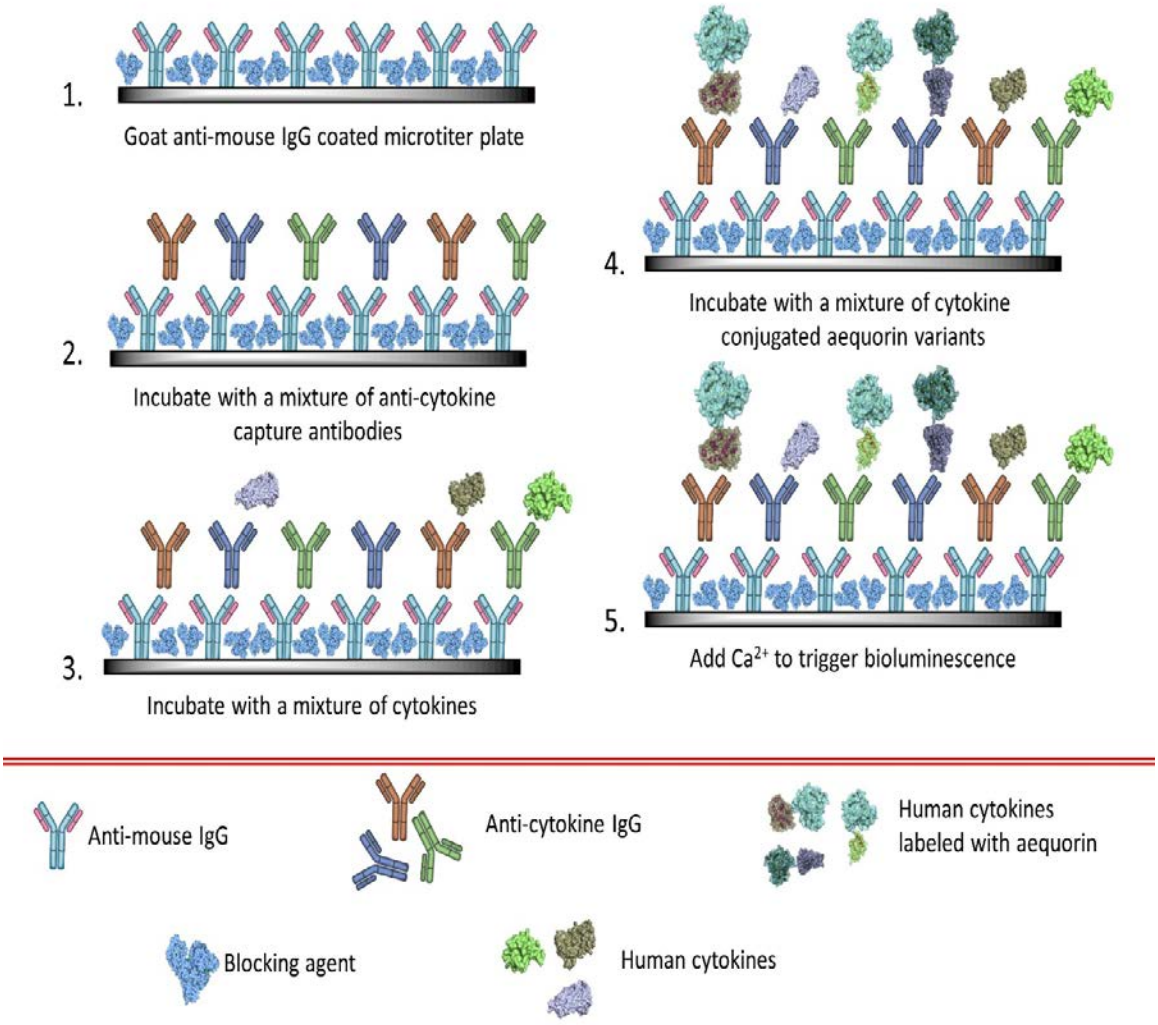

Figure 10. The 2-D scheme of the simultaneous competitive assay for TNF-α, IL-6, and IL-8 using semi-synthetic aequorin mutants.

Our lab have already made a wide range of aequorin mutants which showed greatly shifted emission maximums and half-lives together with different coelenterazine synthetic analogues (21). Taking this work and the individual characteristics and potential of these newly prepared proteins as bioluminescent labels in assays into consideration, the semi-synthetic aequorins have great potential to be used in multiplexed assays. In this study, the aequorin mutant Y82F (AEQY82F) combined with coelenterazine *i,* and the mutant

F113W (AEQF113W) combined with coelenterazine *cp* were chosen to implement this research because they showed maximal spatial and temporal resolutions (**Figure 11**).

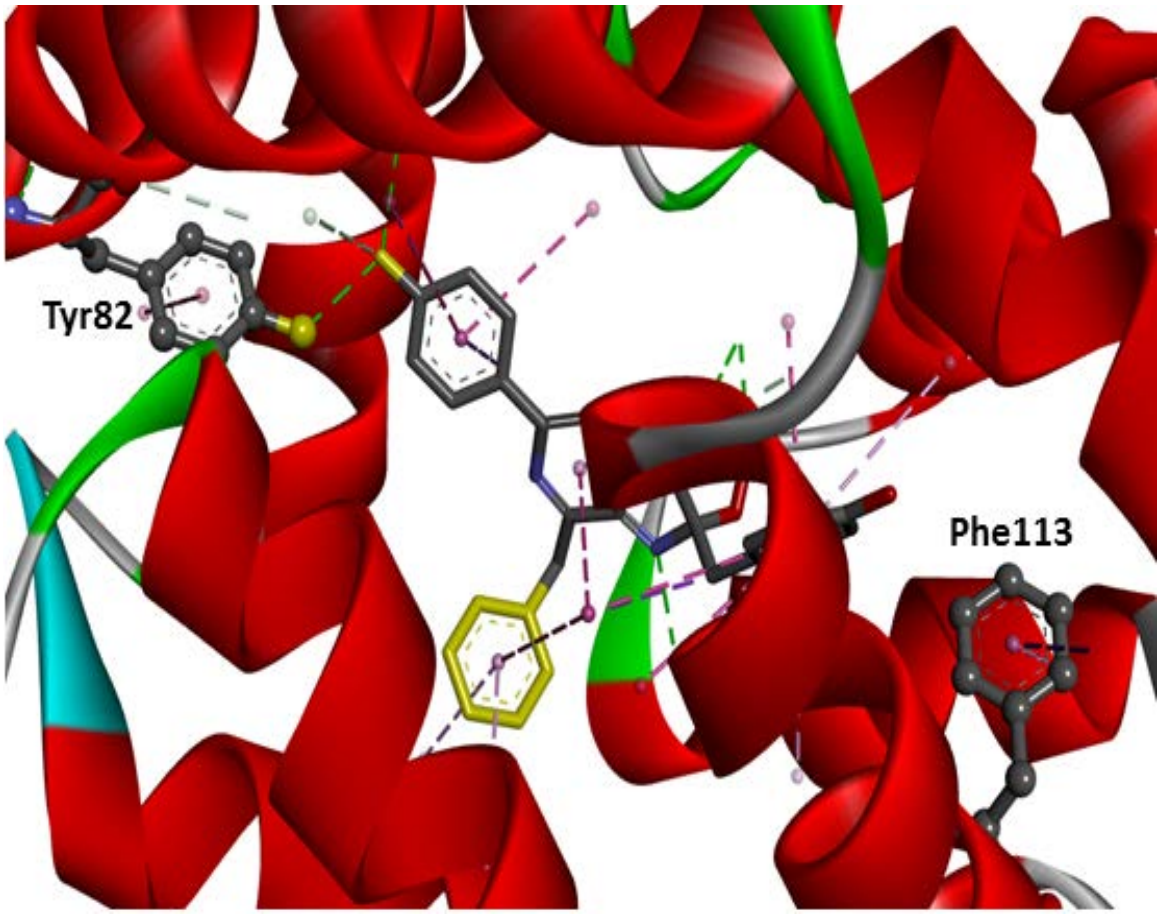

Figure 11. Three-dimensional crystal structure of aequorin with the locations of the Tyr82 and Phe113 highlighted. The dotted lines display the interactions between aequorin and coelenterazine. The tyrosine residue at position 82 was substituted by phenylalanine to decrease the H-bond interaction, and thus red-shifted the emission wavelength. On the other hand, the phenylalanine at position 113 was substituted by tryptophan to increase the π-π interaction, and therefore blue-shifted the emission wavelength.

In our work, we fused the target analytes with the aequorin mutants respectively, and used the fusion proteins to set up competitive immunoassays for the analytes. For this purpose, the genes of aequorin mutants were fused to the c-terminus of the cytokines

through the overlap extension PCR, and then the fused genes were ligated into the pET-30 expression plasmid through the pET-30 Xa/LIC Vector Kit (**Figure 12**).

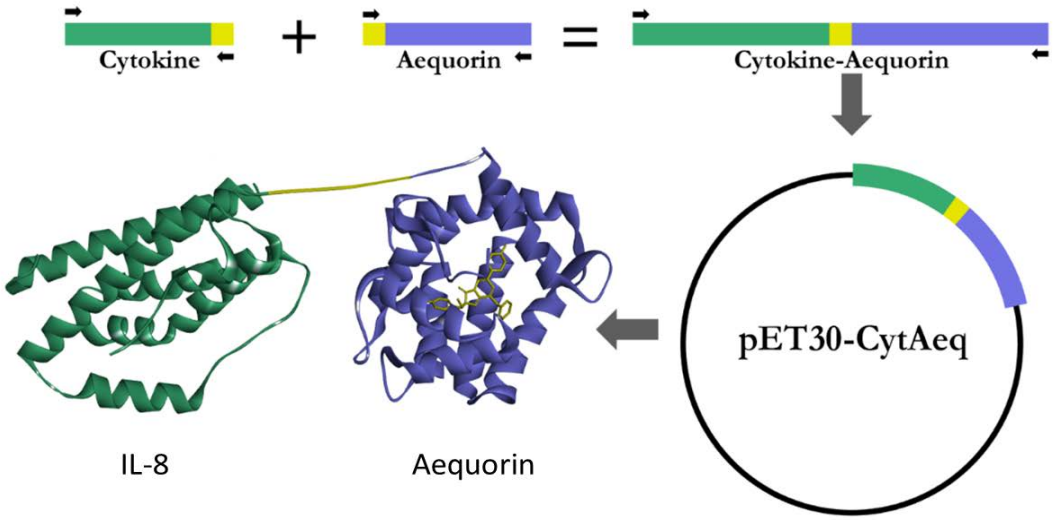

Figure 12. The scheme of the overlap extension PCR. In this figure, IL-8 is used as an example. The green blocks are the genes of the cytokines. The blue blocks are the genes of the aequorin. The yellow blocks are the gene of the linker between cytokines and aequorin. A LIC ligation site is introduced to the N-terminus of IL-8, while the linker sequence is introduced to the C-terminus of IL-8. Similarly, the linker sequence is introduced to the N-terminus of the aequorin mutant, while a LIC ligation site is introduced to the C-terminus of the aequorin mutant. Then, a third PCR is implemented to fuse the genes of the cytokine and the aequorin mutant together. After the ligation, the gene of the cytokine-aequorin fusion proteins are introduced into the pET30 expression plasmid for the expression of the fusion proteins.

After the sequences of these genes were verified, the plasmids containing different genes of the fusion proteins were transfected into different expression vectors to achieve the optimal expression. The plasmids containing the genes of the TNFα-Y82F and IL8-F113W were introduced into *E. coli* BL21(DE3)pLysS strain, while the IL6-Y82F was expressed in a Rosetta(DE3) *E. coli* strain. The fusion proteins were than expressed and

purified according to the optimized procedures. The purity of these proteins has been verified by the protein SDS-PAGE (**Figure 13**).

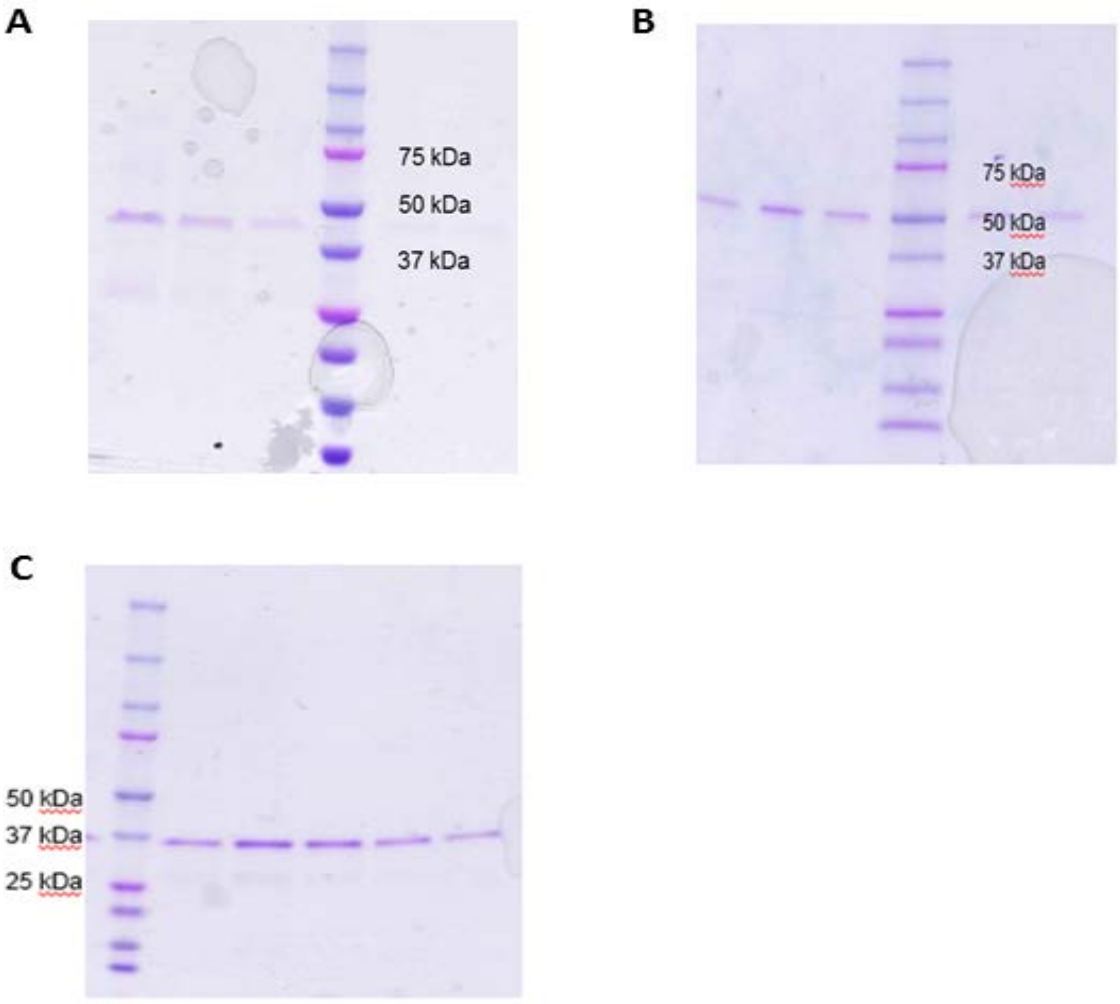

Figure 13. The purity of the cytokine-aequorin fusion proteins was verified by the SDS-PAGE gels. The SDS-PAGE of the three fusion proteins. (A) TNFα-Y82F (B) IL6-Y82F (C) IL8-F113W. The sizes of the fusion proteins with the His-tag are 44.5 kDa for TNFα-Y82F, 50.8 kDa for IL6-Y82F, and 35.7 kDa for IL8-Y82F respectively.

Activities and emission profiles of the proteins were determined by luminometers. In addition, the emission properties including the spectra and the half-lives were measured to

check if the protein engineering affect the emission properties. The emission maxima were shown in **Table II A**, while the emission half-lives were shown in **Table II B**.

Table II. A. The bioluminescence wavelength emission maxima of the cytokine-aequorin fusion proteins combined with different synthetic coelenterazine analogs. B. The bioluminescence emission half-lives of the cytokine-aequorin fusion proteins combined with different synthetic coelenterazine analogs.

A.	TNFα-Y82F	IL6-Y82F	IL8-F113W
Coelenterazine	Emission max (nm)	Emission max (nm)	Emission max (nm)
ntv	501	501	480
i	511	511	481
f	509	509	488
ip	482	480	464
hcp	479	478	463
h	504	503	479
cp	483	477	462
fcp	493	492	472
n	507	498	477

B.	TNFα-Y82F	IL6-Y82F	IL8-F113W
Coelenterazine	Half-life (s)	Half-life (s)	Half-life (s)
ntv	1.1	1.1	2.6
i	13.5	20.00	11.7
f	0.7	0.7	0.6
ip	0.5	0.5	0.4
hcp	0.2	0.1	0.1
h	0.3	0.3	0.3
cp	0.2	0.2	0.2
fcp	0.3	0.3	0.2
n	3.1	3.2	7.4

The results showed that, as expected, the emission properties of the fusion proteins did not change significantly compared to their corresponding free aequorin mutants. Therefore,

the emission maxima of IL8-F113W combined with coelenterazine *cp* blue-shifted from 469 nm of wild-type aequorin to 462 nm because of the tighter binding between apoaequorin and the coelenterazine, while the IL6-Y82F coupled with coelenterazine *i* red-shifted the emission maxima to 511 nm because of the decrease of the H-bond interaction. The detection signals of these two analytes are capable to be separated through the separation of 49 nm. The emission spectra of IL6-Y82F combined with coelenterazine *i* and TNFα-Y82F coupled with coelenterazine *f* are similar to each other, thus cannot be differentiated through different wavelength filters. However, the half-lives of these two fusion proteins are quite different from each other, making it possible to separate their signals. For instance, the half-life of IL6-Y82F with coelenterazine *i* is around 20 s because of heave atom effect, while the half-life of TNFα-Y82F with coelenterazine *f* is less than 1 s. Thus, the signals from these two fusion proteins can be differentiated through different time windows. Therefore, the signals of these three semi-synthetic aequorins can be separated by the combination of different time and wavelength windows. Based on all these information, two band pass filters (420 nm and 520 nm) and two time windows (0-6 s and 6-25 s) were chosen and combined to detect the three cytokines simultaneously. For instance, TNFα-Y82F with coelenterazine *f* was detected in the 0-6 s time window with the 520 nm filter, while IL6-Y82F with coelenterazine *i* was measured in the 6-25 s time window with the 520 nm filter. Similarly, IL8-F113W with coelenterazine *cp* was detected in the 0-6 s time window with the 420 nm filter. Therefore, the spatial resolution was achieved through two filters (420 nm and 520 nm) (**Figure 14A**), as well as the temporal resolution was achieved through two time windows (0-6 s and 6-25 s) (**Figure 14B**).

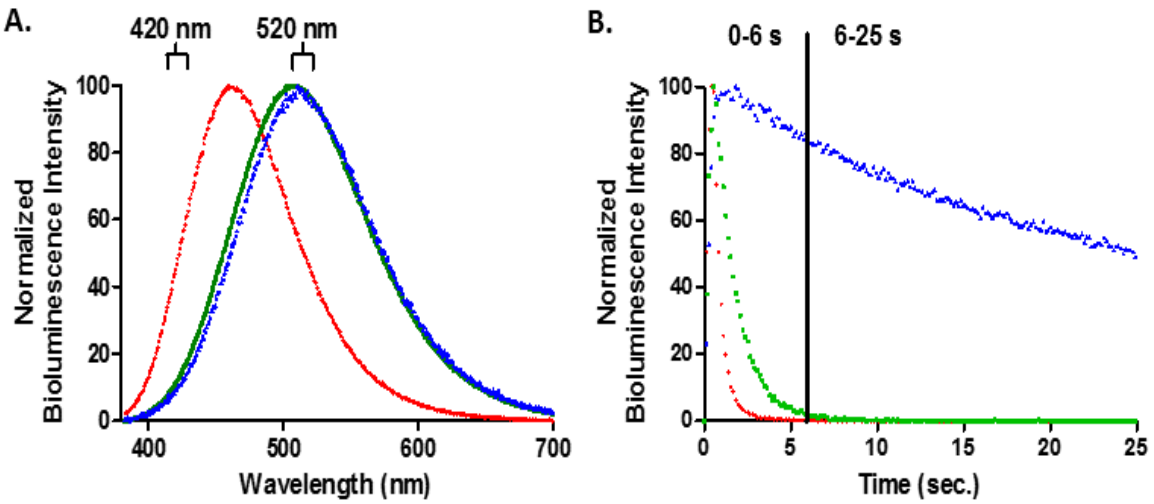

Figure 14. The bioluminescence emission properties of the three cytokine-aequorin fusion proteins coupled with their respective coelenterazine analogs. (A) The emission spectra of the fusion proteins: ■ TNFα-Y82F with coelenterazine *f*, ▲ IL6-Y82F with coelenterazine *i*, and ● IL8-F113W with coelenterazine *cp*. The signals were separated by two optical filters (420 nm and 520 nm). (B) The emission decay kinetics of the three fusion proteins: ■ TNFα-Y82F with coelenterazine *f*, ▲ IL6-Y82F with coelenterazine *i*, and ● IL8-F113W with coelenterazine *cp*. The signals were differentiated through two time windows (0-6 s and 6-25 s). All the measurements were normalized and plotted. The highest intensities were set up to 100, while the lowest readings were set up to 0.

After the appropriate fusion proteins were chosen and the feasibility was verified. The detection assays could be built. The first step was to determine the concentrations of the fusion proteins to be used in the detection assays. The fusion proteins were diluted to different concentrations with buffer A. The bioluminescence intensity was measured by the Polarstar Optima luminometer upon the injection of the buffer B. The signal intensity was plotted against different concentrations. The concentrations along the linear range were chosen because the signal could be differentiated with the background, and avoided to exceed the detection range as well. Based on this study, the concentration of TNFα-Y82F with coelenterazine *f* chosen was 1.04×10^{-8} M. Similarly, the concentration of IL6-Y82F with coelenterazine *i* was 7.00×10^{-8} M, while the concentration of IL8-F113W with coelenterazine *cp* selected was 5.81×10^{-8} M. To establish the detection assay, the other

factor optimized was the concentrations of the antibodies used. The antibodies specific to the three cytokines were diluted to different concentrations, and loaded into the goat anti-mouse IgG plates. The fusion proteins with the concentrations determined in the last step were loaded into the plates. The bioluminescence intensity was measured and plotted against the concentrations of the antibodies (**Figure 15**). The concentrations with the signals that were significantly different from the background, and were within the detection range were chosen. The optimized concentration of the anti-human IL-8 antibody is 0.5 μg/mL, and the concentration of the anti-human IL-6 antibody as well as the anti-human TNF-α antibody is 1.0 μg/mL.

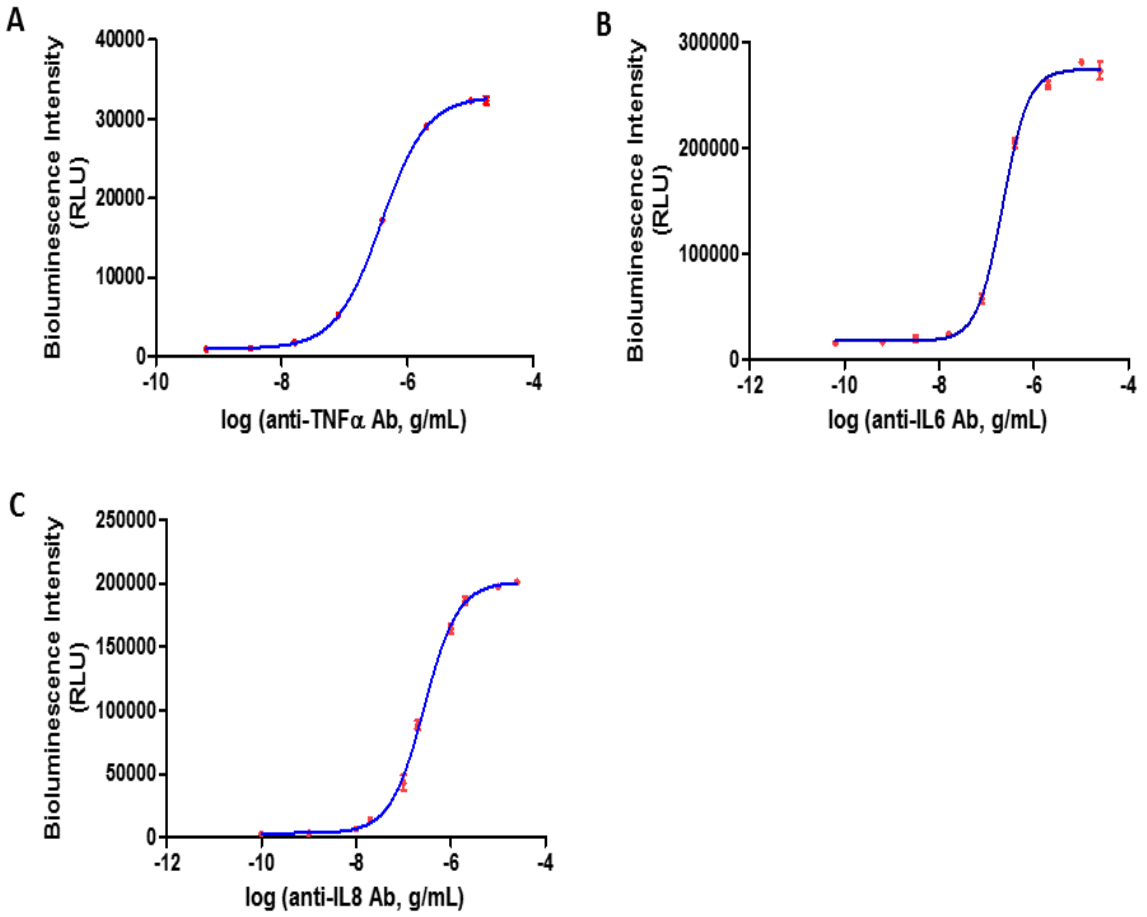

Figure 15. Individual binder dilution curves for the three cytokine-aequorin fusion proteins with the respective cytokine-specific antibodies to determine the optimized concentrations of the antibodies for the development of the bioluminescent assays. (A) TNF-α. (B) IL-6. (C) IL-8. All points are the mean of three measurements ± one standard deviation. Error bar that are not visible are obstructed by the point.

In addition, before the establishment of the multiplexed assays, the competitive immunoassays for single cytokines were developed to check the detection limits of these assays. The optimized concentrations of the anti-human cytokines were loaded into the goat anti-mouse IgG plates. Then a serial dilution of each free cytokine analyte competed with the fixed amount of the corresponding fusion protein to set up a competitive immunoassay. The bioluminescence intensity was plotted against the concentrations of the free cytokine analytes to set up the dose-response curves of the analytes. By this method,

the detection limit of TNF-α was 53 pg/mL, and the detection limit of IL-6 was 184 pg/mL. The dose-response curve for the human IL-8 showed better result with the detection limit of 37 pg/mL (**Figure 16**).

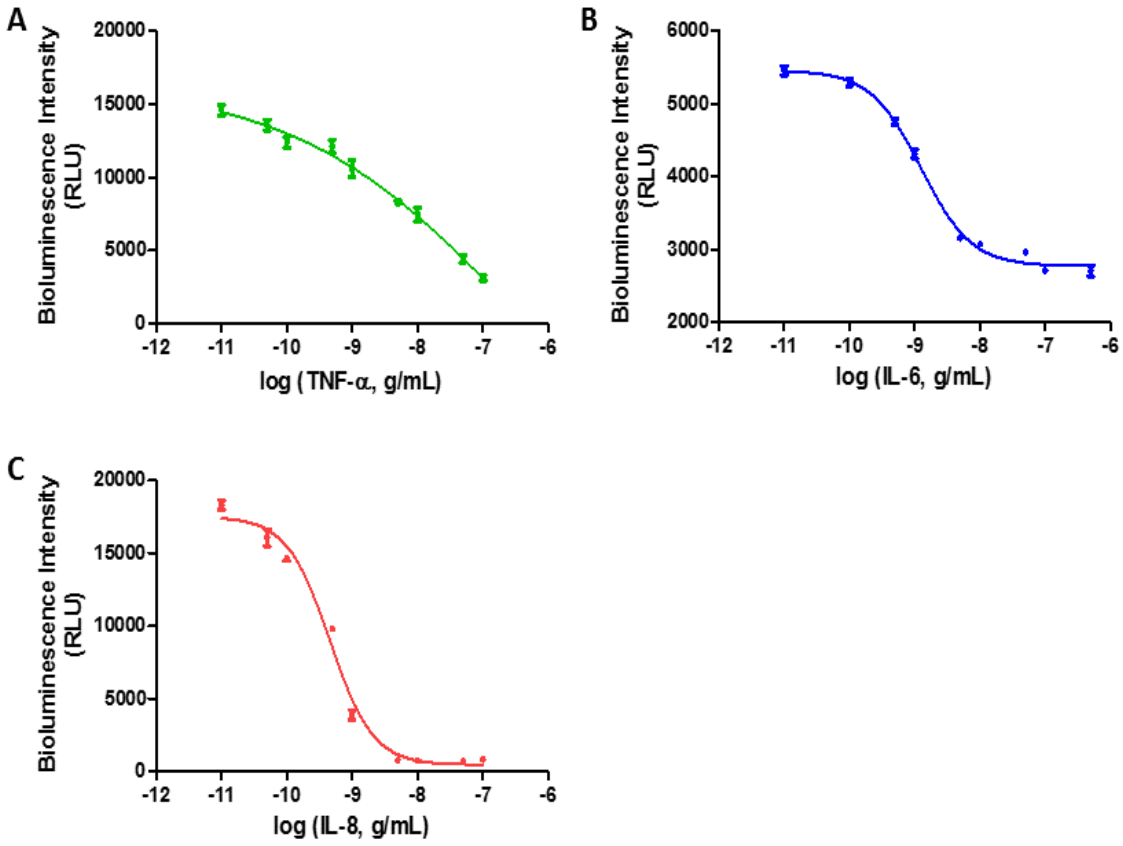

Figure 16. Dose-response curves for the individual cytokines respectively in a buffered solution. (A) TNF-α. (B) IL-6. (C) IL-8. All points are the mean of three measurements ± one standard deviation. Error bar that are not visible are obstructed by the point. The coefficients of variability (CVs) of all the assays are smaller than 10. The coefficients of determination (R^2s) of all the assays are above 95%.

The detection limits of these cytokines are within their relevant elevated concentration ranges (~10 pg-10000 pg) (92-95). After the study of the detection limits of the assays for the single cytokines, the multiplexed assays for all the three cytokines were developed. Instead of only one antibody, one analyte, and one fusion protein, the mixtures of all three

antibodies, three analytes, and three fusion proteins were applied simultaneously in the plates. The concentrations of the antibodies and the fusion proteins were same as the optimized concentrations determined above. The concentration of one free cytokine analyte was serially diluted while keeping the concentrations of the other two cytokines at 1000 pg/mL to determine the interactions of the presence of the other two analytes. This concentration was chosen to simulate the actual concentrations in physiological samples. As expected, the 0-6 s and 420 nm window was only affected by the response for IL-8, and the 6-25 s and 520 nm window only counted the signals responsible to IL-6. However, the 0-6 s and 520 nm window was affected by the response for not only TNF-α, but also the other two analytes. Therefore, a signal deconvolution algorithm (see equation below) was used to subtract the signals response to IL-6 and IL-8 to resolve this issue.

$$[\ \text{signal}_{\text{TNF-}\alpha} = \text{signal}_{520\ \text{nm}\ 0-6\ \text{s}} - 0.72375(\ \text{signal}_{420\ \text{nm}\ 0-6\ \text{s}} - \text{blank}_{420\ \text{nm}\ 0-6\ \text{s}}\ ) - 1.56604(\text{signal}_{520\ \text{nm}\ 6-25\ \text{s}} - \text{blank}_{520\ \text{nm}\ 6-25\ \text{s}})]$$

In the equation, 1.56604 is the ratio of signal intensity between 0-6 s and 6-25 s emitted by IL6-Y82F, and 0.72375 is the ratio between signal intensity emitted by IL8- F113W in 520 nm and 420 nm channels. After the calculations, the bioluminescence intensity from certain detection windows was plotted against the concentrations of the corresponding cytokines to set up the dose-responsive curves for the simultaneous detection of three cytokines. Because of the low background of bioluminescence as well as the low interactions between each cytokine, the detection limits of the multiplexed assays were comparable of the assays for the single cytokines. The detection limit of TNF-α was 250 pg/mL, and the detection limit of IL-6 was 213 pg/mL. The dose-response curve for the human IL-8 showed better result with the detection limit of 19 pg/mL (**Figure 17**).

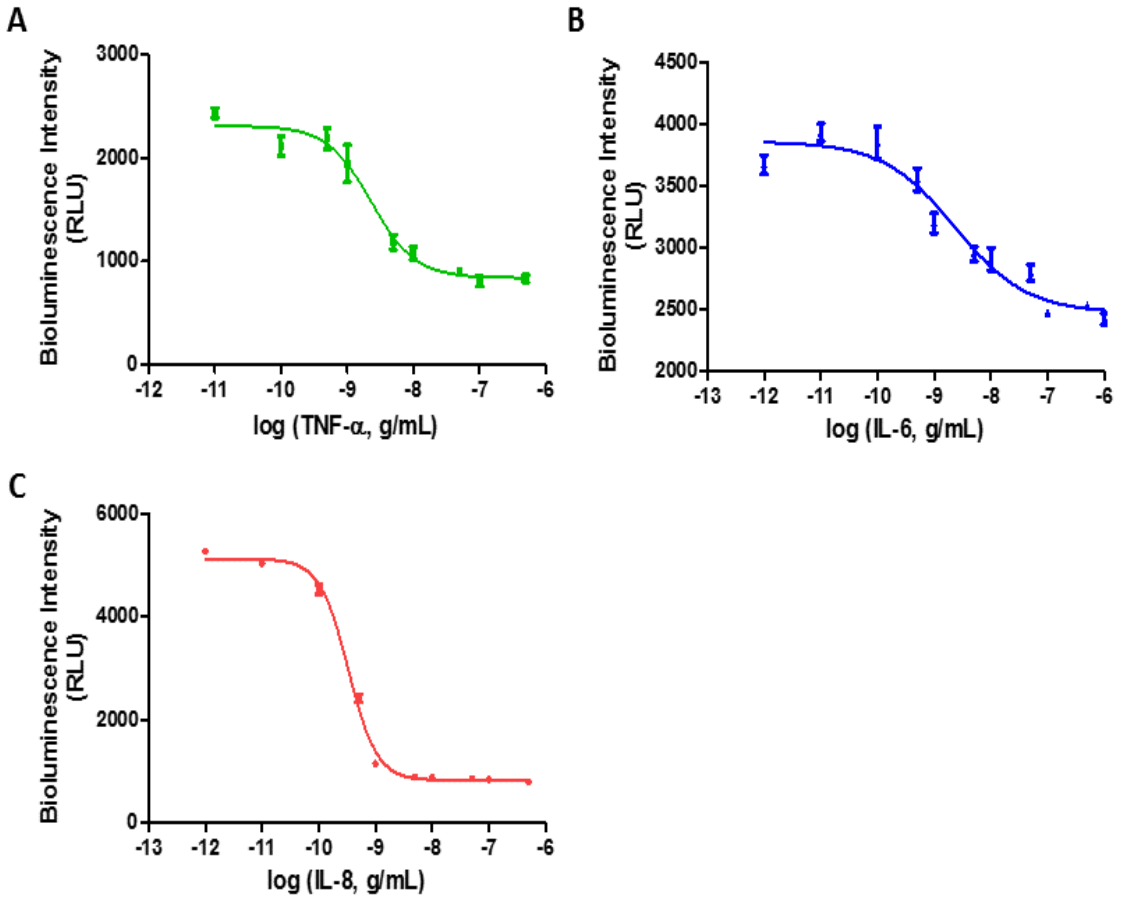

Figure 17. Simultaneous dose-response curves for the multiplexing cytokines in buffer. The bioluminescence intensity from the specific channels was plotted against to the concentrations of the corresponding cytokines. (A) TNF-α. (B) IL-6. (C) IL-8. All points are the mean of three measurements ± one standard deviation. Error bar that are not visible are obstructed by the point. The coefficients of variability (CVs) of all the assays are smaller than 10. The coefficients of determination (R2s) of all the assays are above 90%.

Besides the buffer solution, the multiplexed assays for the three analytes were also developed using human serum as the sample matrix. The inherent ability of bioluminescence-based assays to be performed directly in physiological fluids without the need for sample preparation steps, has numerous advantages such as the ease of the overall analytical method, lower probability to introduce error in the analysis, amenability for incorporation of a variety of platforms, and reduction of analysis time. To that end, our

multiplexed assay showed high sensitivity and specificity in human serum, with the capability to detect all three cytokines with a four order of magnitude linear detection range within their physiological levels. Specifically, the detection limit of the human TNF-α was of 252 pg/mL, and the detection limit of the human IL-6 was 16 pg/mL, while the detection limit of the human IL-8 is 13 pg/mL (**Figure 18**).

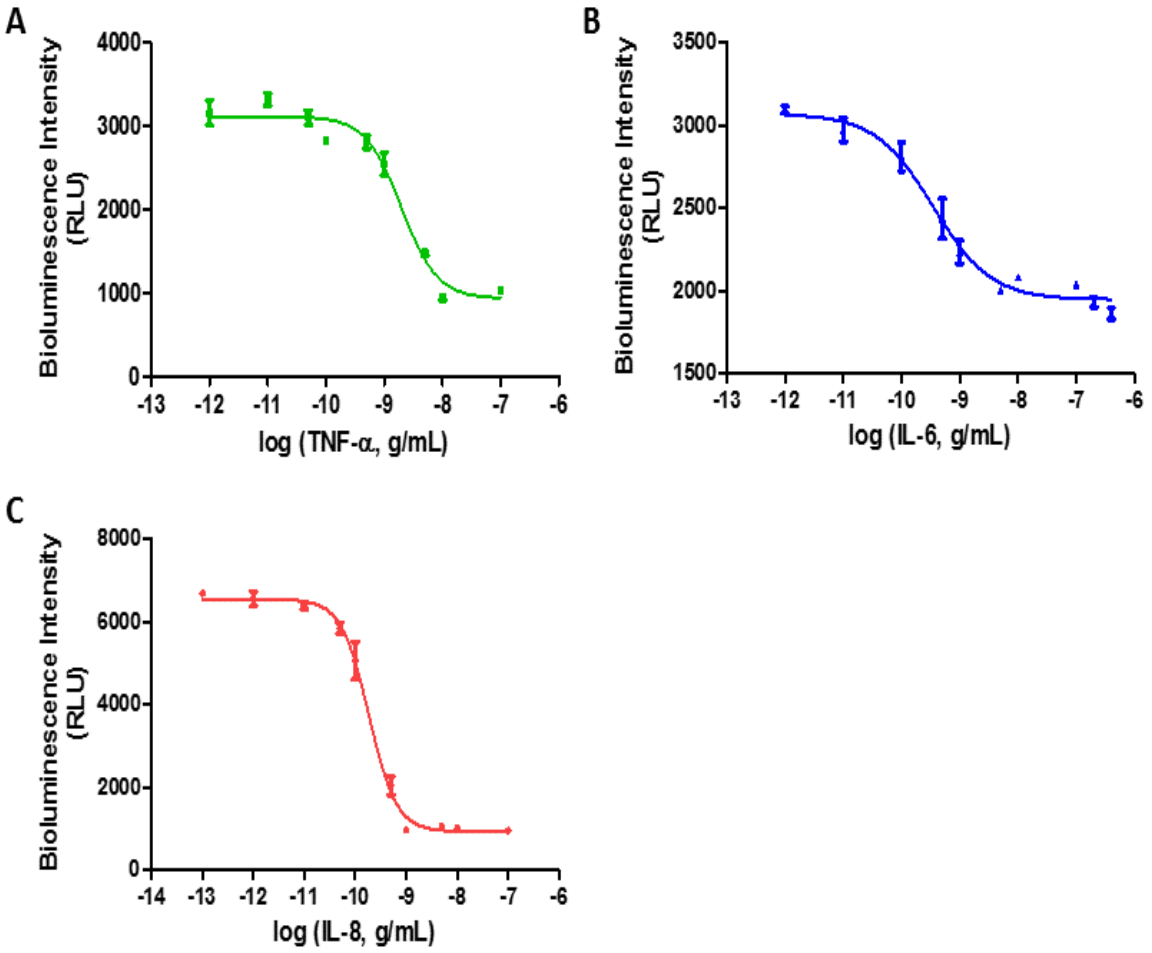

Figure 18. Simultaneous dose-response curves for the multiplexing cytokines in serum. The bioluminescence intensity from the specific channels was plotted against to the concentrations of the corresponding cytokines. (A) TNF-α. (B) IL-6. (C) IL-8. All points are the mean of three measurements ± one standard deviation. Error bar that are not visible are obstructed by the point. The coefficients of variability (CVs) of all the assays are smaller than 10. The coefficients of determination (R^2s) of all the assays are above 95%.

The reproducibility of all the assays has been verified. The intro-assay coefficients of variation (CVs) is smaller than 10, as well as the inter-assays CVs is smaller than 15. Finally, to demonstrate the accuracy of our multiplexed assay, we validated out newly developed multiplexed assay by determining the levels of TNF-α, IL-6 and IL-8 in the human serum spiked samples using both our newly developed multiplexed one pot assay and commercially available ELISA kits for each of the three individual cytokine. The levels measured by our multiplexed one pot assay were within 10% difference from those obtained with the three commercial ELISA assays for each individual cytokine, demonstrating validation of our one pot multiplexed assay against three individually proven commercial cytokine assays (**Table III**). For the validation, the p-values of TNF-α, IL-6 and IL-8 are 0.7331, 0.4488, and 0.2783 respectively, proving that the results from the bioluminescence-based assays and the ELISAs are not significantly different. The recovery rates of TNF-α, IL-6, and IL-8 are 112%, 119%, and 112% respectively.

Table III. Comparison of serum levels of TNF-α, IL-6 and IL-8 measured by the bioluminescent assay and ELISA kits.

	TNF-α (pg/mL)	IL-6 (pg/mL)	IL-8 (pg/mL)
Bioluminescent assay	563 ± 55	119 ± 8	60 ± 3
ELISA	547 ± 23	127 ± 2	62 ± 1
Difference	2.9%	6.3%	3.2%

2.5 Summary and significance

The increasing number of biomarkers available have helped to improve the precision and accuracy of diagnostics and management of disease. However, they also have placed a burden in patients who need to be drawn large volumes of blood for the detection of panels of biomarkers, a process that needs to be repeated as frequently as, on occasions, on a daily

basis if the patients require close management of their therapeutic regime or their disease progression. This has highlighted the need for small volume clinical analysis, which dictates that assays require reagents that achieve the detection limits needed while performing in a fast reproducible, sensitive manner in complex physiological samples. Moreover, it is important that those assays require little or no sample preparation and are simple as possible in order to be amenable for incorporation into miniaturized analytical platforms. In that regard, bioluminescent assays have emerged as great alternatives as more traditional colorimetric and fluorescent assays. Bioluminescent proteins, in that context, have shown that they can be used as labels in multiplexed detection, and could be key in the advancement of such detection systems that can incorporate several biomarkers in an assay. Indeed, the proven ability of bioluminescent proteins as labels in small volume assays (96) makes them ideal for use in miniaturized platforms. To that end, herein, we demonstrate the multiplexed detection of three cytokines in a bioluminescent assay format. Specifically, the system was able to respond quickly and efficiently in a dose-dependent manner over several orders of magnitude, including at physiological and elevated ranges for the target cytokine protein biomarkers of interest. Previously, dual-analyte bioluminescent assays have been reported either based on spectral or time resolved bioluminescent proteins. However, in this study, we have demonstrated that a combination of both, time and space-wavelength resolved aequorin mutants, impart enhanced multiplexing capabilities for the detection systems based on bioluminescence. The low background and high signal-to-background ratio of the emission of aequorin favors the analytical applications of aequorin as a detection probes for quantification in small volumes (70). Moreover, we have prior also demonstrated that bioluminescence-based detection is

compatible and amenable for incorporation into microfluidic platforms (8), an advantage that can be utilized in the development of biomarker detection in microfluidic devices. Herein, we have demonstrated that we have expanded the applications of the semi-synthetic aequorins from dual-analytes detection to the detection of three analytes simultaneously for the first time. As the protein engineering and signal detection techniques improve which can be forecasted, the library of semi-synthetic aequorins has high possibility to be expanded with proteins with emission properties shifted further, which definitely offer a novel tool for the establishment of multiplexed assays beyond detection of three biomarker analytes, and, thus, expand the potential of small volume clinical diagnostics and precise health monitoring systems.

Chapter 3: Detecting and imaging tumor cells *in vivo* using a bioluminescent probe

3.1 Overview

The forecast for cancer, despite all the encouraging advances in its diagnosis and treatment, is that it will remain as a major public health issue in the foreseeable future. Although the overall 5-year relevant survival rate has improved, the treatment efficacy of many cancers, such as pancreatic cancer, has not improved significantly, which is in part due to the lack of early diagnostic and detection methods. Current methods including magnetic resonance imaging (MRI), X-ray radiography, positron-emission computed tomography (PET/CT), and ultrasound (US) are either expensive or lack of sensitivity. Therefore, an ultra-sensitive technique that can detect, diagnose, and image tumors at the molecular level in their early stages is needed. In this research, we demonstrate a bioluminescence-based approach to detect and image different cancer cell lines both *in vitro* and *in vivo*. The bioluminescent protein Gaussia luciferase (Gluc), native from the marine copepod *Gaussia princeps*, was employed as the label, taking advantage of the attractive properties of its bioluminescence emission, including lack of requirement for an excitation source, high signal-to-noise ratio, smaller size, high sensitivity and low detections limits and its non-hazardous nature. In addition, the surface biomarker epidermal growth factor receptor (EGFR) that is overexpressed in various cancer cells was chosen as the binding target to target and home the bioluminescent probe and, thus, increase the specificity of the detection. Herein, Gluc was genetically conjugated to the recognition molecule human epidermal growth factor (EGF), the ligand of EGFR, to construct a bioluminescence-EGRF targeting probe for the cancer cells. The EGF-Gluc fusion protein was employed to detect three common cancers,

namely, head and neck squamous cell carcinoma (HNSCC), breast cancer, and pancreatic cancer, with high sensitivity, specificity, and resolution.

3.2 Introductory remarks

Cancer is the second leading cause of death in the United States, right after cardiovascular disease, and it is forecasted that it will remain as a major public health issue in the foreseeable future. According to the statistics provided by the National Cancer Institute (NCI), which is part of the National Institutes of Health (NIH), around 14 million new cases were reported worldwide with 8.2 million deaths in 2012 (https://www.cancer.gov/about-cancer/understanding/statistics). Furthermore, the estimated annual cost of cancer-related medical care for 2020 will increase to 150 billion dollars.

The relentless efforts and discoveries of the scientific and medical community, have resulted in an increase in the overall 5-year relevant survival rate to 66.9%, albeit with significant variations among different types of cancer. For instance, the average 5-year survival rates of lung cancer and pancreatic cancer are 17.7% and 7.7%, respectively (97) (http://seer.cancer.gov/csr/1975_2013/). Since the survival rate of the disease largely depends on the stage when it is first diagnosed and when the reoccurrence is discovered, an ultra-sensitive method that can detect, diagnose, and even visualize the cancer cells at an early stage has great potential to improve the treatment efficacy and the survival rate.

Conventional detection methods include magnetic resonance imaging (MRI), X-ray radiography, positron-emission computed tomography (PET/CT), and ultrasound (US) (98-101). These detection methods require expensive equipment that increase the financial burden of the health system, especially in developing countries. They also require long

measurement periods and highly trained personnel to operate the expensive equipment preventing them from being employed in the high-throughput screening of populations. In addition, these methods mostly depend on the morphological, structural, and physiological changes at the tissue level, and therefore, lack the ability to detect and monitor cancer at a very early stage before the formation of the macroscopic changes caused by the diseases.

On the other hand, optical methods including fluorescence and bioluminescence have been employed to characterize the biological process at the molecular level, detect cancer cells with low detection limits, and monitor the disease status *in vivo* (102-106). For instance, Heath *et al.* labeled a monoclonal antibody against the epidermal growth factor receptor (EGFR) (panitumumab) with a near-infrared (NIR) fluorescent dye (IRDye800-CW) to image head and neck squamous cell carcinoma (HNSCC) in mice, thereby improving the surgery resection effect (107). Even though fluorescence-based *in vivo* imaging has shown promising results, the early detection of cancer cells is still a problem mainly caused by autofluorescence and photobleaching in mammalian tissues, which decreases the sensitivity of fluorescence as a detection probe. Thus, a novel technique that can offer rapid, affordable, sensitive, and accurate detection, imaging, and diagnosis at the molecular level is needed to tackle these issues. In response to this, we demonstrate a bioluminescence-based approach to detect and image cancer cells both *in vitro* and *in vivo* using the bioluminescent protein *Gaussia* luciferase (Gluc) as the label.

As explained in the prior chapters, bioluminescence is suitable for ultra-sensitive bioanalysis and high-contrast imaging due to its low background and high signal-to-noise ratio in physiological fluids and mammalian tissues (8, 108). Bioluminescence is a phenomenon of light emission generated through an oxidative chemical reaction without

the need for an external excitation energy source, and therefore, eliminates the background signals caused by the excitation process, yielding high signal-to-background ratio. Driven by this unique advantage, bioluminescent proteins have been employed as detection labels in various bioanalytical applications such as calcium detection, various immunoassays, hybridization assays, *in vivo* imaging, BRET assays, and drug discovery (18, 109-112). In addition, the improvements in the imaging instruments, such as the IVIS system (113-115) and bioluminescence tomography (BLT) (116) also spur the *in vivo* applications of bioluminescence as the imaging reagent for sensitive detection, accurate quantification and localization of the tumor growth not only in mice, but also in larger animals. Moreover, bioluminescent proteins are amenable to being engineered and tailored, either genetically or chemically to enhance them with improved characteristics, such as shifted emission wavelength and specific target recognition capabilities. Also, bioluminescent proteins are safe to handle and non-toxic to living organisms (8), significantly improving their uses in *in vivo* pre-clinical applications as well as clinical trials. For example, Cacivis technology, a medical device company, has employed a bioluminescent photoprotein for the detection of trace amounts of free calcium ions demineralized from the tooth surface and, for the first time, completed a clinical trial using bioluminescence, demonstrating its biocompability and sensitivity (http://www.calcivis.com). These unique beneficial properties of bioluminescent proteins highlight its great potential for use as successful next generation detection probes. In this research, the bioluminescent protein Gluc was genetically linked to the recognition molecule human epidermal growth factor (EGF), the ligand of epidermal growth factor receptor (EGFR), to construct a fusion protein EGF-Gluc for the detection

of three common cancers including head and neck squamous cell carcinoma (HNSCC), breast cancer, and pancreatic cancer.

Bioluminescent proteins are comprised of two main groups including photoproteins and luciferases (7). Gluc is originally found in the marine copepod *Gaussia princeps*. It catalyzes the oxidation of the luciferin, the imidazopyrazine chromophore coelenterazine, accompanying with the emission of a blue light with the emission maximum at 480 nm (117). It has been touted that the favorable properties of Gluc may make it surpass other bioluminescent proteins as the preferred reporter protein for biomedical and bioanalytical applications. First, Gluc is a small protein, a 19.9 kDa protein composed of 185 amino acids, and due to its small size compared to the luciferase proteins, its *in vitro* production is easier and its *in vivo* transportation and diffusion (118) are greatly enhanced. Moreover, Gluc has the highest light output among all the commonly used luciferase proteins, which is 1000-fold higher than firefly luciferase (Fluc) and *Renilla* luciferase (Rluc) (119, 120). Also, Gluc is structurally stable due to its high number of disulfide bonds formed by the ten cysteines in its amino acid sequence (118). Moreover, the signal emitted by Gluc can be detected by various types of instruments, such as luminometers and IVIS system with very high sensitivity and contrast. The emission is intense enough to be captured by cost-efficient equipment such as normal digital cameras and can even be visualized by the naked eye. Last but not least, protocols to express the active form of Gluc in both, in vitro *E. coli* system and *in vivo* mammalian cells, in high yields have been developed (121, 122). Thus, although the crystal structure of Gluc has not been fully identified, this protein has been used as a signal generator in a broad range of bioanalytical applications, taking advantage of all its attractive properties. Gluc has been widely used in the design and development of

ultra-sensitive detection assays, monitoring *in vivo* biological processes and observing real-time *in vivo* imaging, all of which contribute to real-time disease management (123-125).

EGFR is a 170 kDa transmembrane protein, which is the surface receptor for the EGF family and belongs to the human epidermal receptor (HER) (ErbB) family of receptor tyrosine kinases (RTK) (126). EGFR has been shown to be overexpressed in a variety of cancer cells, and thus, has been extensively employed as the diagnostic biomarker and a therapeutic target for cancer treatment (126, 127). A monoclonal antibody of EGFR (cetuximab) has been approved as targeted therapy of HNSCC by the US Food and Drug Administration (FDA) (128). Therefore, EGFR has been selected as the binding target of the EGF-Gluc fusion protein to demonstrate its capability in the tumor detection.

Herein, the bioluminescent protein Gluc and EGF, the ligand of the surface biomarker EGFR, were chosen to construct a bioluminescence-based cancer detection and imaging probe. To that end, EGF was genetically conjugated to Gluc resulting in Gluc-labeled EGF fusion protein. The fusion protein EGF-Gluc was employed to detect three common cancer types including HNSCC, breast cancer, and pancreatic cancer *in vitro* and *in vivo*. This research proves that bioluminescent proteins especially Gluc have a great potential to be applied in ultra-sensitive cancer detection and high-contrast imaging to diagnose diseases at an early stage (**Figure 19**).

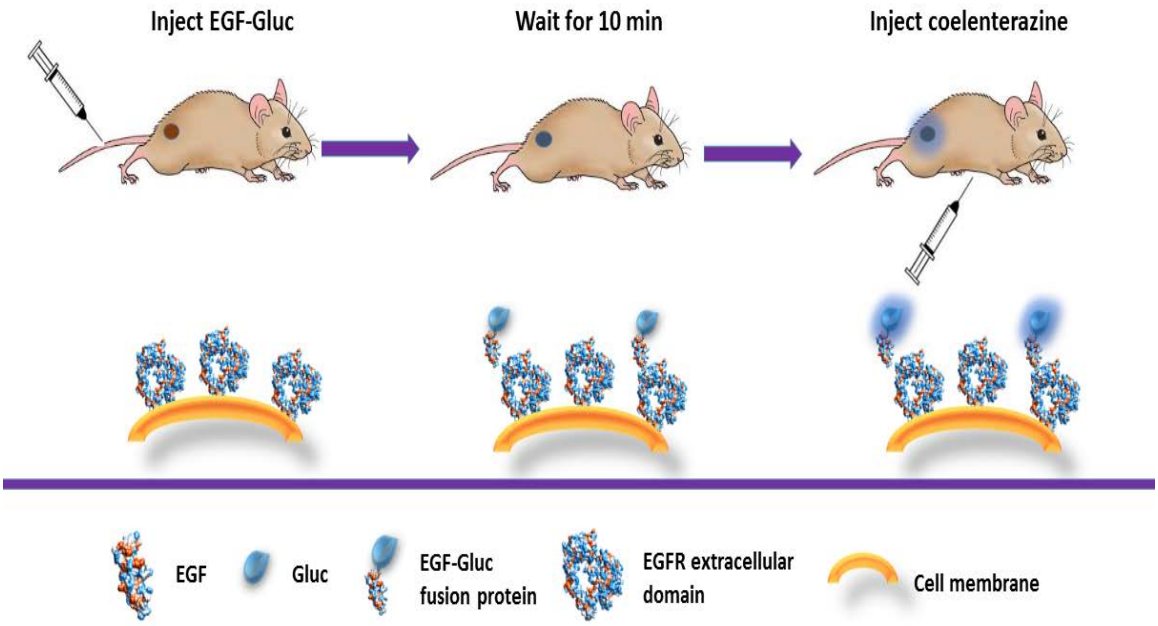

Figure 19. The scheme of imaging tumors *in vivo* using the EGF-Gluc fusion protein.

3.3 Experimental section

3.3.1 Reagents

Luria-Bertani (LB) Agar and LB Broth were purchased from EMD Millipore (Billerica, MA). Disodium ethylenediaminetetraacetate (EDTA) was purchased from CalBiochem (Santa Diego, CA). Agarose, ampicillin sulfate, and sodium phosphate were purchased from Amresco (Solon, OH). Plasmid mini-prep kits and Ni-NTA agarose were purchased from Qiagen (Valencia, CA). Bench top 1Kb DNA ladder was purchased from Promega (Madison, WI). Sodium dodecyl sulfate (SDS) and Tris(hydroxymethyl)amino methane (Tris) free base were purchased from J. T. Baker (Center Valley, PA). Tween-20 was purchased from VWR (Radnor, PA). Isopropyl-beta-D-thiogalactoside (IPTG) was purchased from Gold Biotechnology (St. Louis, MO). Sodium chloride and glycerol were purchased from BDH Chemicals (distributed by VWR, West Chester, PA). SDS-page and

precision plus protein dual color standards were purchased from BIO-RAD (Hercules, CA). Native coelenterazine was ordered from Prolume (Hayward, CA). The phosphate buffer saline (PBS) tablets were purchased from Invitrogen (Camarillo, CA). BCA protein assay reagent (bicinchoninic acid) was from Pierce Biotechnology (St. Louis, MO). The Dulbecco's Modified Eagle Medium (DMEM) cell medium, the Leibovitz's L-15 (L-15) medium, the Eagle's Minimum Essential Medium (EMEM), and the RPMI media 1640 were purchased from Gibco by life technology (Grand Island, NY). Imidazole, fetal bovine serum (FBS), Penicillin-Streptomycin (Pen Strep), and Trypsin-EDTA were purchased from Sigma Aldrich (St. Louis, MO). The MDA-MB-468 cell line and the THP1 cell line were purchased from ATCC (Manassas, VA). The gene of EGF was purchased from GenScript. The CAL-27 cell line was kindly provided by Dr. Franzmann. The EGF-Gluc fusion protein expression vector was developed previously in our lab. The mouse models transplanted with pancreatic tumor and triple-negative breast tumor were kindly provided by Dr.Jimenez. All chemicals were reagent grade or better. All aqueous solutions were prepared using 18 MΩ deionized distilled water produced by the PURELAB flex system from ELGA LabWater (Wohlen, UK).

3.3.2 Apparatus

DNA agarose gels were run by the Kodak BioMax system (Rochester, NY). DNA electrophoresis gels were visualized with a UV Transilluminator (UVP, Upland, CA). The sterile buffers and tools were sterilized by Harvey SterileMax Sterilizer. *E. coli* bacteria culture, for the purpose of expressing our fusion protein, was incubated in the Fisher Scientific orbital shakers (Fair Lawn, NJ). The optical densities (OD) were measured using a Spectronic 21D UV-Vis Spectrophotometer (Ivy Land, PA). The *E. coli* culture that

expressed the protein and the cell lysates were centrifuged using a Beckman Coulter Avanti J-E centrifuge (Palo Alto, CA). The harvested *E. coli* cells were lysed using a Fisher Scientific 550 dismembrator (Pittsburgh, PA). Purified proteins were concentrated by Centrifugal Filter Units Amicon Ultra 10K from Millipore (Darmstadt, Germany). The concentrated protein was dialyzed into the buffer needed by Slide-A-Lyzer Dialysis Cassettes from Thermo Scientific (Rochford, IL). Bioluminescence intensity and decay kinetics were measured by the ClarioStar luminometer from BMG Labtech (Cary, NC). The emission spectra were recorded using a liquid cooled CCD that was custom built by Science Wares Inc (Falmouth, MA). All the mammalian cell cultures were handled in the biosafety safety cabinet from Labconco (Kansas City, MO). All the mammalian cell cultures were incubated in the New Brunswick Galaxy 170S CO_2 incubator from Eppendorf (Hamburg, Germany). The mammalian cells were centrifuged by the Beckman coulter Allegra X-15R centrifuge (Palo Alto, CA). The mammalian cells were observed by OptixCam Summit series P95-C from Microscope (Roanoke, VA). All the cell lines were stored in the VWR CryoPro Canister Storage Tank (Radnor, PA). The in vivo imaging was taken by a Nikon digital camera DSRL (Melville, NY). The bioluminescence intensity was measured using a custom-made instrument constructed with a light-tight chamber and the fiber optic system (FOs). The light intensity was processed with our custom software to firm the bioluminescence imaging.

3.3.3 Engineering, expression and purification of the fusion protein EGF-Gluc

The gene of the EGF-Gluc fusion protein was prepared by Yu-ping Yang. The gene of Gluc was linked to the 3′ end of the gene of EGF genetically through an overlap extension PCR, with a linker composed of serine and glycine (GSSSSGSSSSG). The sequence of

EGF was amplified with the EGF forward primer that introduced a *Nde*I enzyme site on the 5′ end, and the EGF reverse primer that introduced the linker. The sequence of Gluc was amplified using the Gluc forward primer that introduced the linker sequence, and the Gluc reverse primer that introduced a *Kpn*I enzyme site on the 3′ end of the Gluc gene sequence. The amplified products were purified and then combined as the template for the overlap PCR. The mixed products were conjugated using the overlap PCR with the EGF forward primer and the Gluc reverse primer to obtain the gene of the fusion protein EGF-Gluc. The steps of the PCR reaction were started at 95 ºC for 2 min for polymerase activation, and then repeated for 25 cycles for the next steps, 95 ºC for 20 s, and 65 ºC for 10 s, followed by 70 ºC for 30 s, and completed at 70 ºC for 10 min. All the primer sequences are listed in **Table IV**.

Table IV. Primer sequences for each overlap PCR for the construction of the EGF-Gluc fusion protein

Primer	Sequence (5′-3′)
EGF Forward	GAGTCATAACATATGAATAGCGATTCTGAGTGTCCGCTGAGC
EGF Reverse	GGAAGAGCCGCTGCTGCTGGAGCCTGATGAGGAAGAACGCAGTTCCCACCATT TCAGATCGCG
Gluc Forward	GGCTCCAGCAGCAGCGGCTCTTCCTCAAGTGGCATGAAACCGACCGAAAATAA TGAAGAC
Gluc Reverse	CGGGGTACCTTAATCACCACCTGCACCTTTGATTTTGTCCA

The gene of the fusion protein was inserted into the pCold plasmid. The gene sequence was confirmed by sequencing at the Sylvester Comprehensive Cancer Center Oncogenomics Core Facility at the University of Miami. The plasmids were then

transfected into BL21(DE3) *E. coli* cells. The cells containing the EGF-Gluc plasmids were grown through shaking at 250 rpm at 37 ºC in 500 mL LB broth containing 100 µg/mL ampicillin to an OD_{600} ~ 0.6 in the incubator. The cells were then incubated on ice for 1 h using cold shock for the increased yield of the fusion protein. Then IPTG was added into the medium to a final concentration of 1 mM to induce the expression of the protein. The *E. coli* cells were then incubated while shaking at 250 rpm at 15 ºC for two days for the protein expression. The cells were then resuspended in the Ni-NTA native lysis buffer (50 mM NaH_2PO_4 pH 8.0, 300 mM NaCl, and 10 mM imidazole buffer) and lysed by using a sonicator. The lysate was centrifuged again to remove the cell debris. The expressed protein was then purified using immobilized metal affinity chromatography (Ni/NTA). The protein containing lysis buffer was loaded into a gravity column containing Ni/NTA Agarose beads. A sequential washing with buffers of 50 mM NaH_2PO_4 pH 8.0, 300 mM NaCl, and 20, 50 and 70 mM imidazole, was performed on the column. EGF-Gluc was then eluted using the elution buffer (50 mM NaH_2PO_4 pH 8.0, 300 mM NaCl, and 100 mM imidazole). All the fractions containing pure protein (the purity was determined by SDS-PAGE) were pooled together and filtered through a 10K membrane to remove excess imidazole and to concentrate the protein sample. The concentrated EGF-Gluc was then dialyzed in phosphate buffered saline (PBS) with 10 mM sodium phosphate pH 7.5 and 150 mM NaCl (buffer G) for 24 h to change the buffer for the further use on the mammalian cells, and stored at 4 ºC for short-term and at -20 ºC for long term storage. The protein concentration was determined using Pierce BCA protein assay kit following the manufacturer's instructions.

3.3.4 Decay kinetics of EGF-Gluc

The bioluminescence decay kinetics of EGF-Gluc with native coelenterazine analogue was determined using the ClarioStar luminometer. A volume of 10 µL of EGF-Gluc solution was loaded into one well of a 96-well microtiter with in triplicates. Then the emission intensity was collected by the luminometer upon the injection of 100 µL the coelenterazine solution (2.0 µg/mL). The light intensity was recorded for 50 s with readings taken every 0.2 s. The intensity was then imported into the software Grahpad Prism 5.0 for the calculation of the half-life through the non-linear, one phase exponential decay fitting.

3.3.5 Emission spectrum of EGF-Gluc

The emission spectrum of EGF-Gluc was performed using a custom made SpectroScan luminometer containing a liquid cooled Andor CCD detector. The emission signals at different wavelengths (400-700 nm) were measured upon the injection of 100 µL of the coelenterazine solution (2.0 µg/mL) for 5.250 s. The intensity and the wavelengths were then imported into the Microsoft Excel for the calculation of the emission maximum which is the wavelength corresponding to the highest light intensity.

3.3.6 Concentration optimization of the EGF-Gluc fusion protein

The EGF-Gluc fusion protein was serially diluted using Buffer G, and then a volume of 100 µL of each dilution was added to each well of the 96-well microtiter plate in triplicates. The bioluminescence intensity was measured using the ClarioStar luminometer for the duration of 10 s upon the injection of a volume of 100 µL of buffer containing native coelenterazine at a concentration of 2.0 µg/mL into each well. The bioluminescence intensity was imported into GraphPad Prism 5.0 to determine the optimized concentration.

3.3.7 Cell culture

The HNSCC CAL-27 cells were cultured in the DMEM, high glucose, GlutaMAX(TM), pyruvate medium supplemented with 10% FBS and 100 units/ml Pen Strep. The breast cancer MDA-MB-468 cells were cultured in the L-15 medium supplemented with 10% FBS and 100 units/ml Pen Strep. The breast cancer MCF-7 cells with reduced EGFR expression were cultured in the EMEM medium supplemented with 10% FBS, 0.01 mg/mL human recombinant insulin, and 100 units/mL Pen Strep. The negative control THP1 cells with reduced EGFR expression were cultured in the RPMI media supplemented with 10% FBS and 100 units/mL Pen Strep. All the cell lines were incubated at 37 ºC with 5% CO_2. The media of all cell lines was refreshed every two to three days.

3.3.8 Distinguishing cancer cells and normal cells with the EGF-Gluc fusion protein

The bioluminescence emissions from the EGF-Gluc treated EGFR overexpressed cancer cells and negative control cells with little EGFR expression were compared. A volume of 100 µL of the EGF-Gluc fusion protein with the concentration of 5.0×10^{-8} M (determined from the concentration optimization step) was added to 1.0×10^{6} MDA-MB-468, MCF-7, CAL-27, and THP1 cells and incubated for 30 min at room temperature. The cells were then centrifuged and the buffer containing the unbound protein was removed by aspiration. The wells were washed with 200 µL DPBS for three times. The cells were then diluted to the desired numbers with buffer A. The bioluminescence intensity was measured by using the ClarioStar luminometer with an integration time of 10 s following the injection of a volume of 100 µL of the coelenterazine solution into each well. The bioluminescence intensity was imported into GraphPad Prism 5.0 to compare the light intensity between the EGFR overexpressed cells and the negative control.

3.3.9 Detecting EGFR overexpressing HNSCC CAL-27 cells using EGF-Gluc

The capability of the EGF-Gluc fusion protein to detect the HNSCC cell was investigated. For this study, a volume of 100 µL of EGF-Gluc protein with the concentration of 5.0 x 10^{-8} M was added to 1.0 x 10^{6} CAL-27 cells in 100 µL DPBS, and allowed to incubate for 30 min at room temperature. After the incubation, the cells were serially diluted in DPBS buffer to 1.0 x 10^{5}, 5.0 x 10^{4}, 1.0 x 10^{4}, 5.0 x 10^{3}, and 1.0 x 10^{3} cells per mL. Then a volume of 100 µL of each dilution was loaded into each well of a 96-well microtiter plates. Each well contained 1.0 x 10^{4}, 5.0 x 10^{3}, 1.0 x 10^{3}, 5.0 x 10^{2}, and 1.0 x 10^{2} cells respectively. Then the cells were centrifuged down, and the buffer containing the unbounded protein was aspirated. The wells were then washed with 200 µL DPBS for three times to remove the unbound fusion protein. After washing, the bioluminescence intensity was measured using the ClarioStar luminometer for the duration of 10 s upon the injection of a volume of 100 µL of the coelenterazine solution into each well. The bioluminescence intensity was imported into GraphPad Prism 5.0 to generate the detection curve for the CAL-27 cells.

3.3.10 *In vivo* bioluminescence imaging

The bioluminescence imaging using the EGF-Gluc fusion protein as the targeted imaging reagent was also investigated. 100 µL of 1.0 mg/mL EGF-Gluc fusion protein was injected into the tumor bearing nude mice through the tail vain, and the mice were anesthetized in a clear Plexiglas anesthesia box with the mouse anesthesia cocktail (1.5 mg ketamine/20 grams and 0.3 mg xylazine/20 grams. The fusion protein was allowed bind to the receptors on the tumor cells for 10 min, followed by the addition of the coelenterazine solution (< 1.0 mg/g of body weight). After 30 s of the coelenterazine addition, the bioluminescence emission was measured with a digital camera and a fiber optic system (FOs) at various

locations of the mice. The light intensity was processed with a custom software to accomplish the bioluminescence imaging for quantification and localization.

3.4 Results and discussion

In this study, we demonstrated a bioluminescence-based method as a platform for ultra-sensitive cancer cell detection for the targeted, high-resolution, non-invasive, and quantitative *in vivo* imaging of cancer cells in nude mouse models.

As mentioned above, our goal was to develop technologies that are cost-effective, easy to use and highly sensitive to aid in the early stage diagnosis of cancer and increase the survival of patients suffering from this devastating disease. In that regard, we genetically fused the bioluminescent protein Gluc and the recognition molecule EGF to construct a novel imaging reagent, aiming at imaging tumors in cancer mouse models. This fusion protein EGF-Gluc successfully maintained both the bioluminescence signal generating ability of Gluc and the targeted binding ability of EGF to EGFR. In that regard, we demonstrated that EGF-Gluc was able to recognize and specifically bind to the EGFR-overexpressed in cancer cells *in vitro* in cell lines and *in vivo* in mouse animal model of three different types of cancer, which demonstrated the feasibility of employing bioluminescence in high-resolution imaging and ultra-sensitive detection.

The crystal structures of human EGF and the extracellular domain of EGFR are shown in **Figure 20**. The genetic sequence of Gluc was fused to the C-terminus of EGF through an overlap extension PCR (**Figure 21**). Then, the sequence of the resulting fusion-protein EGF-Gluc was ligated into a cold-induced expression system pCold to increase the yield of the soluble portion of the expressed protein. The pCold plasmids containing the gene of EGF-Gluc were transfected into the *E. coli* BL21(DE3) strain for the optimal expression.

The fusion protein was purified through using immobilized metal affinity chromatography and the purity of the protein was verified by protein SDS-PAGE (**Figure 22**).

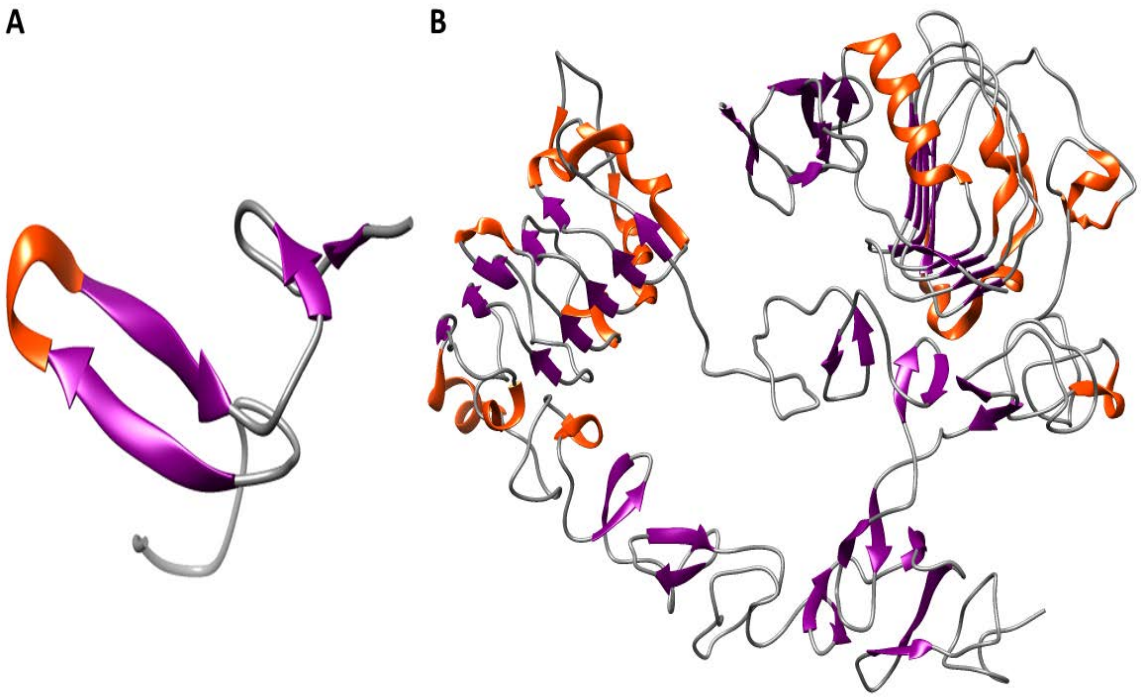

Figure 20. Crystal structures of (A) Human EGF (PDB ID Code: 1JL9) and (B) Extracellular domain of EGFR (PDB Code: 1NQL)

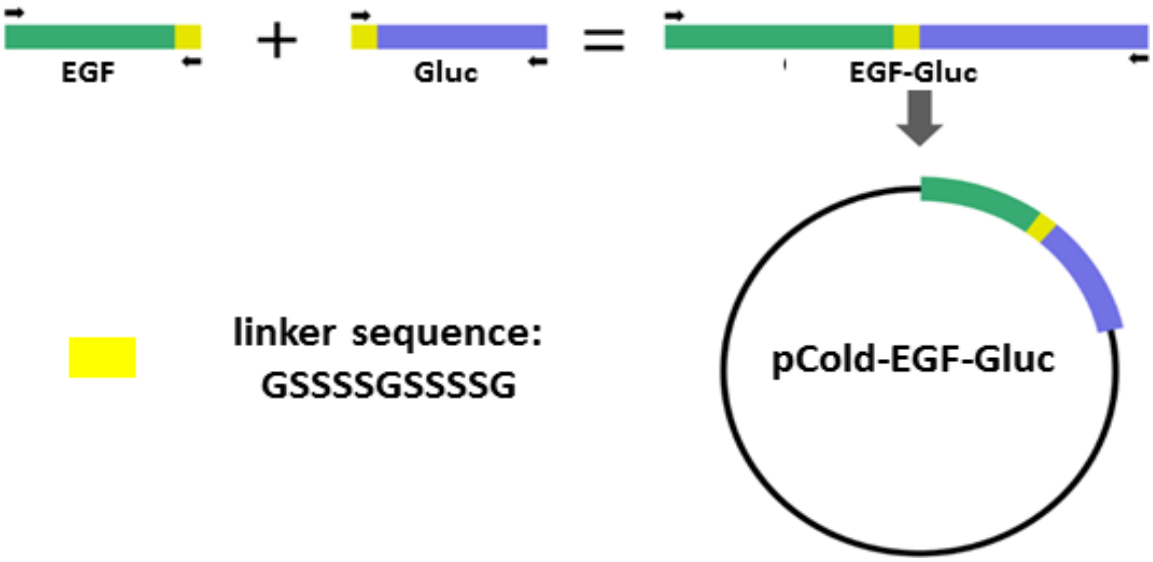

Figure 21. The scheme of the overlap extension PCR. The green blocks represent the gene of EGF. The blue blocks represent the gene of Gluc. The yellow blocks represent the gene of the linker.

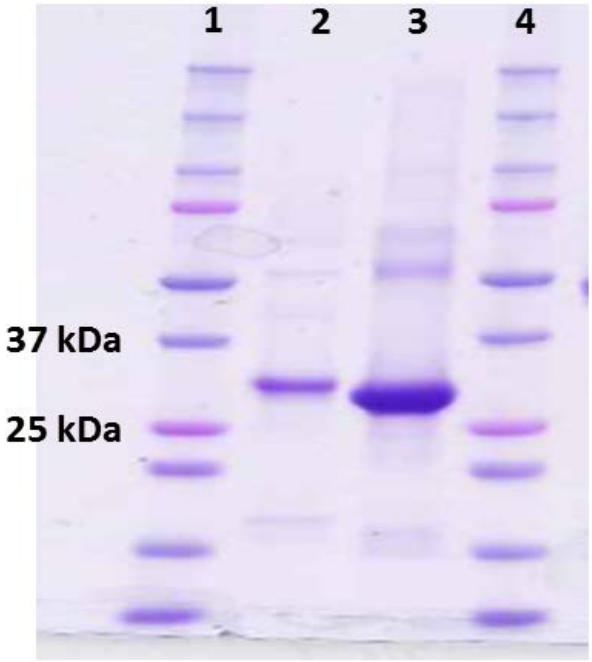

Figure 22. SDS-PAGE of the fusion protein EGF-Gluc. Lane 1 and lane 4 contained Precision Plus Protein Dual Color Standard (Bio-Rad Laboratories Inc., Hercules, California). Lane 2 contained the fusion protein EGF-Gluc. Lane 3 contained concentrated EGF-Gluc.

The purity of the protein was verified by SDS-PAGE, which showed the presence of a pure protein band with an apparent molecular weight of around 30 kDa which is consistent with the molecular weight of the EGF-Gluc fusion protein (GLuc with Hig-tag from pCold is 22 kDa and EGF is 6.2 kDa).

In addition, the maximum wavelength of the bioluminescence emission and the decay kinetics of the EGF-Gluc fusion protein along with the native coelenterazine were determined to characterize its bioluminescence properties. The emission properties of the fusion protein and the wild type Gluc were also compared to test the potential effect of the genetic fusion on the bioluminescence characteristics (**Table V)**; the bioluminescence emission properties of Gluc had been previously reported by Hunt *et al.* (129).

Table V. Bioluminescence maximum wavelengths and half-lives of the fusion protein EGF-Gluc and Gluc complexed with native coelenterazine.

Protein	Coelenterazine	Emission max (nm)	Half-life (s)
EGF-Gluc	native	487	7.8
Gluc	native	480	7.0

The concentration of the fusion protein used in the *in vitro* study was also investigated. EGF-Gluc was diluted to various concentrations with PBS buffer. The bioluminescence emission intensity was measured using a microtiter plate luminometer ClarioStar upon the injection of the native coelenterazine solution (2.0 μg/mL in PBS). The signal intensity was plotted against the concentrations of the fusion protein. We selected 5.0×10^{-8} M as the concentration for the remainder of the *in vitro* study because it is close to the maximum linear value of the dilution plot which can increase the detection sensitivity without much waste.

Then the binding affinity of the fusion protein EGF-Gluc to its receptor EGFR was investigated. For this purpose, two different cancer cell-lines that overexpresses EGFR on their cell surface, head and neck squamous cell carcinoma (HNSCC CAL-27) and breast cancer cell line MDA-MB-468 were chosen. On the other hand, the monocyte THP1 cell line with low EGFR expression was chosen as the negative control. In addition, human breast adenocarcinoma cell line (MCF-7) with low EGFR expression level (130) was chosen as the negative control for EGFR overexpressed breast cancer cells specifically.

An aliquot of 5000 CAL-27 cells were treated with (5.0×10^{-8} M) EGF-Gluc in an Eppendorf test tube. The same number of THP1 cells were also exposed to the same conditions and used as the negative control. After an incubation of 30 min the excess fusion protein was washed using PBS buffer. The cells were transferred into the wells of a 96-well plate. A solution of coelenterazine was added into each well and the resulting bioluminescence was measured. The bioluminescence signals from 5000 EGF-Gluc treated CAL-27 cells and THP1 were compared with t-test using GraphPad Prism version 5.0 (**Figure 23 A**). Similar experiments were performed using 1000 MDA-MB-468 cells and MCF-7 cells and the light signals were compared using the same software (**Figure 23 B**). The bioluminescence intensity from the cancer cells was significantly higher ($p<0.0001$) than the signal from the control cells, demonstrating the targeted binding of the fusion protein to the EGFR expressed on the surface of cells.

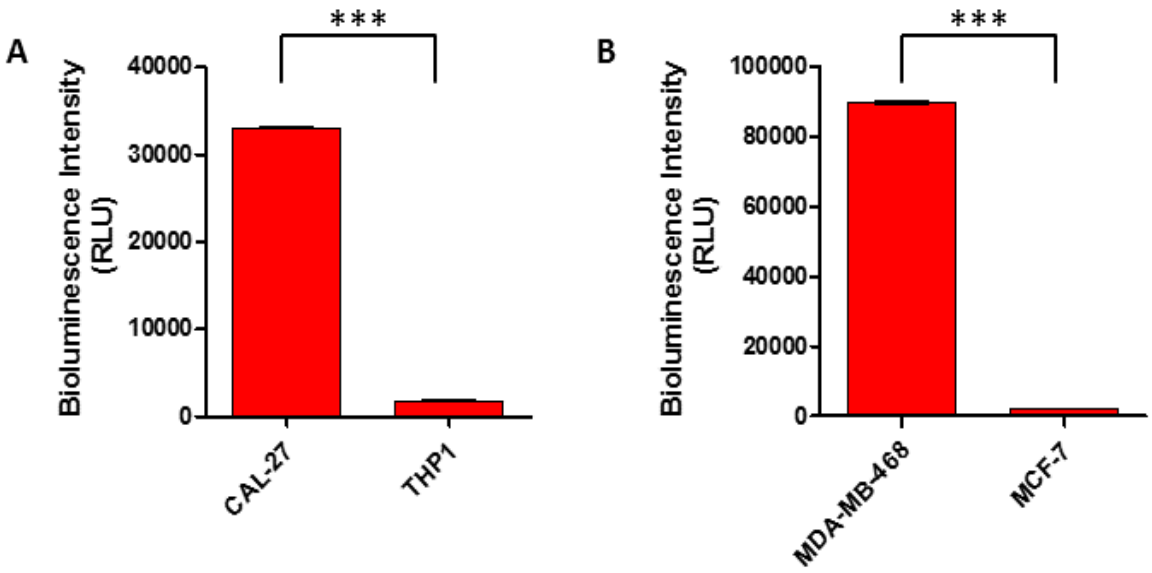

Figure 23. (A) Bioluminescence intensity from 5000 EGFR-overexpressed CAL-27 cells and EGFR-negative THP-1 labeled with EGF-Gluc. (B) Bioluminescence intensity compared between 1000 EGFR-overexpressed MDA-MB-468 cells and MCF-7 with low EGFR expression. All data columns represent the mean of three replicates ± one standard deviation. *** $p<0.0001$

An additional experiment was performed to confirm the targeting of the fusion protein EGF-Gluc to the cancer cells expressing the EGF receptors in cell lines. A Gluc solution was added into 1.0×10^6 CAL-27 cells to a final concentration of 5.0×10^{-8} M and incubated for 30 min at the room temperature. After the wash step to remove unbound fusion protein, CAL-27 cells now labeled with Gluc were serially diluted to concentrations ranging from 1.0×10^2 to 1.0×10^4 cells/100 µL. The bioluminescence intensity from each well was collected and plotted to establish a relationship between the light intensity and the cell counts (**Figure 24**).

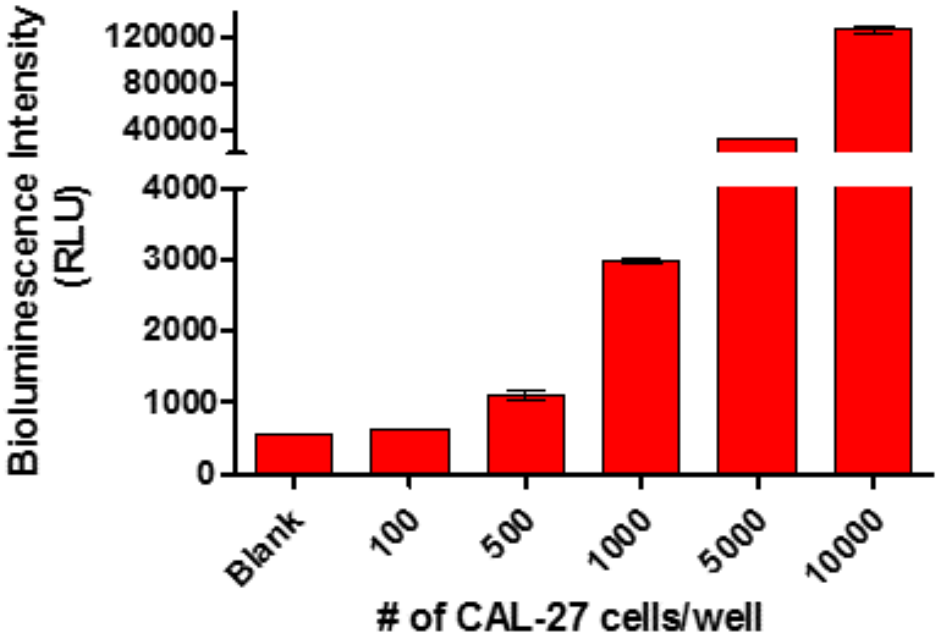

Figure 24. Bioluminescence emission from the EGFR-overexpressed CAL-27 cells labeled with EGF-Gluc. All the columns are the mean of three replicates ± one standard deviation.

The results showed that the bioluminescence intensity increased as the number of cancer cells increased, and the light intensity from 500 cancer cells was significantly above the background signal ($p=0.0014$). The particular *in vitro* experiment demonstrated the binding of the fusion protein to the EGFR-overexpressed cells. This experiment also demonstrated that bioluminescent labels have the potential to be employed to develop sensitive detection platforms for cancer cells *in vitro* in cell lines. Moreover, the targeted biomarkers and the bioluminescent labels can be chosen to tailor specific cells and detection needs. For example, the EGF portion of the fusion protein can be replaced with a different selective targeting moiety for the type of cancer cell line of interest.

We also have investigated the feasibility of using bioluminescent labels to image and localize tumor/lesion sites in animal models. We have selected pancreatic and breast cancer

as our model systems because pancreatic cancer continuously has the lowest 5-year survival rate, while breast cancer is the most common cancer in North America. Tumors for pancreatic cancer and triple-negative breast cancer were grown in xenograft mouse models to investigate the feasibility of the non-invasive, *in vivo*, detection. For this study, a Nikon digital single lens reflex (DSLR) camera was used to take photographs and image the light emission from the tumors. Also, a first-generation, custom-built instrument, which was constructed in our lab by combining a dark light-tight chamber and a fiber optic system (FOs), was employed to measure externally the bioluminescence intensity, emitted from the tumors, in a quantitative manner. Briefly, a volume of 100 μL of the fusion protein EGF-Gluc with a concentration of 1.0 mg/mL was injected to the tumor-bearing nude mice through the tail vein and was allowed to bind to the tumor sites for 10 min. The coelenterazine solution (< 1.0 mg/g of body weight) was then injected into the animals by intraperitoneal injection (IP injection) and allowed to diffuse for 30 s. After that, the bioluminescent signals from different sites were imaged using the digital camera to take a photo. The light emitted was quantified by placing the FOs on top of the tumor site and collecting the light with the FOs that is equipped with custom software to localize and quantify the light intensity. The results obtained by imaging the pancreatic tumor and the triple-negative breast cancer are displayed in **Figures 25** and **26,** respectively.

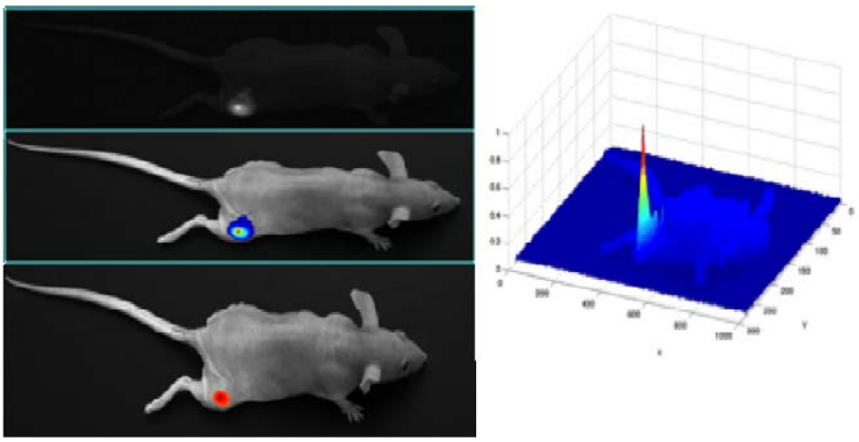

Figure 25. Image of the mouse showing the transplanted pancreatic tumor by the bioluminescence emitted by the fusion protein EGF-Gluc bound at the EGFR receptors on the tumor cells. Top: Image of the light emission obtained with the digital camera. Middle: Processed image collected using the light-tight chamber/FOs and a digital camera, and processed with a custom software showing the localization and quantification of the light intensity emitted by the tumor. Bottom: Processed image showing the localization and intensity of the bioluminescence peak. Right: Mesh plot of the light emission of the tumor site in relation to the whole body.

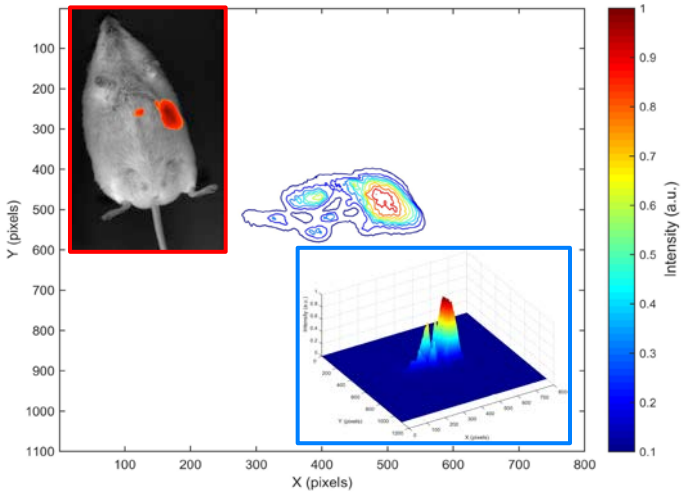

Figure 26. Image of the mouse with a transplanted triple-negative breast tumor and metastasized (smaller) tumor labeled by the binding of the EGF-Gluc fusion protein with the EGFR receptors on the surface fo the tumor cells. Top: Processed image measured using the light-tight chamber/FOs and a digital camera, and processed with a custom software showing the localization and quantification of the light intensity. Middle and bottom: contour and mesh plot of the light emission of the tumor site in relation to the whole body.

The results showed that both tumors were detected, localized, and imaged using the digital camera. The emitted light intensity was quantified using our custom instrument. Since the emitted bioluminescence is only observed around the grafted tumor sites, while other locations including the reagent injection sites showed little or no bioluminescence emission, our targeting of Gluc-EGF to the EGFR receptors in the tumor sites in mouse models is very specific. The light intensity of the bioluminescence emission was monitored using the FOs for up to 80 min (**Figure 27**) indicating the circulating time of the native coelenterazine in the mouse body (**Figure 26**). We envision that our bioluminescent fusion proteins and our imaging technology can be used to study the progression of tumor growth or the efficacy of a particular drug treatment by correlating the measured light intensity from the tumor with the disease state and/or the efficacy of the drug.

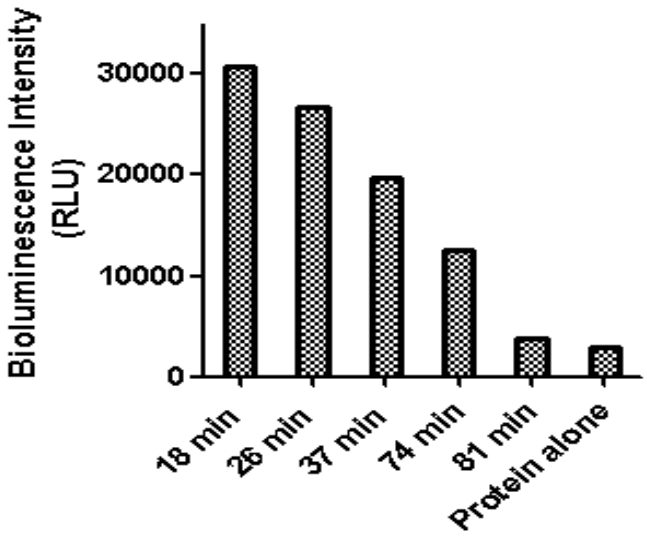

Figure 27. Light intensity from the triple negative breast cancer detection in mouse with the FOs during a 80-min period

3.5 Summary and significance

Herein, we demonstrated a sensitive method for the detection and imaging of epithelial growth factor receptors (EGFR) overexpressed on the surface of cancer cells using the fusion protein EGF-Gluc as a bioluminescent imaging probe. Bioluminescence offers high sensitivity and resolution due to its low background signals in mammalian tissues. The fusion protein was able to bind to the EGFR expressed on the cancer cells, yielding higher bioluminescence signals from head and neck squamous cell carcinoma (HNSCC CAL-27) and breast cancer MDA-MB-468 cells than their corresponding negative controls. The bioluminescence signals from different numbers of EGF-Gluc labeled CAL-27 cells was plotted against the corresponding cell numbers. The light intensity increased as the number of cancer cells increased, demonstrating the effective binding of the EGF-Gluc fusion protein to the EGFR-overexpressed cells. We employed both, our custom-made instrument composed of a light-tight chamber and a FOs combined and a digital camera for the bioluminescence imaging of the tumors. The bioluminescence emitted was collected and processed with a custom software for bioluminescence imaging to localize and quantify the light intensity. Using this system, we were able to image the pancreatic tumor and the triple-negative breast cancer as well as its metastasis in the mouse models with the engrafted tumors, demonstrating the feasibility of employing bioluminescence for cancer detection and diagnosis. Other advantages of our technology involve the cost-effective production of the bioluminescent probes for imaging, the simple assay method *in vitro* and *in vivo*, fast data acquisition, and easy data processing. Finally, we anticipate that our novel bioluminescence-based detection method has a great potential to be used in early cancer diagnosis, which is critical for improved prognosis and better disease management.

Chapter 4: Detection of the biomarker CD44 expressed on the head and neck cancer cells using an aequorin variant

4.1 Overview

Head and neck squamous cell carcinoma (HNSCC) has been a serious public health issue for a long time. More than half a million new cases are diagnosed annually worldwide, among those more than 42,000 new cases occur in the USA, representing 3% of all the cancers diagnosed. Although billions of dollars are spent for medical care of HNSCC patients per year, the survival rate has not improved much for many years. This is potentially caused by the lack of an early diagnostic method. A sensitive detection technique that can diagnose this cancer at an early stage is an imperative need. In our research, the biomarker CD44 that is overexpressed on the surface of the HNSCC cells was chosen as the binding target of our bioluminescence detection probe. We then designed a bioluminescence-based detection probe targeting CD44 for the detection of the HNSCC cells when present at low levels. The photoprotein aequorin, native from the jellyfish *Aequorea victoria*, was employed as the detection probe, taking advantage of the properties of its bioluminescence emission, including no need for an excitation source, high signal-to-background ratio, and tunable emission properties. In this study, the aequorin mutant S5CF113W (AEQS5CF113W) with blue-shifted wavelength of emission spectrum was chemically conjugated to the anti-human CD44 antibody to construct a detection probe with specific targeting capability. The anti-CD44 antibody-AEQS5CF113W conjugate fusion was applied in the development of the bioluminescent assay of the HNSCC cells, proving the sensitivity of aequorin as a new detection probe to report the presence of HNSCC in tumors

4.2 Introductory remarks

Head and neck squamous cell carcinoma (HNSCC) represents cancers that happen in the squamous cells located in the head and neck regions, including the oral cavity, pharynx, larynx, and salivary glands. As stated above, HNSCC has been a significant public problem for a long time with causing about 12,000 deaths per year (131). Furthermore, more than half a million HNSCC cases are reported worldwide with 300,000 deaths, encompassing different ethnic backgrounds and races (132). Over three billion dollars is spent on the medical care of head and neck cancer per year (https://costprojections.cancer.gov/graph.php). Unfortunately, the efficacy of the current treatments of HNSCC such as surgery, chemotherapy, and radiation therapy do not offer significant, shown by that the five-year survival rate improves slightly within the recent thirty years (133). The slow improvement of the survival rate mainly results from lack of the early diagnostic methods, which highlights the importance of the discovery of an ultra-sensitive detection method that can diagnose the cancer cells at an early stage, which would have the potential to improve the survival rate significantly.

The receptors overexpressed on the surface of the HNSCC cell can be used as the targets for homing the bioluminescence detection probes by virtue of the binding specificity afforded by the molecular recognition between the CD44 and its ligand or binding partner. CD44 is an important biomarker of HNSCC. CD44 is comprised of more than 20 isoforms of a transmembrane glycoprotein involved in a variety of cell activities such as cell adhesion, migration, and signaling (134). CD44 has been found to be overexpressed on the cell surface of certain types of HNSCC (135, 136). Additionally, cell-

free CD44 has been found in high levels in saliva of HNSCC patients at all stages of the cancer, and thus, is a diagnostic biomarker of choice for CD44 (137).

Currently, the most novel optical detection method of HNSCC is based on fluorescence (138). This method suffers from the drawbacks associated with fluorescence, among which is compromised sensitivity and detection limits due to the autofluorescence inherent to physiological samples and the fluorescence background caused by the excitation of the fluorescent probe. On the contrary, bioluminescence is generated through an oxidation chemical reaction, eliminating the need of the external energy source, and thus, yielding high signal-to-noise ratio (8). In the work described in this chapter, a mutant of the photoprotein aequorin with shifted bioluminescence wavelength emission properties was used as the detection label for the development of a sensitive bioluminescent assay of HNSCC.

The photoprotein aequorin is originally found in the jellyfish *Aequorea victoria*, comprising apoaequorin, the chromophore coelenterazine, and molecular oxygen (78, 79). This 22 kDa protein is composed of 189 amino acids, which fold into four EF-hand domains and a hydrophobic pocket (14). Three of the four EF-hand domains (I, III, and IV) contain the high-affinity calcium binding sites on the EF-hand loops, while EF-hand II may help form the scaffold (12). In the active form of aequorin, the imidazopyrazine chromophore coelenterazine is incorporated into the hydrophobic pocket non-covalently. Upon binding three calcium ions, the protein undergoes a conformational change, catalyzing the oxidation of the bound coelenterazine to excited coelenteramide (12). A flash-type light with the wavelength of 469 nm is emitted when the excited coelenteramide relaxes to its ground state.

The crystal structure and the emission mechanism of aequorin have been studied thoroughly, and the bioluminescence emission spectra and the decay kinetics of aequorin have been tuned through random (139) and site-specific mutagenesis (15), the incorporation of non-natural amino acids (18), and the formation of semi-synthetic aequorins through the use of synthetic coelenterazine analogs (19). Our group has done a lot of work on protein engineering to create detection labels with enhanced properties. Three aequorin mutants with distinct bioluminescence properties have been employed in the simultaneous detection of three cytokines (tumor necrosis factor-α, interleukin-6, and interleukin-8) in both buffered solution and serum using a two-dimensional approach that combines both temporal and spatial resolution, which has been discussed in Chapter two, demonstrating the multiplexing capability of the aequorin variants. Among all the aequorin variants, the aequorin mutant F113W (AEQF113W) combined with coelenterazine *cp* (*ctz cp*) was chosen as the detection label in this study because this combination can shift the wavelength of emission maximum from 469 nm to 446 nm (21). In further research, bioluminescent probes with distinct light properties can be used to construct probes targeting biomarkers other than CD44. These probes have the potential to measure multiple biomarkers simultaneously, which can increase the diagnostic accuracy.

In this work, the surface biomarkers CD44 and the AEQF113W mutant were chosen to build the bioluminescence-based assay for the detection of HNSCC as a proof of concept. To that end, the serine at the position five of the AEQF113W mutant was replaced by a unique cysteine to introduce a sulfhydryl group into the protein for chemical conjugation to form the AEQS5CF113W mutant. The anti-CD44 antibody was chosen as the recognition molecule. The AEQS5CF113W mutant was chemically conjugated to the anti-

CD44 antibody through a heterobifunctional crosslinker Sulfo-LC-SPDP to construct the detection probe. The anti-CD44 antibody-AEQS5CF113W conjugate was employed to measure HNSCC CAL-27 cells, allowing the detection of HNSCC at low levels (**Figure 28**).

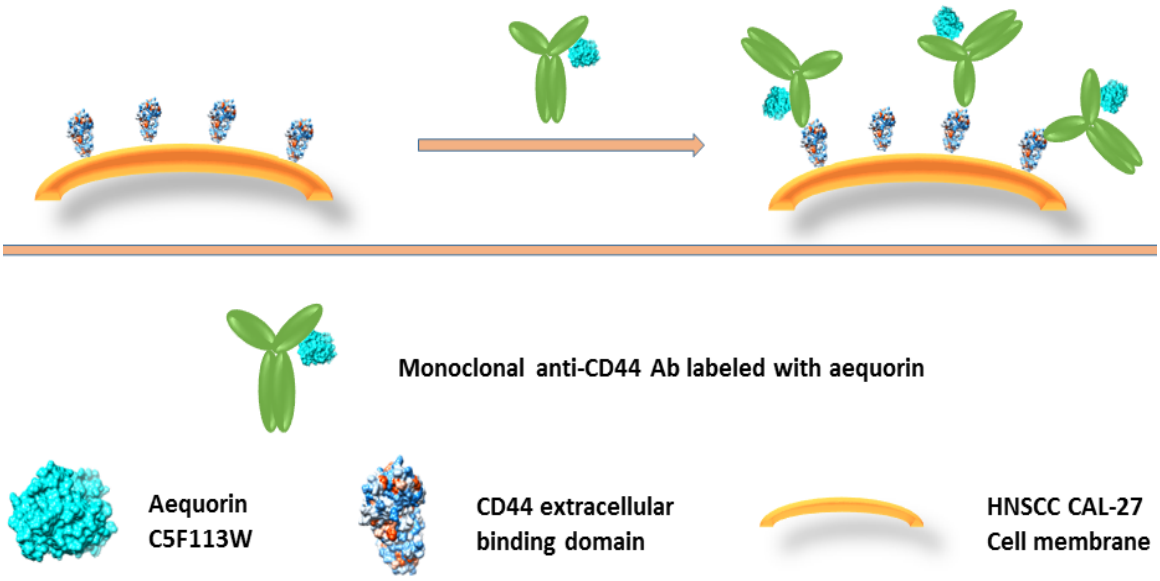

Figure 28. Scheme of the binding of AEQS5CF113W mutant labeled anti-CD44 antibody to the CD44 expressed HNSCC CAL-27 cells.

4.3 Experimental section

4.3.1 Reagents

Luria-Bertani (LB) Agar and LB Broth were purchased from EMD Millipore (Billerica, MA). *Eco*RI, *Hin*dIII restriction enzymes, *Taq* DNA polymerase, and deoxynucleotide (dNTP) were purchased from New England BioLabs (Ipswich, MA). Plasmid mini-prep kits, gel extraction kits and Ni-NTA agarose were purchased from Qiagen (Valencia, CA). Bench top 1Kb DNA ladder was purchased from Promega (Madison, WI). Disodium ethylenediaminetetraacetate (EDTA) was purchased from CalBiochem (Santa Diego, CA).

Agarose, kanamycin sulfate, and sodium phosphate were purchased from Amresco (Solon, OH). Sodium dodecyl sulfate (SDS) and Tris(hydroxymethyl)amino methane (Tris) free base were purchased from J. T. Baker (Center Valley, PA). Imidazole and calcium chloride were purchased from Sigma Aldrich (St. Louis, MO). Tween-20 was purchased from VWR (Radnor, PA). Isopropyl-beta-D-thiogalactoside (IPTG) was purchased from Gold Biotechnology (St. Louis, MO). Sodium chloride and glycerol were purchased from BDH Chemicals (distributed by VWR, West Chester, PA). SDS-page and precision plus protein dual color standards were purchased from BIO-RAD (Hercules, CA). Gel-red and coelenterazine sampler kit was ordered from Biotium (Hayward, CA). The anti-human CD44 monoclonal antibody was purchased from R&D systems (Minne-apolis, MN). The heterobifunctional crosslinker Sulfo-LC-SPDP (sulfosuccinimidyl 6-(3'-(2-pyridyldithio)propionamido)hexanoate), immobilized TCEP disulfide reducing gel, and the Zeba spin desalting columns (7 kDa MWCO) were purchased from Thermo Fisher Scientific (Rockford, IL). The phosphate buffer saline (PBS) tablets were purchased from Invitrogen (Camarillo, CA). The protein-free (PBS) blocking buffer, BCA protein assay reagent (bicinchoninic acid) and goat anti-mouse IgG coated white 96-well plates were from Pierce Biotechnology (St. Louis, MO). The DMEM cell medium was purchased from Gibco by life technology (Grand Island, NY). Fetal bovine serum (FBS), Penicillin-Streptomycin (Pen Strep), and Trypsin-EDTA were purchased from Sigma Aldrich (St. Louis, MO). The gene of the aequorin mutant F113W, the PIN IV vectors, and the Top 10F′ competent cells were obtained from our lab. The CAL 27 cell line was kindly provided by Dr. Franzmann. All the aqueous solutions were prepared using 18 MΩ deionized distilled water.

4.3.2 Apparatus

Polymerase chain reactions (PCR) were performed with the Eppendorf gradient thermo-cycler (Hamburg, Germany). DNA agarose gels were run on the Kodak BioMax system (Rochester, NY). DNA electrophoresis gels were showed with a UV Transilluminator (UVP, Upland, CA). The medium for the bacteria growth were sterilized by Harvey SterileMax Sterilizer. Protein expression bacterial *E. coli* were incubated in the Fisher Scientific orbital shakers (Fair Lawn, NJ). The optical densities (OD) of the *E. coli* culture were monitored using a Spectronic 21D UV-Vis Spectrophotometer (Ivy Land, PA). The *E. coli* cells were centrifuged down by a Beckman coulter Avanti J-E centrifuge (Palo Alto, CA) and lysed with a Fisher Scientific 550 dismembrator (Pittsburgh, PA). Purified proteins were concentrated by Centrifugal Filter Units Amicon Ultra 10K from Millipore and the chemical conjugation product was separated with the unbound aequorin mutant AEQC5F113W by the Amicon Ultra 100K centrifugal filters (Darmstadt, Germany). The concentrated protein was dialyzed into the chemical conjugation buffer by Slide-A-Lyzer Dialysis Cassettes from Thermo Scientific (Rochford, IL). Light intensity and decay kinetics were read by the Polarstar Optima luminometer from BMG Labtech (Cary, NC). The emission spectrum was scanned with a liquid cooled CCD named SpectroScan. The CAL-27 cell culture was handled in the biosafety safety cabinet from Labconco (Kansas City, MO), incubated in the New Brunswick Galaxy 170S CO_2 incubator from Eppendorf (Hamburg, Germany), and observed by OptixCam Summit series P95-C from Microscope (Roanoke, VA). The CAL-27 cells were centrifuged down and stocked by the Beckman coulter Allegra X-15R centrifuge (Palo Alto, CA) and the VWR CryoPro Canister Storage Tank (Radnor, PA) respectively.

4.3.3 Engineering, expression, and purification of AEQS5CF113W

For this study, the serine (Ser) at the position 5 of the aequorin mutant AEQF113W was replaced by a tyrosine (Tyr) to introduce one sulfhydryl group into the protein for the chemical conjugation, forming the gene of AEQS5CF113W. The sequence of AEQF113W was amplified with the F113W forward primer that introduced an *Eco*RI restriction site and a tyrosine at the positon 5 on the 5′ end, and the F113W reverse primer that introduced a *Hin*dIII restriction site. The steps of the PCR reaction were started at 95 ºC for 5 min, and then repeated for 40 cycles for the next steps, 95 ºC for 1 min, and 60 ºC for 1 min, followed by 72 ºC for 2 min, and then the reaction was completed at 72 ºC for 10 min. Then the gene of AEQS5CF113W was ligated into the pIN IV vector and transmitted into the TOP 10F′ *E. coli* for the plasmid amplification. Then the gene of AEQS5CF113W was amplified with the C5F113W forward and reverse primers that introduced the LIC/Xa cloning sites on the 5′ end and the 3′ end respectively. The steps of the PCR reaction were started at 95 ºC for 5 min, and then repeated for 25 cycles for the next steps, 95 ºC for 20 s, and 65 ºC for 10 s, followed by 70 ºC for 10 s, and then the reaction was completed at 70 ºC for 10 min. All the primer sequences are listed in **Table VI**.

Table VI. The primer sequences for the engineering of the AEQS5CF113W mutant.

Primer	Sequence (5′-3′)
F113W Forward	GTGGAATTCCAATGGTGAAACTGACCTGCGACTTCGACAACCCAAGATGGA
F113W Reverse	CACAAGCTTTTAGGGGACAGCTCCACCG
S5CF113W Forward	GGTATTGAGGGTCGCGAATTCCCATCAATGGTGAAACTGACCTGCGACTTCG ACAACCCA
S5CF113W Reverse	AGAGGAGAGTTAGAGCCCAAGCTTTGATTGTTAGGGGACAGCTCCACCGTA GAGCTTTTC

The gene of the AEQS5CF113W mutant was ligated into the pET-30 plasmids through the Novagen pET-30 Xa/LIC Cloning Kits. The gene sequence of AEQS5CF113W was confirmed by the Sylvester Comprehensive Cancer Center Oncogenomics Core Facility. The plasmids containing the gene of AEQS5CF113W were then transferred into BL21(DE3) *E. coli* cells for the *in vitro* protein expression. The culture was grown in 500 mL LB broth containing 30 μg/mL Kanamycin and incubated through shaking at 250 rpm at 37 ºC. When the OD_{600} reached to 0.6, IPTG with a final concentration of 1 mM was added into the medium to induce the protein expression. The *E. coli* cells were then collected after three h's incubation at 37 ºC. The harvested cells were lysed in the Ni-NTA native lysis to release the soluble expressed protein in the buffer. The protein containing buffer solution was separated with the pellet through centrifuging. The AEQS5CF113W mutant was purified using immobilized metal affinity chromatography (Ni/NTA). The AEQS5CF113W containing native lysis buffer (50 mM NaH_2PO_4 pH 8.0, 300 mM NaCl, and 10 mM imidazole buffer) was loaded into a gravity column containing pre-washed Ni/NTA Agarose beads. A sequential washing with buffers of 50 mM NaH_2PO_4 pH 8.0, 300 mM NaCl, and 20, 50 and 70 mM imidazole, were performed on the column. The

AEQS5CF113W mutant was then washed off from the column by the elution buffer (50 mM NaH_2PO_4 pH 8.0, 300 mM NaCl, and 100 mM imidazole). All the fractions containing the pure AEQS5CF113W were pooled together through a 10K membrane. The concentrated AEQS5CF113W was then dialyzed into the conjugation coupling buffer phosphate buffered saline with EDTA (PBS-EDTA) with 20 mM sodium phosphate pH 7.5, containing 1 mM EDTA, 150 mM NaCl, 0.02% sodium azide (buffer H) for 24 h to change the buffer, and stored at 4 ^{o}C for further uses. The protein concentration was measured through the Pierce BCA protein assay kit.

4.3.4 Chemical conjugation of the anti-human CD44 antibody and AEQS5CF113W

The mouse anti-human CD44 monoclonal antibody and the AEQS5CF113W aequorin mutant were conjugated chemically through a heterobifunctional crosslinker Sulfo-LC-SPDP. The Sulfo-LC-SPDP molecule reacted with the primary amine group of the antibody through the NHS ester end, and then reacted with the sulfhydryl group of the AEQS5CF113W mutant through its 2-pyridyldithiol group, labeling the antibody molecule with the aequorin mutant. In this research, 2 mg Sulfo-LC-SPDP was dissolved in 200 µL water to obtain the linker solution with the 20 mM concentration right before the conjugation. Then 100 µg mouse anti-CD44 monoclonal antibody powder that was dissolved in 50 µL buffer H was mixed with 1 µL of the linker solution and allowed to incubate for 1 h at room temperature. After the conjugation, the excess linker was removed through the Zeba spin desalting column (7 kDa MWCO) pre-equilibrated with buffer H. A amount of 180 µg AEQS5CF113W (ten molar excess of the antibody) was mixed with the TCEP reducing gel slurry pre-equilibrated with buffer H, and allowed to incubate at room temperature for 1 h. The volume of the TCEP slurry equaled to two times the volume of

the aequorin mutant. The TCEP was removed through centrifugation at 1000 x g for 1 min. Then the crosslinker activated anti-CD44 antibody and the reduced aequorin were mixed and incubated at 30 ºC for 1 h, followed by the incubation at 4 ºC for overnight. After the conjugation, the unconjugated AEQS5CF113W mutant was removed from the conjugation product through the Amicon Ultra 4 centrifugal filter (100 kDa MWCO). The conjugation product (AEQS5CF113W labeled anti-human CD44 antibody) was stored at -20 ºC for further use.

4.3.5 Decay kinetics of free and conjugated AEQS5CF113W

The bioluminescence decay kinetics of the AEQS5CF113W mutant with each coelenterazine analogue (coelenterazine *ntv, i, f, cp, hcp, fcp, n, fcp, h*) were measured by the Polarstar Optima luminometer respectively. Each combination was incubated for 24 h at 4 ºC. The concentration of the coelenterazine analogue is three times of the concentration of the protein. A volume of 10 µL of each combination was loaded into one well of a 96-well microtiter in triplicate. The bioluminescence emission intensity was recorded with the Polarstar Optima luminometer after the injection of 100 µL 30 mM Tris/HCl buffer containing 100 mM $CaCl_2$, pH 7.5 (buffer I) to trigger the bioluminescence emission. The light intensity for the AEQS5CF113W mutant combined with coelenterazine *i* were recorded for 50 s with readings taken every 200 ms. For other combinations, the light intensity was read for 25 s with readings taken every 100 ms.

For the conjugated AEQS5CF113W, the conjugate was mixed with coelenterazine *cp* for 24 h. The goat anti-mouse IgG coated plate was washed with the protein-free (PBS) blocking buffer (buffer J). A volume of 100 µL of the conjugate was then loaded into each well of the goat anti-mouse IgG coated plate, and incubated for 1 h at room temperature to

capture the conjugated AEQS5CF113W. Then the wells were washed three times with 10 mM phosphate, pH 7.5 containing 2mM EDTA, 150mM NaCl and 0.05% Tween-20 (buffer K) to remove the unbounded free AEQS5CF113W mutant. The light intensity was measured for 25 s with readings taken every 100 ms using the Polarstar Optima luminometer. The intensity was plotted against the time series and analyzed through the non-linear, one phase exponential decay fitting to calculate the half-lives using Grahpad Prism 5.0.

4.3.6 Bioluminescence emission spectra of free and conjugated AEQS5CF113W

The emission spectra were scanned by a liquid cooled SpectroScan CCD camera in the SpectroScan. Same steps as the measurement of decay kinetics were taken to prepare the samples. The emission signals at different wavelengths (400-700 nm) were measured upon the injection of 100 µL of buffer I for 5.250 s. The emission maximum is the wavelength corresponding to the highest light intensity.

4.3.7 Bioluminescent detection of CD44 overexpressed in HNSCC cells

The capability of using the aequorin labeled anti-CD44 antibody to detect the CD44 overexpressed CAL-27 cells was investigated. The HNSCC cell line CAL-27 was cultured in the Dulbecco's Modified Eagle Medium (DMEM), 10% fetal bovine serum (FBS), and 1% Penicillin-Streptomycin (Pen Strep) at 37 ºC in the CO_2 incubator. For this study, a volume of 50 µL of the AEQS5CF113W mutant labeled anti-CD44 antibody coupled with coelenterazine *cp* was added to 1.0 x 10^6 CAL-27 cells in 100 µL DPBS with 1 mM EDTA (buffer L), and allowed to incubate for 30 min at room temperature. After the incubation, the cells were serially diluted in buffer L to 5.0 x 10^5, 1.0 x 10^5, 5.0 x 10^4, 1.0 x 10^4, 5.0 x 10^3, and 1.0 x 10^3 cells per mL, and then 100 µL of each dilution was loaded into each well

of the 96-well microtiter plate, yielding 1.0 x 10^5, 5.0 x 10^4, 1.0 x 10^4, 5.0 x 10^3, 1.0 x 10^3, 5.0 x 10^2, and 1.0 x 10^2 cells per well. The cells were then centrifuged down, and the buffer containing the unbounded conjugate was vacuumed out. Each well was washed with 200 μL buffer L three times to remove the unbounded AEQS5CF113W mutant labeled anti-CD44 antibody. The bioluminescence intensity of each well was then measured by the Polarstar Optima luminometer for 10 s upon the injection of 100 μL buffer I. The light intensity was plotted against the number of cells using the software GraphPad Prism 5.0.

4.4 Results and discussion

Diagnosis of HNSCC at an early stage is of utmost importance as it could save lives and increase the survival rate of patients suffering from this devastating cancer. Our approach to help solve this problem was to develop a bioluminescent probe that can bind specifically to the HNSCC cells. Specifically, we were set to establish a sensitive detection platform for the HNSCC cells based on bioluminescence, aiming at achieving the early diagnosis of HNSCC.

The aequorin mutant AEQF113W was chosen for this work because of its substantial blue-shifted wavelength of emission. A cysteine was incorporated into the AEQF113W mutant at the position 5 to introduce a free sulfhydryl group into the protein, enabling the chemical conjugation to the specific targeting moiety, namely an anti-CD44 antibody (**Figure 29**). The gene sequence of the AEQS5CF113W mutant was ligated into the pET-30 plasmid through the pET-30 Xa/LIC Vector Kit to incorporate a His-tag into the protein to facilitate protein purification. The AEQS5CF113W-containing plasmid was transfected into *E. coli* BL21(DE3) cells for expression. The purity of the expressed, isolated and purified AEQS5CF113W was verified by SDS-PAGE (**Figure 30**).

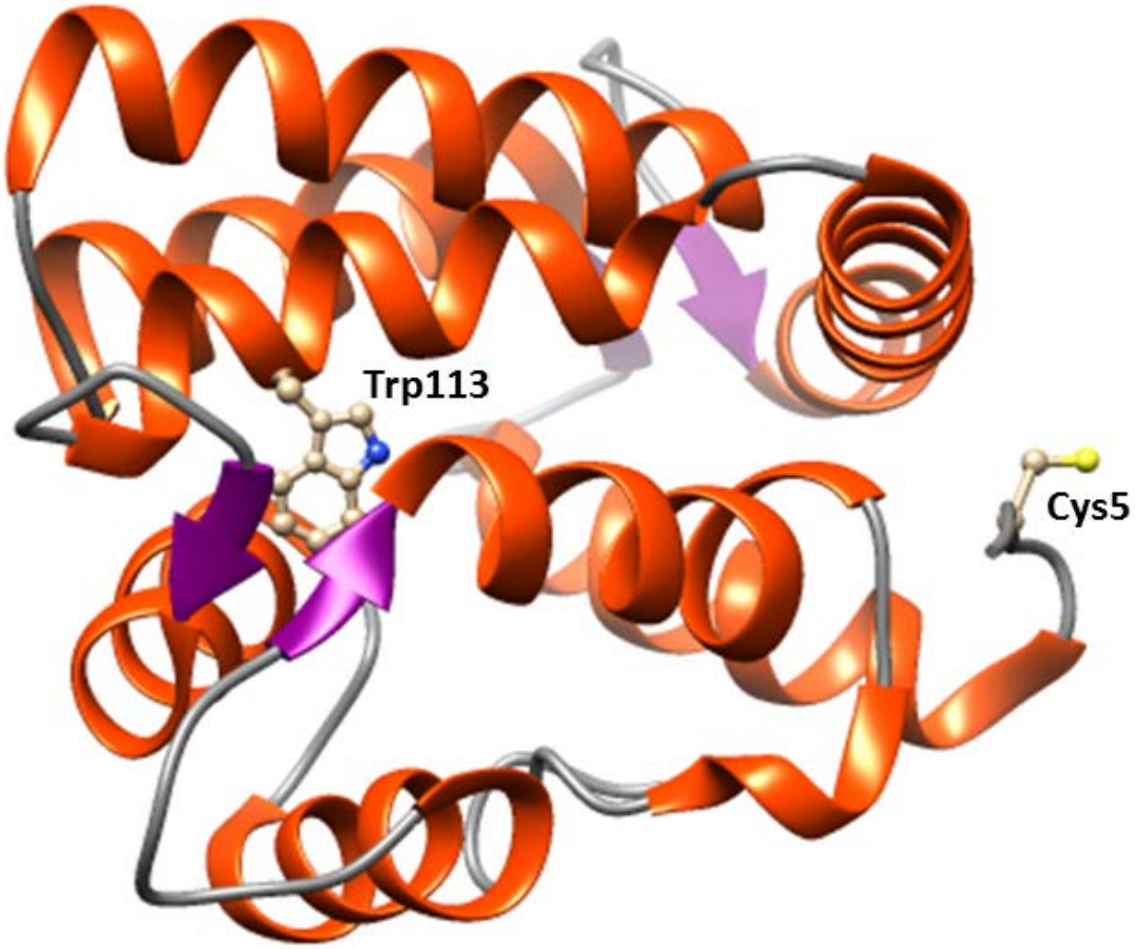

Figure 29. Crystal structure of the aequorin mutant AEQS5CF113W showing the locations of the two mutations, Cys5 and Trp113, on the protein structure.

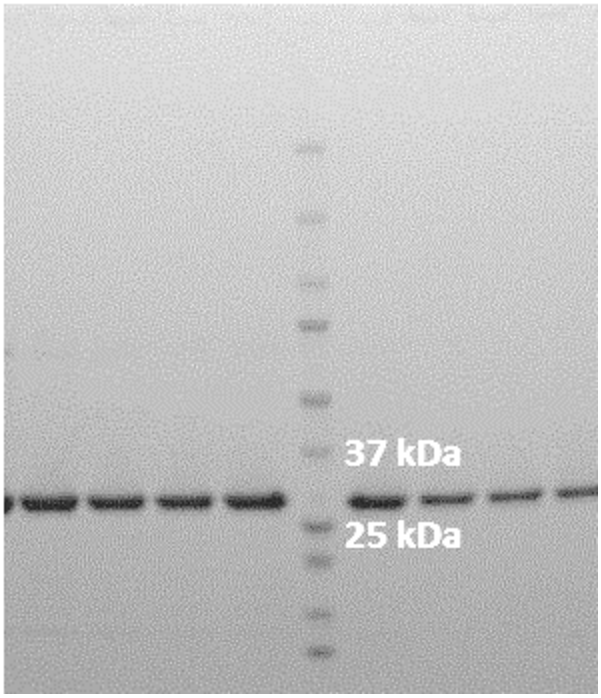

Figure 30. SDS-PAGE of the prepared aequorin mutant AEQS5CF113W. The SDS-PAGE showed the presence of pure protein bands with a molecular weight of around 27-29 kDa, which is consistent with the aequorin mutant (aequorin: 22 kDa and Hig-tag: 5kDa).

The bioluminescence characteristics of the AEQS5CF113W mutant were obtained and compared with those of aequorin. The wavelength of maximum emission and the decay kinetics of the AEQS5CF113W along with a series of coelenterazine analogs were determined to confirm that it inherited the desired bioluminescence emission properties of AEQF113W (Table VII). The spectrum maxima of AEQS5CF113W aequorin combined with coelenterazine *cp* is 455 nm, demonstrating that the blue-shifted emission was not affected by the amino acid incorporation.

Table VII. Bioluminescence emission maxima and half-lives of AEQS5CF113W complexed with different synthetic coelenterazine analogs.

Coelenterazine	Emission max (nm)	Half-life (s)
ntv	483	1.5
i	486	12.7
f	482	0.7
ip	457	0.6
hcp	458	0.2
h	474	0.7
cp	455	0.3
fcp	463	0.20
n	475	9.6

CD44 has been proven to be a potential biomarker for the detection of HNSCC at early stages of cancer (136, 137). Because of that, CD44 was chosen as the target biomarker for the detection of HNSCC cells. An anti-human CD44 antibody was chosen as the recognition molecule incorporated into the bioluminescent probe to target the CD44 overexpressed on the cell surface of the HNSCC cells. The anti-human CD44 antibody was chemically linked to the aequorin mutant AEQS5CF113W through the heterobifunctional crosslinker Sulfo-LC-SPDP for the construction of the probe. The NHS ester end of the Sulfo-LC-SPDP reacted with the primary amine group of the antibody. The TCEP reducing gel slurry was used to reduce the disulfide bonds to produce free sulfhydryl groups. After the removal of the excess Sulfo-LC-SPDP and the TCEP gel, the linker activated antibody and the AEQS5CF113W aequorin mutant were conjugated through the reaction between the sulfhydryl group of the AEQS5CF113W aequorin and the 2-pyridyldithiol group of the linker. Verification of the success of the conjugation reaction was verified using the goat

anti-mouse IgG plate. The crosslinking conditions were optimized as well by performing the reaction at different temperatures and times (**Figure 31**).

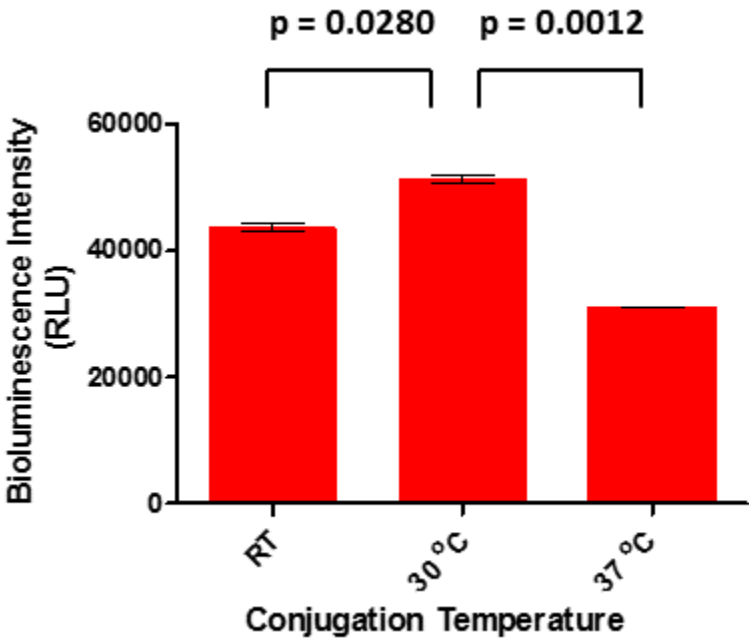

Figure 31. Optimization for the conjugation temperature for the first hour. After the removal of the excess Sulfo-LC-SPDP linker and the TCEP gel, the mouse IgG and the aequorin mutant AEQS5CF113W were mixed together and allowed to incubate at a higher temperature for 1 h, followed by the incubation at 4 °C overnight. The temperature for the first h's incubation was optimized. Three different temperatures, i.e., room temperature, 30 °C, and 37 °C, were chosen to be compared. The same amount of each conjugation product combined with coelenterazine *cp* was loaded into the anti-mouse IgG plate. The bioluminescence intensity was measured by a microtiter plate luminometer, and analyzed by GraphPad Prism 5.0 software. The p-value of the bioluminescence intensity between room temperature and 30 °C is 0.0008, proving that they are significantly different. All the columns are the mean of three replicates ± one standard deviation.

The bioluminescence emission maximum and decay kinetics of the anti-CD44 antibody/AEQS5CF113W conjugate combined with coelenterazine *cp* were determined to be 456 nm and 0.40 s, respectively, as anticipated. After the characterization of the anti-CD44 antibody/AEQS5CF113W conjugate, this bioluminescent probe was employed to detect CD44 expressed on the surface of the HNSCC CAL-27 cells *in vitro* in a cell line.

For this purpose, a volume of 50 μL anti-CD44 antibody/AEQS5CF113W aequorin conjugate was added to 1.0 x 10^6 CAL-27 cells, and allowed to incubate for 30 min at room temperature to allow for the specific binding to occur. The cells were serially diluted to different concentrations ranging from 1.0 x 10^2 to 5.0 x 10^4/100 μL. The cells were then centrifuged down and washed with EDTA-containing DPBS buffer (buffer L). The unbound anti-CD44 antibody/AEQS5CF113W aequorin conjugate were aspirated removed. After washing, the bioluminescence emission was measured with a microtiter plate luminometer upon injection of the calcium-containing buffer (buffer I) for 10 s. The bioluminescence intensity was plotted against the number of cells, and analyzed by the Grahpad Prism 5.0, yielding a detection limit of 100 cells (**Figure 32**).

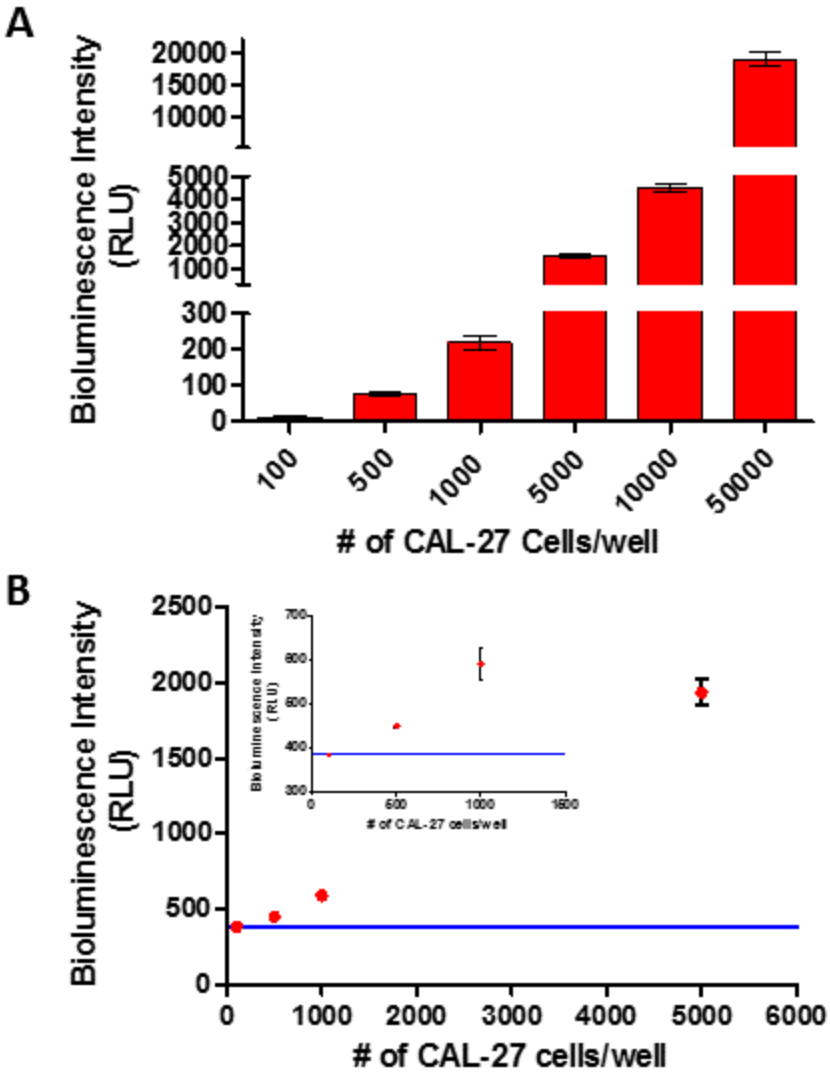

Figure 32. Bioluminescence intensity emitted by different amounts of the CD44 overexpressed CAL-27 cells. (A) The bioluminescence was measured from different numbers of CAL-27 cells (1.0×10^2 to 5.0×10^4 cells per well). (B) Bioluminescence intensity from low amounts of CAL-27 cells (1.0×10^2 to 5.0×10^3 cells per well). The blue line represents the detection limit. The smaller insert figure is the low part of the curve. All the columns and points are the mean of three replicates ± one standard deviation.

4.5 Summary and significance

Recent advancements in cancer diagnostics and treatments have significantly improved the treatment efficacy and survival rates of many types of cancer. However, the survival rate of HNSCC, which counts with more than half a million new cases per year worldwide, has not improved much during the recent two decades. The lag of advancement in this field is

due to the lack of sensitive detection methods that can diagnose this cancer at an early stage. Specifically, this has highlighted the need for methods that enable the measurement of HNSCC cells, even if a low number of cells are present. In that regard, our goal was to create highly sensitive bioluminescent probes that target specifically HNSCC cells. For that, we chemically conjugated the anti-human CD44 monoclonal antibody to the aequorin mutant AEQS5CF113W through Sulfo-LC-SPDP a crosslinker to yield the bioluminescent targeting probe for the detection of the HNSCC CAL-27 cells. This probe was able to achieve a detection limit of 100 HNSCC cells. Bioluminescent probes constructed with varied aequorin mutants with different emission properties coupled to different molecular recognition molecules could provide with a set of probes that could be employed for the detection of more than one cellular biomarker in the cancerous cells, thus leading to a multi-prone detection that should result in improved detection and more accurate diagnosis.

Chapter 5: Conclusions and future perspectives

Bioluminescence has unique properties, such as the capability of emitting light without the need for an excitation source, low background in physiological samples, high signal-to-noise ratio, and its non-hazardous nature. Moreover, driven by its biocompatibility and simple sample preparation process, bioluminescent labels are amenable to be incorporated into miniaturized analytical platforms such as lab-on-a-chip or lab-on-a-CD, as well as in high-throughput systems. Therefore, bioluminescence has been widely employed in many bioanalytical systems such as immunoassays, calcium detection, ATP detection, hybridization assays, BRET assays, and *in vivo* imaging (8). This dissertation describes several novel applications of bioluminescence in the bioanalytical field, including multiplexed cytokine detection, cancer biomarker detection, and *in vivo* tumor imaging.

In Chapter 2, we demonstrated the multiplexed detection of three cytokines in a bioluminescent assay format. Specifically, the system was able to respond quickly and efficiently in a dose-dependent manner over several orders of magnitude, including at physiological and elevated ranges for the target cytokine protein biomarkers of interest. Previously, dual-analyte bioluminescent assays had been reported either based on spectral or time resolved bioluminescent proteins. Here, we have demonstrated that a combination of both, time and spatially (wavelength) resolved aequorin mutants, impart enhanced multiplexing capabilities for detection systems based on bioluminescence. The low background and high signal-to-background ratio of the emission of the aequorin variants allows their analytical application as detection probes for quantification in small volumes (70). Moreover, previously, it had also demonstrated that bioluminescence-based detection is compatible and amenable for incorporation into microfluidic platforms (8), an

advantage that can be utilized in the development of biomarker detection in microfluidic devices. Herein, we have demonstrated that we have expanded the application of the semi-synthetic aequorin variants from dual-analyte detection to the detection of three analytes simultaneously for the first time. Protein engineering and signal detection techniques will continue to improve, and, therefore, the library of semi-synthetic aequorins could be expanded with proteins that have further shifted emission properties, thus offering additional tools for the establishment of multiplexed assays beyond the detection of three biomarker analytes. Thus, the potential of small volume clinical diagnostics and precise health monitoring systems could be expanded.

In Chapter 3, a sensitive method for the detection and imaging of cancer cells that has overexpressed epithelial growth factor receptors (EGFR) using a fusion protein EGF-Gluc as the bioluminescent probe was described. Here, a recognition molecule EGF was genetically incorporated into the bioluminescent protein Gluc for the specific binding to the cancer cells and tumor sites overexpressing the EGF receptors on their surfaces. This fusion protein bound to the EGFR expressed on the surface of cancer cells, yielding higher bioluminescence intensity from head and neck squamous cell carcinoma (HNSCC CAL-27) and breast cancer MDA-MB-468 cells than their corresponding negative controls. The bioluminescence intensity of EGF-Gluc labeled CAL-27 cells were plotted against the corresponding cell numbers. The bioluminescence emission intensity increased as the number of cancer cells increased, demonstrating the binding of the fusion protein to the EGFR-overexpressed cells, yielding a detection limit of 500 cells per well in 100 μL of buffer. A custom-made instrument that is constructed with a light-tight chamber and a fiber optic light guide combined with a digital camera was used for the bioluminescence

detection and *in vivo* imaging of animals bearing cancer tumors. The light signals were processed with custom software for bioluminescence imaging to localize and quantify the light intensity, whereas the digital camera was used to acquire pictures of the animals emitting bioluminescence from their tumors. Using this system, we were able to image pancreatic and triple-negative breast cancer tumors as well as its breast cancer metastasis in mouse models, demonstrating the feasibility of employing bioluminescence for cancer detection and diagnosis. The method developed is cost-effective, non-invasive, sensitive, and selective. The data acquisition is fast, and the data processing is quite simple. All these characteristics point out to the usefulness of our method in the early diagnosis of cancer, which is critical for improved prognosis and disease management.

In Chapter 4, a bioluminescent probe of HNSCC CAL-27 cells was constructed using the photoprotein aequorin as the reporter in order to take advantage of its sensitivity and the multiplexing capability. Here, we chemically conjugated the anti-human CD44 monoclonal antibody to the aequorin mutant AEQS5CF113W through a crosslinker Sulfo-LC-SPDP to incorporate specific targeting capabilities to the probe. This selective bioluminescent probe enabled the measurement of HNSCC CAL-27 cells with a detection limit of 100 cells per well.

We envision that, in the future, bioluminescent probes with different emission properties and binding targets will be produced, and applied to the detection of diverse cancer cells both *in vitro* and *in vivo* by employing different cancer cell biomarkers, which would provide sensitive detection and more accurate cancer diagnostic platforms.

References

1. Shimomura O, Johnson FH, Saiga Y. Extraction, purification and properties of aequorin, a bioluminescent protein from the luminous hydromedusan, *Aequorea*. *Journal of Cellular Physiology*. 1962;59(3):223-239.

2. Markova SV, Vysotski ES, Blinks JR, Burakova LP, Wang BC, Lee J. Obelin from the bioluminescent marine hydroid *Obelia geniculata*: cloning, expression, and comparison of some properties with those of other Ca^{2+}-regulated photoproteins. *Biochemistry*. 2002;41(7):2227-2236.

3. Dewet JR, Wood KV, Deluca M, Helinski DR, Subramani S. Firefly luciferase gene - structure and expression in mammalian-cells. *Molecular and Cellular Biology*. 1987;7(2):725-737.

4. Verhaegen M, Christopoulos TK. Recombinant *Gaussia* luciferase. Overexpression, purification, and analytical application of a bioluminescent reporter for DNA hybridization. *Analytical Chemistry*. 2002;74(17):4378-4385.

5. Lorenz WW, Mccann RO, Longiaru M, Cormier MJ. Isolation and expression of a cDNA encoding *Renilla-Reniformis* luciferase. *Proceedings of the National Academy of Sciences of the United States of America*. 1991;88(10):4438-4442.

6. Widder EA. Bioluminescence in the ocean: origins of biological, chemical, and ecological diversity. *Science*. 2010;328(5979):704-708.

7. Rowe L, Dikici E, Daunert S. Engineering bioluminescent proteins: expanding their analytical potential. *Analytical Chemistry*. 2009;81(21):8662-8668.

8. Scott D, Dikici E, Ensor M, Daunert S. Bioluminescence and its impact on bioanalysis. *Annual Review Analytical Chemistry*. 2011;4:297-319.

9. Weiss PS. 2008 Nobel Prize in chemistry: green fluorescent protein, its variants and implications. *ACS Nano*. 2008;2(10):1977-1977.

10. Prendergast FG. Bioluminescence illuminated. *Nature*. 2000;405(6784):291-293.

11. Marques SM, da Silva JCGE. Firefly bioluminescence: a mechanistic approach of luciferase catalyzed reactions. *IUBMB Life*. 2009;61(1):6-17.

12. Head JF, Inouye S, Teranishi K, Shimomura O. The crystal structure of the photoprotein aequorin at 2.3 Å resolution. *Nature*. 2000;405(6784):372-376.

13. Inouye S, Noguchi M, Sakaki Y, Takagi Y, Miyata T, Iwanaga S, Tsuji FI. Cloning and sequence analysis of cDNA for the luminescent protein aequorin. *Proceedings of the National Academy Sciences of the United States of America*. 1985;82(10):3154-3158.

14. Lewit-Bentley A, Rety S. EF-hand calcium-binding proteins. *Current Opinion Structural Biology*. 2000;10(6):637-643.

15. Stepanyuk GA, Golz S, Markova SV, Frank LA, Lee J, Vysotski ES. Interchange of aequorin and obelin bioluminescence color is determined by substitution of one active site residue of each photoprotein. *FEBS Letters*. 2005;579(5):1008-1014.

16. Rowe L, Rothert A, Logue C, Ensor CM, Deo SK, Daunert S. Spectral tuning of photoproteins by partnering site-directed mutagenesis strategies with the incorporation of chromophore analogs. *Protein Engineering Design & Selection*. 2008;21(2):73-81.

17. Ohmiya Y, Ohashi M, Tsuji FI. 2 Excited-states in aequorin bioluminescence induced by tryptophan modification. *FEBS Letters*. 1992;301(2):197-201.

18. Grinstead KM, Rowe L, Ensor CM, Joel S, Daftarian P, Dikici E, Zingg JM, Daunert S. Red-shifted aequorin variants incorporating non-canonical amino acids: applications in *in vivo* imaging. *PLoS One*. 2016;11(7).

19. Shimomura O, Musicki B, Kishi Y. Semi-synthetic aequorin - an improved tool for the measurement of calcium-ion concentration. *Biochemical Journal*. 1988;251(2):405-410.

20. Shimomura O, Kishi Y, Inouye S. The relative rate of aequorin regeneration from apoaequorin and coelenterazine analogs. *Biochemical Journal*. 1993;296:549-551.

21. Dikici E, Qu X, Rowe L, Millner L, Logue C, Deo SK, Ensor M, Daunert S. Aequorin variants with improved bioluminescence properties. *Protein Engineering Design & Selection*. 2009;22(4):243-248.

22. Nijegorodov N, Mabbs R. The influence of molecular symmetry and topological factors on the internal heavy atom effect in aromatic and heteroaromatic compounds. *Spectrochimica Acta Part A: Molecular and Biomolecular Spectroscopy*. 2001;57(7):1449-1462.

23. Granatiero V, Patron M, Tosatto A, Merli G, Rizzuto R. The use of aequorin and its variants for Ca^{2+} measurements. *Cold Spring Harbor Protocols*. 2014;2014(1):9-16.

24. Clapham DE. Calcium signaling. *Cell*. 2007;131(6):1047-1058.

25. Berchtold MW, Brinkmeier H, Muntener M. Calcium ion in skeletal muscle: its crucial role for muscle function, plasticity, and disease. *Physiological Reviews*. 2000;80(3):1215-1265.

26. Ohmiya Y, Hirano T. Shining the light: the mechanism of the bioluminescence reaction of calcium-binding photoproteins. *Chemical Biology*. 1996;3(5):337-347.

27. de la Fuente S, Fonteriz RI, de la Cruz PJ, Montero M, Alvarez J. Mitochondrial free [Ca^{2+}] dynamics measured with a novel low-Ca^{2+}-affinity aequorin probe. *Biochemical Journal*. 2012;445(3):371-376.

28. Bonora M, Giorgi C, Bononi A, Marchi S, Patergnani S, Rimessi A, Rizzuto R, Pinton P. Subcellular calcium measurements in mammalian cells using jellyfish photoprotein aequorin-based probes. *Nature Protocols*. 2013;8(11):2105-2018.

29. Ordenes VR, Moreno I, Maturana D, Norambuena L, Trewavas AJ, Orellana A. *In vivo* analysis of the calcium signature in the plant Golgi apparatus reveals unique dynamics. *Cell Calcium*. 2012;52(5):397-404.

30. Zonin E, Moscatiello R, Miuzzo M, Cavallarin N, Di Paolo ML, Sandona D, Marin O, Brini M, Negro A, Navazio L. TAT-mediated aequorin transduction: an alternative approach for effective calcium measurements in plant cells. *Plant and Cell Physiology*. 2011;52(12):2225-2235.

31. Zhu XH, Feng Y, Liang GM, Liu N, Zhu JK. Aequorin-based luminescence imaging reveals stimulus- and tissue-specific Ca^{2+} dynamics in *Arabidopsis* plants. *Molecular Plant*. 2013;6(2):444-455.

32. Shimomura O. The discovery of aequorin and green fluorescent protein. *Journal of Microscopy-Oxford*. 2005;217:3-15.

33. Rodriguez-Garcia A, Rojo-Ruiz J, Navas-Navarro P, Aulestia FJ, Gallego-Sandin S, Garcia-Sancho J, Alonso MT. GAP, an aequorin-based fluorescent indicator for imaging Ca^{2+} in organelles. *Proceedings of the National Academy of Sciences of the United States of America*. 2014;111(7):2584-2589.

34. Xiong TC, Ronzier E, Sanchez F, Corratge-Faillie C, Mazars C, Thibaud JB. Imaging long distance propagating calcium signals in intact plant leaves with the BRET-based GFP-aequorin reporter. *Frontiers in Plant Science*. 2014;5(43).

35. Jacobson KA. New paradigms in GPCR drug discovery. *Biochemical Pharmacology*. 2015;98(4):541-555.

36. Lappano R, Maggiolini M. G protein-coupled receptors: novel targets for drug discovery in cancer. *Nature Reviews Drug Discovery*. 2011;10(1):47-60.

37. Menon V, Ranganathn A, Jorgensen VH, Sabio M, Christoffersen CT, Uberti MA, Jones KA, Babu PS. Development of an aequorin luminescence calcium assay for high-throughput screening using a plate reader, the LumiLux. *Assay and Drug Development Technologies*. 2008;6(6):787-793.

38. Hattori M, Ozawa T. Bioluminescent tools for the analysis of G-protein-coupled receptor and arrestin interactions. *RSC Advances*. 2015;5(17):12655-12663.

39. Qu XG, Deo SK, Dikici E, Ensor M, Poon M, Daunert S. Bioluminescence immunoassay for angiotensin II using aequorin as a label. *Analytical Biochemistry*. 2007;371(2):154-161.

40. Inouye S, Sato J. Comparison of luminescent immunoassays using biotinylated proteins of aequorin, alkaline phosphatase and horseradish peroxidase as reporters. *Bioscience Biotechnology, and Biochemistry*. 2008;72(12):3310-3313.

41. Inouye S, Sato J. Recombinant aequorin with a reactive cysteine residue for conjugation with maleimide-activated antibody. *Analytical Biochemistry*. 2008;378(1):105-107.

42. Galvan B, Christopoulos TK. Bioluminescence hybridization assays using recombinant aequorin. Application to the detection of prostate-specific antigen mRNA. *Analytical Chemistry*. 1996;68(20):3545-3550.

43. Doleman L, Davies L, Rowe L, Moschou EA, Deo S, Daunert S. Bioluminescence DNA hybridization assay for *Plasmodium falciparum* based on the photoprotein aequorin. *Analytical Chemistry*. 2007;79(11):4149-4153.

44. Rowe L, Deo S, Shofner J, Ensor M, Daunert S. Aequorin-based homogeneous cortisol immunoassay for analysis of saliva samples. *Bioconjugate Chemistry*. 2007;18(6):1772-1777.

45. Yagi K. Applications of whole-cell bacterial sensors in biotechnology and environmental science. *Applied Microbiology and Biotechnology*. 2007;73(6):1251-1258.

46. Date A, Pasini P, Sangal A, Daunert S. Packaging sensing cells in spores for long-term preservation of sensors: a tool for biomedical and environmental analysis. *Analytical Chemistry*. 2010;82(14):6098-6103.

47. Bjerketorp J, Hakansson S, Belkin S, Jansson JK. Advances in preservation methods: keeping biosensor microorganisms alive and active. *Current Opinion in Biotechnology*. 2006;17(1):43-49.

48. Araki N, Iida M, Amino N, Morita S, Ide A, Nishihara E, Ito M, Saito J, Nishikawa T, Katsuragi K, Miyauchi A. Rapid bioassay for detection of thyroid-stimulating antibodies using cyclic adenosine monophosphate-gated calcium channel and aequorin. *European Thyroid Journal*. 2015;4(1):14-19.

49. Kozlova O, Zwinderman M, Christofi N. A new short-term toxicity assay using *Aspergillus awamori* with recombinant aequorin gene. *BMC Microbiology*. 2005;5(40).

50. Rider TH, Petrovick MS, Nargi FE, Harper JD, Schwoebel ED, Mathews RH, Blanchard DJ, Bortolin LT, Young AM, Chen JZ, Hollis MA. A B cell-based sensor for rapid identification of pathogens. *Science*. 2003;301(5630):213-215.

51. Zeinoddini M, Khajeh K, Behzadian F, Hosseinkhani S, Saeedinia AR, Barjesteh H. Design and characterization of an aequorin-based bacterial biosensor for detection of toluene and related compounds. *Photochemistry and Photobiology*. 2010;86(5):1071-1075.

52. Xie Q, Soutto M, Xu X, Zhang Y, Johnson CH. Bioluminescence resonance energy transfer (BRET) imaging in plant seedlings and mammalian cells. *Methods in Molecular Biology* Methods. 2011;680:3-28.

53. Pfleger KD, Seeber RM, Eidne KA. Bioluminescence resonance energy transfer (BRET) for the real-time detection of protein-protein interactions. *Nature Protocols*. 2006;1(1):337-345.

54. Xu Y, Piston DW, Johnson CH. A bioluminescence resonance energy transfer (BRET) system: application to interacting circadian clock proteins. *Proceedings of the National Academy of Sciences of the United States of America*. 1999;96(1):151-156.

55. Morise H, Shimomura O, Johnson FH, Winant J. Intermolecular energy transfer in the bioluminescent system of *Aequorea*. *Biochemistry*. 1974;13(12):2656-2662.

56. Bakayan A, Vaquero CF, Picazo F, Llopis J. Red fluorescent protein-aequorin fusions as improved bioluminescent Ca^{2+} reporters in single cells and mice. *PLoS ONE*. 2011;6(5).

57. Rowe L, Combs K, Deo S, Ensor C, Daunert S, Qu X. Genetically modified semisynthetic bioluminescent photoprotein variants: simultaneous dual-analyte assay in a single well employing time resolution of decay kinetics. *Analytical Chemistry*. 2008;80(22):8470-8476.

58. Hamorsky KT, Ensor CM, Wei Y, Daunert S. A bioluminescent molecular switch for glucose. *Angewandte Chemie-International Edition*. 2008;47(20):3718-3721.

59. Scott D, Hamorsky KT, Ensor CM, Anderson KW, Daunert S. Cyclic AMP receptor protein-aequorin molecular switch for cyclic AMP. *Bioconjugate Chemistry*. 2011;22(3):475-481.

60. Weissleder R. A clearer vision for *in vivo* imaging. *Nature Biotechnology*. 2001;19(4):316-317.

61. Jacques SL. Optical properties of biological tissues: a review. *Physics in Medicine and Biology*. 2013;58(14):5007-5008.

62. Bakayan A, Domingo B, Miyawaki A, Llopis J. Imaging Ca^{2+} activity in mammalian cells and zebrafish with a novel red-emitting aequorin variant. *Pflügers Archiv European Journal of Physiology*. 2015;467(9):2031-2042.

63. Henry NL, Hayes DF. Cancer biomarkers. *Molecular Oncology*. 2012;6(2):140-146.

64. Tseng GC, Ghosh D, Feingold E. Comprehensive literature review and statistical considerations for microarray meta-analysis. *Nucleic Acids Research*. 2012;40(9):3785-3799.

65. Miller MB, Tang YW. Basic concepts of microarrays and potential applications in clinical microbiology. *Clinical Microbiology Reviews*. 2009;22(4):611-633.

66. Liu H, Li S, Liu L, Tian L, He N. An integrated and sensitive detection platform for biosensing application based on Fe@Au magnetic nanoparticles as bead array carries. *Biosensensors and Bioelectronics*. 2010;26(4):1442-1448.

67. Elshal MF, McCoy JP. Multiplex bead array assays: performance evaluation and comparison of sensitivity to ELISA. *Methods*. 2006;38(4):317-323.

68. Roda A, Guardigli M, Michelini E, Mirasoli M. Bioluminescence in analytical chemistry and *in vivo* imaging. *TrAC Trends in Analytical Chemistry*. 2009;28(3):307-322.

69. Inouye S, Sato J. Purification of histidine-tagged aequorin with a reactive cysteine residue for chemical conjugations and its application for bioluminescent sandwich immunoassays. *Protein Expression and Purification*. 2012;83(2):205-210.

70. Hamorsky KT, Ensor CM, Dikici E, Pasini P, Bachas L, Daunert S. Bioluminescence inhibition assay for the detection of hydroxylated polychlorinated biphenyls. *Analytical Chemistry*. 2012;84(18):7648-7655.

71. Martin JR, Rogers KL, Chagneau C, Brulet P. *In vivo* bioluminescence imaging of Ca^{2+} signalling in the brain of *Drosophila*. *PLoS ONE*. 2007;2(3).

72. Hamorsky KT, Ensor CM, Pasini P, Daunert S. A protein switch sensing system for the quantification of sulfate. *Analytical Biochemistry*. 2012;421(1):172-180.

73. Manjarres IM, Chamero P, Domingo B, Molina F, Llopis J, Alonso MT, Garcia-Sancho J. Red and green aequorins for simultaneous monitoring of Ca^{2+} signals from two different organelles. *Pflügers Archiv European Journal of Physiology*. 2008;455(5):961-970.

74. Kain SR. Green fluorescent protein (GFP): applications in cell-based assays for drug discovery. *Drug Discovery Today*. 1999;4(7):304-312.

75. Eglen RM, Reisine T. Photoproteins: important new tools in drug discovery. *Assay and Drug Development Technologies*. 2008;6(5):659-671.

76. Frank LA, Borisova VV, Markova SV, Malikova NP, Stepanyuk GA, Vysotski ES. Violet and greenish photoprotein obelin mutants for reporter applications in dual-color assay. *Analytical and Bioanalytical Chemistry*. 2008;391(8):2891-2896.

77. Van de Bittner GC, Bertozzi CR, Chang CJ. Strategy for dual-analyte luciferin imaging: *in vivo* bioluminescence detection of hydrogen peroxide and caspase activity in a murine model of acute inflammation. *Journal of the American Chemical Society*. 2013;135(5):1783-1795.

78. Shimomura O. A short story of aequorin. *The Biological Bulletin*. 1995;189(1):1-5.

79. Shimomura O, Johnson FH. Peroxidized coelenterazine, the active group in the photoprotein aequorin. *Proceedings of the National Academy of Sciences of the United States of America*. 1978;75(6):2611-2615.

80. Qu X, Rowe L, Dikici E, Ensor M, Daunert S. Aequorin mutants with increased thermostability. *Analytical and Bioanalytical Chemistry*. 2014;406(23):5639-5643.

81. Sriramula S, Francis J. Tumor necrosis factor - alpha is essential for angiotensin II-induced ventricular remodeling: role for oxidative stress. *PLoS ONE*. 2015;10(9).

82. Rincon M. Interleukin-6: from an inflammatory marker to a target for inflammatory diseases. *Trends in Immunology*. 2012;33(11):571-577.

83. Akdis M, Burgler S, Crameri R, Eiwegger T, Fujita H, Gomez E, Klunker S, Meyer N, O'Mahony L, Palomares O, Rhyner C, Ouaked N, Schaffartzik A, Van de Veen W, Zeller S, Zimmermann M, Akdis CA. Interleukins, from 1 to 37, and interferon-gamma: receptors, functions, and roles in diseases. *Journal of Allergy and Clinical Immunology*. 2011;127(3):701-721.

84. Diamandis EP. Theranos phenomenon: promises and fallacies. *Clinical Chemistry and Laboratory Medicine*. 2015;53(7):989-993.

85. Li M, Diamandis EP. Theranos phenomenon - part 2. *Clinical Chemistry and Laboratory Medicine*. 2015;53(12):1911-1912.

86. Li M, Diamandis EP. Theranos phenomenon - part 3. *Clinical Chemistry and Laboratory Medicine*. 2016;54(5):145-146.

87. Diamandis EP. Theranos phenomenon - part 4: Theranos at an international conference. *Clinical Chemistry and Laboratory Medicine*. 2016;54(8):243-244.

88. Garcia-Hernandez P, Prieto B, Martinez-Morillo E, Rodriguez V, Alvarez FV. Interleukin-6 in cerebrospinal fluid as a biomarker of acute meningitis. *Annals of Clinical Biochemistry*. 2016;53(1):155-163.

89. Scheller J, Chalaris A, Schmidt-Arras D, Rose-John S. The pro- and anti-inflammatory properties of the cytokine interleukin-6. *Biochimica et Biophysica*. 2011;1813(5):878-888.

90. Paquette SG, Banner D, Zhao Z, Fang Y, Huang SSH, Leon AJ, Ng DCK, Almansa R, Martin-Loeches I, Ramirez P, Socias L, Loza A, Blanco J, Sansonetti P, Rello J, Andaluz D, Shum B, Rubino S, de Lejarazu RO, Tran D, Delogu G, Fadda G, Krajden S, Rubin BB, Bermejo-Martin JF, Kelvin AA, Kelvin DJ. Interleukin-6 is a potential biomarker for severe Pandemic H1N1 influenza a infection. *PLoS ONE*. 2012;7(6).

91. Urquidi V, Chang M, Dai YF, Kim J, Wolfson ED, Goodison S, Rosser CJ. IL-8 as a urinary biomarker for the detection of bladder cancer. *BMC Urology*. 2012;12(12).

92. Dos Santos PL, de Oliveira FA, Santos ML, Cunha LC, Lino MT, de Oliveira MF, Bomfim MO, Silva AM, de Moura TR, de Jesus AR, Duthie MS, Reed SG, de Almeida RP. The severity of visceral leishmaniasis correlates with elevated levels of serum IL-6, IL-27 and sCD14. *PLoS Neglected Tropical Diseases*. 2016;10(1).

93. Kobawala TP, Patel GH, Gajjar DR, Patel KN, Thakor PB, Parekh UB, Patel KM, Shukla SN, Shah PM. Clinical utility of serum interleukin-8 and interferon-alpha in thyroid diseases. *Journal of Thyroid Research.* 2011;2011.

94. Tefferi A, Vaidya R, Caramazza D, Finke C, Lasho T, Pardanani A. Circulating interleukin (IL)-8, IL-2R, IL-12, and IL-15 levels are independently prognostic in primary myelofibrosis: a comprehensive cytokine profiling study. *Journal of Clinical Oncology*. 2011;29(10):1356-1363.

95. Malamitsi-Puchner A, Protonotariou E, Boutsikou T, Makrakis E, Sarandakou A, Creatsas G. The influence of the mode of delivery on circulating cytokine concentrations in the perinatal period. *Early Human Development*. 2005;81(4):387-392.

96. Feltus A, Grosvenor AL, Conover RC, Anderson KW, Daunert S. Detection of biotin in individual sea urchin oocytes using a bioluminescence binding assay. *Analytical Chemistry*. 2001;73(7):1403-1407.

97. Howlander N, Noone AM, Krapcho M, Miller D, Bishop K, Altekruse SF, Kosary CL, Yu M, Ruhl J, Tatalovich Z, Mariotto A, Lewis DR, Chen HS, Feuer EJ, Cronin KA. SEER cancer statistics review (CSR) 1975-2013 https://seer.cancer.gov/csr/1975_2013/: National Cancer Institute; 2016. Available from: https://seer.cancer.gov/csr/1975_2013/.

98. Smith BR, Gambhir SS. Nanomaterials for *in vivo* imaging. *Chemical Reviews*. 2017;117(3):901-986.

99. Patel UB, Brown G, Machado I, Santos-Cores J, Pericay C, Ballesteros E, Salud A, Isabel-Gil M, Montagut C, Maurel J, Ramon-Ayuso J, Fernandez-Martos C. MRI assessment and outcomes in patients receiving neoadjuvant chemotherapy only for primary rectal cancer: longterm results from the GEMCAD 0801 trial. *Annals of Oncology*. 2017; 28(2):344-353.

100. Kobayashi M, Kikuchi D, Okamura H. Imaging of ultraweak spontaneous photon emission from human body displaying diurnal rhythm. *PLoS One*. 2009;4(7).

101. Pinto PA, Chung PH, Rastinehad AR, Baccala AA, Jr., Kruecker J, Benjamin CJ, Xu S, Yan P, Kadoury S, Chua C, Locklin JK, Turkbey B, Shih JH, Gates SP, Buckner C, Bratslavsky G, Linehan WM, Glossop ND, Choyke PL, Wood BJ. Magnetic resonance imaging/ultrasound fusion guided prostate biopsy improves cancer detection following transrectal ultrasound biopsy and correlates with multiparametric magnetic resonance imaging. *Journal of Urology*. 2011;186(4):1281-1285.

102. Willmann JK, van Bruggen N, Dinkelborg LM, Gambhir SS. Molecular imaging in drug development. *Nature Reviews Drug Discovery*. 2008;7(7):591-607.

103. O'Neill K, Lyons SK, Gallagher WM, Curran KM, Byrne AT. Bioluminescent imaging: a critical tool in pre-clinical oncology research. *The Journal of Pathology*. 2010;220(3):317-327.

104. Massoud TF, Gambhir SS. Molecular imaging in living subjects: seeing fundamental biological processes in a new light. *Genes and Development*. 2003;17(5):545-580.

105. Prescher JA, Contag CH. Guided by the light: visualizing biomolecular processes in living animals with bioluminescence. *Current Opinion in Chemical Biology*. 2010;14(1):80-89.

106. Chinen AB, Guan CM, Ferrer JR, Barnaby SN, Merkel TJ, Mirkin CA. Nanoparticle probes for the detection of cancer biomarkers, cells, and tissues by fluorescence. *Chemical Reviews*. 2015;115(19):10530-10574.

107. Heath CH, Deep NL, Beck LN, Day KE, Sweeny L, Zinn KR, Huang CC, Rosenthal EL. Use of panitumumab-IRDye800 to image cutaneous head and neck cancer in mice. *Otolaryngology-Head and Neck Surgery*. 2013;148(6):982-990.

108. Dothager RS, Flentie K, Moss B, Pan MH, Kesarwala A, Piwnica-Worms D. Advances in bioluminescence imaging of live animal models. *Current Opinion in Biotechnology*. 2009;20(1):45-53.

109. Paley MA, Prescher JA. Bioluminescence: a versatile technique for imaging cellular and molecular features. *Medchemcomm*. 2014;5(3):255-267.

110. Kenakin T, Christopoulos A. Signalling bias in new drug discovery: detection, quantification and therapeutic impact. *Nature Reviews Drug Discovery*. 2013;12(3):205-216.

111. Frank LA, Krasitskaya VV. Application of enzyme bioluminescence for medical diagnostics. *Advances in Biochemistry Engineering/Biotechnology*. 2014;144:175-197.

112. Burakova LP, Kudryavtsev AN, Stepanyuk GA, Baykov IK, Morozova VV, Tikunova NV, Dubova MA, Lyapustin VN, Yakimenko VV, Frank LA. Bioluminescent detection probe for tick-borne encephalitis virus immunoassay. *Analytical and Bioanalytical Chemistry*. 2015;407(18):5417-5423.

113. De A, Gambhir SS. Noninvasive imaging of protein-protein interactions from live cells and living subjects using bioluminescence resonance energy transfer. *The FASEB Journal*. 2005;19(14):2017-2019.

114. Dragulescu-Andrasi A, Chan CT, De A, Massoud TF, Gambhir SS. Bioluminescence resonance energy transfer (BRET) imaging of protein-protein interactions within deep tissues of living subjects. *Proceedings of the National Academy of Sciences of the United States of America*. 2011;108(29):12060-12065.

115. Negrin RS, Contag CH. In vivo imaging using bioluminescence: a tool for probing graft-versus-host disease. *Nature Reviews Immunology*. 2006;6(6):484-490.

116. Wang G, Cong W, Durairaj K, Qian X, Shen H, Sinn P, Hoffman E, McLennan G, Henry M. *In vivo* mouse studies with bioluminescence tomography. *Optics Express*. 2006;14(17):7801-7809.

117. Shimomura O, Teranishi K. Light-emitters involved in the luminescence of coelenterazine. *Luminescence*. 2000;15(1):51-58.

118. Inouye S, Sahara Y. Identification of two catalytic domains in a luciferase secreted by the copepod *Gaussia princeps*. *Biochemical and Biophysical Research Communications*. 2008;365(1):96-101.

119. Goerke AR, Loening AM, Gambhir SS, Swartz JR. Cell-free metabolic engineering promotes high-level production of bioactive *Gaussia princeps* luciferase. *Metabolic Engineering*. 2008;10(3-4):187-200.

120. Tannous BA, Kim DE, Fernandez JL, Weissleder R, Breakefield XO. Codon-optimized *Gaussia* luciferase cDNA for mammalian gene expression in culture and *in vivo*. *Molecular Therapy*. 2005;11(3):435-443.

121. Wurdinger T, Badr C, Pike L, de Kleine R, Weissleder R, Breakefield XO, Tannous BA. A secreted luciferase for *ex vivo* monitoring of *in vivo* processes. *Nature Methods*. 2008;5(2):171-173.

122. Rathnayaka T, Tawa M, Sohya S, Yohda M, Kuroda Y. Biophysical characterization of highly active recombinant *Gaussia* luciferase expressed in *Escherichia coli*. *Biochimica et Biophysica Acta*. 2010;1804(9):1902-1907.

123. Remy I, Michnick SW. A highly sensitive protein-protein interaction assay based on *Gaussia* luciferase. *Nature Methods*. 2006;3(12):977-979.

124. Maguire CA, Deliolanis NC, Pike L, Niers JM, Tjon-Kon-Fat LA, Sena-Esteves M, Tannous BA. *Gaussia* luciferase variant for high-throughput functional screening applications. *Analytical Chemistry*. 2009;81(16):7102-7106.

125. Hughes C, Rabinowitz A, Tate M, Birrell L, Allsup J, Billinton N, Walmsley RM. Development of a high-throughput *Gaussia* luciferase reporter assay for the activation of the GADD45a gene by mutagens, promutagens, clastogens, and aneugens. *Journal Biomolecular Screening*. 2012;17(10):1302-1315.

126. Yarden Y. The EGFR family and its ligands in human cancer signalling mechanisms and therapeutic opportunities. *European Journal of Cancer*. 2001;37(Suppl 4):3-8.

127. Nicholson RI, Gee JM, Harper ME. EGFR and cancer prognosis. *European Journal of Cancer*. 2001;37(Suppl 4):9-15.

128. Hansen AR, Siu LL. Epidermal growth factor receptor targeting in head and neck cancer: have we been just skimming the surface? *Journal of Clinical Oncology*. 2013;31(11):1381-1383.

129. Hunt EA, Moutsiopoulou A, Ioannou S, Ahern K, Woodward K, Dikici E, Daunert S, Deo SK. Truncated variants of *Gaussia* luciferase with tyrosine linker for site-specific bioconjugate applications. *Scientific Reports*. 2016;6.

130. Subik K, Lee JF, Baxter L, Strzepek T, Costello D, Crowley P, Xing L, Hung MC, Bonfiglio T, Hicks DG, Tang P. The expression patterns of ER, PR, HER2, CK5/6, EGFR, Ki-67 and AR by immunohistochemical analysis in breast cancer cell lines. *Breast Cancer: basic and clinical research*. 2010;4:35-41.

131. Wilken R, Veena MS, Wang MB, Srivatsan ES. Curcumin: a review of anti-cancer properties and therapeutic activity in head and neck squamous cell carcinoma. *Molecular Cancer*. 2011;10:(12).

132. Safdari Y, Khalili M, Farajnia S, Asgharzadeh M, Yazdani Y, Sadeghi M. Recent advances in head and neck squamous cell carcinoma-a review. *Clinical Biochemistry*. 2014;47(13-14):1195-1202.

133. Pulte D, Brenner H. Changes in survival in head and neck cancers in the late 20th and early 21st century: a period analysis. *The Oncologist*. 2010;15(9):994-1001.

134. Ponta H, Sherman L, Herrlich PA. CD44: from adhesion molecules to signalling regulators. *Nature Reviews Molecular Cell Biology*. 2003;4(1):33-45.

135. Chen J, Zhou J, Lu J, Xiong H, Shi X, Gong L. Significance of CD44 expression in head and neck cancer: a systemic review and meta-analysis. *BMC Cancer*. 2014;14:(15).

136. Franzmann EJ, Reategui EP, Carraway KL, Hamilton KL, Weed DT, Goodwin WJ. Salivary soluble CD44: a potential molecular marker for head and neck cancer. *Cancer Epidemiology, Biomarkers & Prevention*. 2005;14(3):735-739.

137. Franzmann EJ, Reategui EP, Pedroso F, Pernas FG, Karakullukcu BM, Carraway KL, Hamilton K, Singal R, Goodwinl WJ. Soluble CD44 is a potential marker for the early detection of head and neck cancer. *Cancer Epidemiology, Biomarkers & Prevention*. 2007;16(7):1348-1355.

138. Day KE, Sweeny L, Kulbersh B, Zinn KR, Rosenthal EL. Preclinical comparison of near-infrared-labeled cetuximab and panitumumab for optical imaging of head and neck squamous cell carcinoma. *Molecular Imaging and Biology*. 2013;15(6):722-729.

139. Tricoire L, Tsuzuki K, Courjean O, Gibelin N, Bourout G, Rossier J, Lambolez B. Calcium dependence of aequorin bioluminescence dissected by random mutagenesis. *Proceedings of the National Academy of Sciences of the United States of America*. 2006;103(25):9500-9505.